VOLUMETRIC MUSCLE LOSS INJURY AND MITOCHONDRIA: THE INTERSECTION OF MITOCHONDRIAL BIOENERGETICS, REDOX HOMEOSTASIS, AND SEX DIFFERENCES

by

JUNWON HEO

(Under the Direction of Jarrod Call)

ABSTRACT

Volumetric muscle loss (VML) is an irrecoverable skeletal muscle injury that leads to permanent functional deficits and long-term disability. It affects both military and civilian populations, with blast exposure being a primary cause in the military, while accidents and tumor ablation contribute to cases in civilians. Despite its prevalence, there is no clinical standard of care for VML rehabilitation and treatment. While extensive efforts have been made to comprehend the pathophysiology of VML, the metabolic impact of a Western diet (WD) on VML-injured muscle remains unclear. Additionally, evidence for mitochondrial ROS-associated oxidative stress following VML is circumstantial, primarily characterized by hyperpolarized mitochondrial membrane potential ($\Delta\psi m$) and lower respiratory capacity (JO_2). Furthermore, most VML studies rely on male animal models, leaving a critical gap in understanding sex-specific responses to injury and recovery. This dissertation addresses these knowledge gaps through three studies. Study 1 examined the impact of WD on muscle metabolism post-VML in both sexes. In males, WD worsened carbohydrate-supported mitochondrial respiration, impairing pyruvate dehydrogenase (PDH) enzyme kinetics and complexes I and II, while no significant effects were observed in females. Study 2 explored the relationship between VML and

mitochondrial ROS in male mice and assessed the effects of the mitochondrial-targeted antioxidant SS-31. While SS-31 improved mitochondrial function and fixed ROS, it had limited effects on muscle contractility, suggesting that oxidative stress alone is not the primary driver of impaired muscle adaptation. The combination of SS-31 with rehabilitation modestly improved metabolic outcomes but did not restore muscle function, emphasizing the need for multifaceted therapeutic approaches. Study 3 investigated the role of 17β-estradiol (E2) in muscle metabolism and redox balance in E2-deficient mice post-VML injury. Ovariectomy exacerbated mitochondrial dysfunction, increased ROS emission, and impaired antioxidant capacity after VML injury, while E2 replacement improved mitochondrial bioenergetic efficiency and antioxidant defense. Together, these studies enhance our understanding of VML pathophysiology in a sex-dependent manner, highlight the metabolic consequences of WD, and underscore the role of ovarian hormones. The findings provide a foundation for developing targeted therapeutic strategies to optimize muscle metabolic function and redox homeostasis post-VML injury.

INDEX WORDS: Exerkines; Volumetric muscle loss injury; Metabolism; Mitochondrial Bioenergetics; Reactive Oxygen Species; Sex Differences

VOLUMETRIC MUSCLE LOSS INJURY AND MITOCHONDRIA: THE INTERSECTION OF MITOCHONDRIAL BIOENERGETICS, REDOX HOMEOSTASIS, AND SEX DIFFERENCES

by

JUNWON HEO

BEd, Inha University, 2016

MS, Inha University, 2018

A Dissertation Submitted to the Graduate Faculty of The University of Georgia in Partial Fulfillment of the Requirements for the Degree

DOCTOR OF PHILOSOPHY

ATHENS, GEORGIA

2025

VOLUMETRIC MUSCLE LOSS INJURY AND MITOCHONDRIA: THE INTERSECTION OF MITOCHONDRIAL BIOENERGETICS, REDOX HOMEOSTASIS, AND SEX DIFFERENCES

by

JUNWON HEO

Major Professor:	Jarrod Call
Committee:	Emily Noble
	Tony Wolf
	Kelsey Fisher-Wellman

Electronic Version Approved:

Ron Walcott
Vice Provost for Graduate Education and Dean of the Graduate School
The University of Georgia
May 2025

DEDICATION

This work is dedicated to my wife Ji Won. Her unwavering support, love, and encouragement have been the foundation of this PhD journey. Without her by my side, I would not have been able to reach this milestone. She is not only my greatest champion but also the true MVP in every sense.

ACKNOWLEDGEMENTS

My PhD work would not have been possible without the invaluable support of my lab mates, Dr. Jennifer McFaline-Figueroa, Dr. Albino Schifino, Jessica Hoffman, David Miller, Katelyn Castelli, and Reese Groover, and my mentor, Dr. Jarrod Call. Their guidance, collaboration, and encouragement have been instrumental in my PhD journey, and I am deeply grateful for their contributions.

I would also like to express my heartfelt gratitude to my parents and my parents-in-law for their love, sacrifices, and support throughout this journey. Their encouragement and belief in me have been a constant source of strength, and I could not have done this without them.

TABLE OF CONTENTS

Page

LIST OF TABLES

Page

LIST OF FIGURES

Page

CHAPTER 1

INTRODUCTION

Volumetric muscle loss (VML) injury represents a severe and often irrecoverable musculoskeletal trauma that results in a permanent loss of skeletal muscle mass and function (Greising et al., 2018). The injury is characterized by a compromised regenerative response, leading to persistent fibrosis (Hoffman et al., 2022), chronic inflammation (Larouche et al., 2023), metabolic dysfunction (Dalske et al., 2021; McFaline-Figueroa et al., 2022, 2023; Southern et al., 2019), and mitochondrial impairment (McFaline-Figueroa et al., 2022, 2023; Southern et al., 2019). VML injuries are observed in military personnel due to combat-related trauma, but they are also prevalent in civilian populations following open fractures, gunshot wounds, surgical resections, and soft-tissue sarcomas (Testa et al., 2021). Given the long-term disability associated with VML injuries, understanding the underlying pathophysiology is critical for developing targeted therapeutic interventions.

Mitochondria play a pivotal role in skeletal muscle function, regulating bioenergetics, metabolic flexibility, and redox balance. The impairment of mitochondrial function in VML-injured muscle has been associated with decreased respiratory efficiency and hyperpolarized mitochondrial membrane potential (McFaline-Figueroa et al., 2023), all of which contribute to poor muscle recovery and adaptation. Intriguingly, there is a lack of evidence where (a) WD would impact muscle metabolism and contractile function after VML injury in both sexes, (b) VML is associated with mitochondrial ROS and the role of mitochondrial-targeted antioxidants

on mitochondrial bioenergetic and ROS following VML, and (c) the sex hormone would influence muscle metabolism following VML injury in female mice.

This dissertation aims to explore the complex interplay between mitochondrial bioenergetics, redox homeostasis, and sex differences in VML injury. The subsequent chapters delve into the role of exerkines in modulating brain mitochondria (Chapter 2), the combined impacts of WD and VML on skeletal muscle metabolic regulation in male and female mice (Chapter 3), the impact of mitochondrial-targeted antioxidants in mitigating oxidative stress and improving bioenergetic function in VML-injured muscle (Chapter 4), and the influence of estradiol on skeletal muscle metabolism and ROS homeostasis in female VML-injured mice (Chapter 5). Together, these studies provide a comprehensive understanding of the mitochondrial pathophysiology and the potential for targeted interventions to optimize muscle regeneration and functional recovery against VML injury.

To address the important questions raised above, my dissertation had the following specific aims and hypotheses:

Specific Aim 1: Determine how exercises such as myokines, hepatocytes, and adipokines influence mitochondrial bioenergetics, content, and dynamics, potentially mitigating neurocognitive decline and metabolic dysfunction.

Hypothesis 1: This review paper provides an overview of how physical activity-induced exerkines modulate mitochondrial function in the brain, with implications for broader systemic metabolic health.

Specific Aim 2: Investigate the extent to which Western diet (WD) affects skeletal muscle metabolic and contractile function following VML injury in both male and female mice.

Hypothesis 2: WD would worse muscle metabolic dysfunction following VML injury regardless of sex.

Specific Aim 3: Determine whether VML is associated with mitochondrial ROS and exogenous mitochondrial antioxidant would enhance contractile and metabolic function after rehabilitation.

Hypothesis 3: VML injury would be associated with greater mitochondrial ROS production, while mitochondrial-targeted antioxidants would improve the contractile and metabolic function after exercise rehabilitation.

Specific Aim 4: Determine the role of estradiol in protecting against mitochondrial dysfunction and redox homeostasis following VML injury in female mice.

Hypothesis 4: Estradiol would attenuate ovariectomy-induced mitochondrial dysfunction and oxidative stress following VML-injured female mice.

References:

Dalske, K. A., Raymond-Pope, C. J., McFaline-Figueroa, J., Basten, A. M., Call, J. A., & Greising, S. M. (2021). Independent of physical activity, volumetric muscle loss injury in a murine model impairs whole-body metabolism. *PloS One*, *16*(6), e0253629. https://doi.org/10.1371/journal.pone.0253629

Greising, S. M., Warren, G. L., Southern, W. M., Nichenko, A. S., Qualls, A. E., Corona, B. T., & Call, J. A. (2018). Early rehabilitation for volumetric muscle loss injury augments endogenous regenerative aspects of muscle strength and oxidative capacity. *BMC Musculoskeletal Disorders*, *19*, 173. https://doi.org/10.1186/s12891-018-2095-6

Hoffman, D. B., Raymond-Pope, C. J., Sorensen, J. R., Corona, B. T., & Greising, S. M. (2022). Temporal changes in the muscle extracellular matrix due to volumetric muscle loss injury. *Connective Tissue Research*, *63*(2), 124–137. https://doi.org/10.1080/03008207.2021.1886285

Larouche, J. A., Wallace, E. C., Spence, B. D., Buras, E., & Aguilar, C. A. (2023). Spatiotemporal mapping of immune and stem cell dysregulation after volumetric muscle loss. *JCI Insight*, *8*(7), e162835. https://doi.org/10.1172/jci.insight.162835

McFaline-Figueroa, J., Hunda, E. T., Heo, J., Winders, E. A., Greising, S. M., & Call, J. A. (2023). The bioenergetic “CK Clamp” technique detects substrate-specific changes in mitochondrial respiration and membrane potential during early VML injury pathology. *Frontiers in Physiology*, *14*, 1178213. https://doi.org/10.3389/fphys.2023.1178213

McFaline-Figueroa, J., Schifino, A. G., Nichenko, A. S., Lord, M. N., Hunda, E. T., Winders, E. A., Noble, E. E., Greising, S. M., & Call, J. A. (2022). Pharmaceutical Agents for

Contractile-Metabolic Dysfunction After Volumetric Muscle Loss. *Tissue Engineering. Part A*, *28*(17–18), 795–806. https://doi.org/10.1089/ten.TEA.2022.0036

Southern, W. M., Nichenko, A. S., Tehrani, K. F., McGranahan, M. J., Krishnan, L., Qualls, A. E., Jenkins, N. T., Mortensen, L. J., Yin, H., Yin, A., Guldberg, R. E., Greising, S. M., & Call, J. A. (2019). PGC-1α overexpression partially rescues impaired oxidative and contractile pathophysiology following volumetric muscle loss injury. *Scientific Reports*, *9*(1), 4079. https://doi.org/10.1038/s41598-019-40606-6

Testa, S., Fornetti, E., Fuoco, C., Sanchez-Riera, C., Rizzo, F., Ciccotti, M., Cannata, S., Sciarra, T., & Gargioli, C. (2021). The War after War: Volumetric Muscle Loss Incidence, Implication, Current Therapies and Emerging Reconstructive Strategies, a Comprehensive Review. *Biomedicines*, *9*(5), 564. https://doi.org/10.3390/biomedicines9050564

CHAPTER 2

THE ROLE OF EXERKINES ON BRAIN MITOCHONDRIA: A MINI-REVIEW [1]

[1] Heo J, Noble EE, Call JA. *Journal of Applied Physiology* (1985). 2023 Jan 1;134(1):28-35.

Abstract

Exercise benefits many organ systems, including having a panacea-like effect on the brain. For example, aerobic exercise improves cognition and attention and reduces the risk of brain-related diseases, such as dementia, stress, and depression. Recent advances suggest that endocrine signaling from peripheral systems, such as skeletal muscle, mediates the effects of exercise on the brain. Consequently, it has been proposed that factors secreted by all organs in response to physical exercise should be more broadly termed the "exerkines". Accumulating findings suggest that exerkines derived from skeletal muscle, liver, and adipose tissues directly impact brain mitochondrial function. Mitochondria play a pivotal role in regulating neuronal energy metabolism, neurotransmission, cell repair, and maintenance in the brain, and therefore exerkines may act via impacting brain mitochondria to improve brain function and disease resistance. Therefore, herein we review studies investigating the impact of muscle-, liver-, and adipose tissue-derived exerkines on brain cognitive and metabolic function via modulating mitochondrial bioenergetics, content, and dynamics under healthy and/or disease conditions.

Running title: Exerkines and Brain Mitochondria

Key words: Exercise; Myokines; Hepatokines; Adipokines; Mitochondria

INTRODUCTION

The discovery in the late 20th century that exercise enhances neurogenesis and neuroplasticity has resulted in a burgeoning area of research investigating the impact of exercise on brain function in health and disease. Given the tremendous impact of exercise on the organ systems of the body, identifying the precise mechanisms by which exercise improves brain function remains challenging. Physical activity reduces cognitive decline associated with Parkinson's and Alzheimer's disease, and an individual's physical activity levels are positively associated with a lower risk of developing several neurocognitive disorders and depression (Fonte et al., 2019). Cellular mechanisms of neurocognitive decline are complicated and multifaceted; however, there is robust literature supporting changes in brain mitochondrial bioenergetics as playing a role in several brain disorder pathophysiologies (Raefsky & Mattson, 2017). Herein we investigate the existing literature that physical activity-induced secretory factors (i.e., exerkines) promote brain health by modulating mitochondrial bioenergetics.

Mitochondrial Bioenergetics and Dynamics

Mitochondrial bioenergetics describes the redox systems (e.g., dehydrogenases), electron transport chain (ETC) activities (e.g., oxygen reduction), and mitochondrial membrane potential ($\Delta\Psi_m$) regulation that participates in matching ATP re-synthesis with energetic demand [for comprehensive review (Schmidt et al., 2021)]. In the neuron, for example, mitochondria are spread throughout the dendrites and axons where they produce ATP to support neurotransmission and cell maintenance. Importantly, mitochondria are structurally dynamic organelles that are continuously regulated by biogenesis and dynamics (fusion; mitochondrial elongation and fission; mitochondrial fragmentation) to maintain mitochondrial quality control in response to

physiological and/or pathological stimuli (Raefsky & Mattson, 2017). In the process of mitochondrial dynamics, dynamin-related protein 1 (Drp1) and mitochondrial fission protein I (Fis1) primarily regulate mitochondrial fission; meanwhile, mitochondrial fusion is mediated by mitofusin 1 and 2 (Mfn1 and Mfn2; outer membrane), and optic atrophy protein 1 (Opa1; inner membrane) (Raefsky & Mattson, 2017). Furthermore, mitochondrial autophagy, called mitophagy, is crucial for neuronal health by recycling the impaired mitochondria (Martín-Maestro et al., 2016). Since there is a dearth of direct evidence linking myo-, hepato-, and adipose tissue-mediated exerkines to mitophagy in the brain, in this review, we have not addressed the link between exerkines and mitophagy; however, given that exercise has been shown to activate mitophagy and improve mitochondrial function (Liang et al., 2021), future research is required to explore the direct relationship between exerkines-mediated mitophagy and brain function. Dysfunctional mitochondrial dynamics, content, and bioenergetics are associated with reduced neuronal activity and greater cell death during the neurodegeneration (Raefsky & Mattson, 2017), and exercise has been shown to improve mitochondrial function, neuronal activity, and neuroprotection. In this review, we discuss the evidence for the beneficial impacts of exerkines modulating mitochondrial bioenergetics, content, and dynamics.

Brain-Derived Neurotrophic Factor

Brain-Derived Neurotrophic Factor (BDNF) plays a dominant role in mediating the beneficial effects of exercise on brain function, especially hippocampal-cognitive function (Marosi & Mattson, 2014). BDNF activates neuronal differentiation from stem cells, augments neurite outgrowth and synaptogenesis, and impedes apoptosis. In neurons, BDNF is expressed throughout development and the adult mammalian nervous system (Marosi & Mattson, 2014). Greater levels of BDNF mRNA and protein are associated with the beneficial effects of exercise

in rodents and humans and contribute to better cognitive function [see these reviews (Marosi & Mattson, 2014; Severinsen & Pedersen, 2020)]. While BDNF is not believed to cross the blood-brain barrier (BBB) [e.g., (Matthews et al., 2009)] many of the exerkines reviewed herein act via engaging a BDNF-mediated mechanism in the brain. Additionally, BDNF impacts mitochondrial bioenergetics, content, and dynamics in the brain. For example, BDNF enhances the complex I substrate-mediated respiratory control index, which indicates mitochondrial integrity by measuring the coupling of the respiratory chain and improves the efficiency of respiratory coupling (Markham et al., 2004, 2012). BDNF activates peroxisome proliferator-activated receptor γ coactivator 1 alpha (PGC1α), resulting in an increase in mitochondrial biogenesis, and a corresponding elevation in cellular energy substrates such as ATP and NAD^+, as well as the maintenance and formation of the synapses (Cheng et al., 2012). Importantly, PGC1α augments BDNF expression levels, supported by evidence that following the knockdown of PGC1α, synapse formation decreases, and the capability of BDNF to stimulate synaptogenesis is impeded (Cheng et al., 2012). These findings suggest a positive feedback loop mechanism whereby BDNF stimulates PGC1α and vice versa. Overall, current findings suggest BDNF is directly associated with mitochondrial biogenesis and respiratory coupling efficiency. Next, we summarize how the exerkines released from skeletal muscle, liver, and adipose tissues directly impact the parameters of mitochondrial bioenergetics, content, and dynamics in the brain **(Table 1)**.

EXERKINES

Exerkines are defined, broadly, as the secretory factors from any organ in response to physical activity (Safdar et al., 2016). The concept of physical activity-induced secretory factors began to

emerge in the early 2000s when Steensberg et al. (Steensberg et al., 2000) demonstrated that interleukin-6 (IL-6) is secreted from skeletal muscle into the circulation following acute exercise and acts as an endocrine factor. Later, Pedersen and colleagues (Pedersen et al., 2003) introduced the term "myokines" referring to the specific autocrine, paracrine, and endocrine effects of muscle-secreted factors. To date, the biological and physiological functions for a minority of myokines (~5%) have been defined (Severinsen & Pedersen, 2020). Furthermore, additional organs are now recognized for their physical activity-induced release of secretory factors, such as the liver (hepatokines) and adipose tissue (adipokines). Presently, there is growing recognition that exerkines impact cognitive function [see the review (Chow et al., 2022)].

Herein we review exerkines that *i*) pass through the BBB and *ii*) show evidence of influencing mitochondrial bioenergetics, content, and/or dynamics. The revelations from this review highlight a potential mechanism of physical activity-related brain benefits and also recognize a significant knowledge gap in the field, i.e., that there is a critical need for additional brain region-specific studies.

Myokines

The first discovered and most well-studied myokine is interleukin-6 (IL-6). The role of IL-6 in skeletal muscle adaptations to exercise has been demonstrated extensively. Skeletal muscle contraction promotes IL-6 independent of tumor necrosis factor-alpha (Febbraio & Pedersen, 2002), suggesting that muscle-mediated IL-6 increases metabolic function rather than inflammatory function. Several studies have demonstrated that peripherally secreted IL-6 crosses the BBB (Timper et al., 2017) and regulates food intake, possibly suppressing obesity and obesity-mediated neuronal disorders [see the review (Severinsen & Pedersen, 2020)]. For

example, enhancing muscle-derived IL-6 suppresses food intake and reduces body weight in rodent models by regulating the expression of hypothalamic peptides relevant for energy balance, suggesting that IL-6 may contribute to exercise-induced reductions in body weight (Shirazi et al., 2013).

More recently, the discovery of Irisin renewed interest exercise-induced myokine influences on the brain. Irisin is a membrane molecule that is the cleavage product of fibronectin type III domain containing 5 (FNDC5) and is secreted from muscle in circulation and might cross the BBB (Islam et al., 2021), and potentially mediates the effects of exercise on BDNF expression in the brain. Exercise upregulates the *fndc5* expression via increasing the transcription factor, PGC1α in skeletal muscle, and circulating Irisin also upregulates PGC1α- mediated *fndc5* expression and irisin in the brain (Wrann et al., 2013). Specifically, in rodents, greater plasma Irisin is associated with elevated *Bdnf* gene expression in the hippocampus. In primary cortical neurons, *in vitro* Irisin treatment promotes *Bdnf* gene expression, while RNA-interference-mediated knockdown of *fndc5* results in a reduced *Bdnf* gene expression, suggesting that in both the hippocampus and cortical cells, the BDNF levels are increased by circulating Irisin. In further support of the idea that Irisin may mediate some of the benefits of exercise to prevent neurodegenerative disorders, Irisin has recently been identified to improve synaptic plasticity and memory function in an Alzheimer's disease mouse model (Islam et al., 2021). However, one caveat to consider is that it has been controversial whether exercise elevates plasma levels of irisin in humans (Albrecht et al., 2015).

Lactate is also one of the major exerkines derived from the skeletal muscle following exercise (Brooks et al., 2022). There is accumulating evidence that exercise-derived lactate passes through BBB and engages BDNF-mediated signaling in the hippocampus and improves

learning and memory (El Hayek et al., 2019). Furthermore, lactate directly augments metabolic function in brain regions such as the hypothalamus and hippocampus. For instance, hypothalamic sensing of lactate in circulation maintains glucose production which is critical for glucose homeostasis (Kokorovic et al., 2009).

Taken together, the evidence suggests that exercise-mediated myokines such as lactate, Irisin, and IL-6 are released into circulation, cross the BBB, and influence brain function.

Myokines and Brain Mitochondria

Irisin (FNDC5), IL-6, and lactate each have been shown to impact mitochondrial bioenergetics, content, and dynamics **(Table 1)**. In 2013, Wrann et al. (Wrann et al., 2013) demonstrated that the neuronal gene expression of *Fndc5* is controlled by PGC1α, and the knockout of PGC1α in mice induced a decrease in *Fndc5* gene expression in the brain, suggesting that PGC1α regulates *Fndc5*. Conversely, other studies have demonstrated Irisin controls mitochondrial biogenesis, bioenergetics, and structures (P. Guo et al., 2021; Tu et al., 2021; S. Wang & Pan, 2016). For example, Irisin treatment increases mitochondrial complex I, II, and IV activities, and ATP levels following chronic unpredictable stress (a rodent model of depression) in rats (S. Wang & Pan, 2016). *In vivo* intracerebroventricular administration of irisin increases mitochondrial biogenesis following subarachnoid hemorrhage in rodents by increasing PGC1α and the mitochondrial transcription factor A (TFAM) protein expression levels (Tu et al., 2021). Furthermore, the mitochondrial structure observed by transmission electron microscope (TEM) showed that nascent mitochondria increased, with less swelling in mitochondria and fewer vacuoles. Another study has shown that intravenous treatment of Irisin increases nuclear respiratory factor-2 (NRF-2) protein levels and reduces $\Delta\Psi_m$ and ROS formation following traumatic brain injury (P. Guo

et al., 2021). Taken together, Irisin treatment attenuates disease-induced impaired mitochondrial biogenesis, bioenergetics, and structure by enhancing biogenesis factors and structure and lowering ROS and $\Delta\Psi_m$.

Similar to Irisin, IL-6 improves mitochondrial content, mitochondrial bioenergetics, and structure in astrocytes under the lipopolysaccharide-induced sepsis model (Chen et al., 2018). In this study, *in vitro* treatment of IL-6 to astrocytes enhanced PGC1α, NFR1, and TFAM protein levels, accompanied by an increase in mtDNA content and mitochondrial volume density, increased intracellular ATP levels, and improved mitochondrial morphology observed via TEM. Surprisingly, although IL-6 is the first discovered myokine, there is a dearth of studies on the link between IL-6 and brain mitochondria. Considering that IL-6 treatment has been shown to directly control mitochondrial dynamics in skeletal muscle (Fix et al., 2019), future research is necessary to investigate the exercise-derived IL-6 would directly influence mitochondrial bioenergetics and quality control in the brain.

Muscle-derived lactate is associated with mitochondrial bioenergetics, content, and dynamics in the brain. For instance, i.p. lactate injections activate the histone deacetylase SIRT1, which engages the hippocampal PGC1α/FNDC5 pathway, resulting in elevated BDNF and TrkB protein levels (El Hayek et al., 2019). Similarly, i.p. injection of lactate elevates hippocampal PGC1α and TFAM mRNA expression (Park et al., 2021). Blood lactate injection increases hippocampal lactate levels similar to that in blood, suggesting that lactate crosses the BBB, and the effects of lactate are suppressed by UK5099, a lactate transporter inhibitor, demonstrating that blood lactate elevates hippocampal mitochondrial biogenesis markers (Park et al., 2021). In addition, Hu et al. (Hu et al., 2021) suggest lactate has a role in regulating mitochondrial bioenergetics and structure. They treated lactate to primary hippocampal neurons and

demonstrated that lactate increases hippocampal ATP levels and enhances OxPhos-related genes, such as Ubiquinol-Cytochrome C Reductase Core Protein 1 (Uqcrc1; complex III) and ATP synthase subunit alpha 1 (Atp5a1; complex V). Corroborating previous studies, lactate also induced an increase in mitochondrial biogenesis factors, including PGC1α, NRF2, TFAM gene expression levels, and mtDNA copy number. Lastly, the authors demonstrated that mitochondrial dynamics is regulated by lactate treatment in primary hippocampal neurons (Hu et al., 2021). Although there was no change in Opa1 protein levels, Mfn1 and 2 protein levels are significantly higher after lactate treatment; conversely, mitochondrial Drp1 and Fis1 protein levels were reduced by lactate (Hu et al., 2021), shifting to more fused mitochondria. Together, these findings suggest that lactate elicited by exercise can directly influence brain mitochondria, regulating mitochondrial bioenergetics, biogenesis, and dynamics.

Hepatokines

Fibroblast growth factor 21 (FGF21) is an exercise-mediated hepatokine that crosses the BBB (Kang et al., 2020) and has neuroregulatory actions in the brain (Kang et al., 2020; Sa-Nguanmoo et al., 2016). Especially, in the hypothalamus, FGF 21 regulates sugar intake (von Holstein-Rathlou et al., 2016) and circadian behavior (Bookout et al., 2013), and in the hippocampus, FGF21 is shown to protect against cognitive decline by not only enhancing synaptic plasticity in the obese rat (Sa-Nguanmoo et al., 2016) but also reducing inflammation and oxidative stress in the *db/db* and aged mouse (Kang et al., 2020).

Ketone bodies, similar to lactate, are metabolites that double as signaling molecules and act as exerkines with effects in the brain (Camandola & Mattson, 2017). Ketone bodies are produced in the liver during conditions of limited glucose availability, such as fasting and

exercise (Mattson et al., 2018). Under limited glucose conditions, adipocytes secrete fatty acids, which are then converted into the ketone bodies β-hydroxybutyrate (BHB) and acetoacetate by the liver. The metabolic demands of exercise have a potent effect on increasing BHB synthesis and secretion from the liver. BHB passes through the BBB and accumulates in the hippocampus, increasing the histone acetylation in the BDNF promoters, particularly activity-dependent promoter 1, and in turn, increased BDNF expression (Sleiman et al., 2016). These findings suggest that BHB as an exerkine provides a link between exercise and BDNF expression in the brain.

Hepatokines and Brain Mitochondria

Hepatokines, such as BHB and FGF21, augment brain function by modulating mitochondrial bioenergetics, content, and dynamics **(Table 1)**. For example, FGF21 treatment to the human dopaminergic neurons increases PGC1α protein levels, oxygen consumption rate, and NAD^+/NADH ratio (which is a marker of ETC efficiency) under normal conditions, although mtDNA copy number and mitochondrial surface area are not changed following FGF21 treatment (Mäkelä et al., 2014). Furthermore, Sa-Nguanmoo et al. (Sa-Nguanmoo et al., 2016) found that following 6 weeks of high-fat diet consumption, i.p. FGF21 injection for 6 weeks increased PGC1α protein levels and attenuated ROS production, normalized $\Delta\Psi_m$, and decreased mitochondrial swelling in rat brain. These results suggest that *in vivo* injection of FGF21 exerts a neuroprotective effect in obese rats by enhancing mitochondrial bioenergetics, (specifically i.e., amelioration of ROS and $\Delta\Psi_m$, and mitochondrial morphology). Another study showed that *in vitro* and *in vivo* treatment of FGF21 improved mitochondrial bioenergetics ($\Delta\Psi_m$), biogenesis, and content under the MPTP-induced Parkinson's disease (PD) model supported by the evidence

where FGF21 treatment improved $\Delta\Psi_m$ (*in vitro*) and the mitochondrial ETC-related gene and proteins expression (*in vivo*) in the PD model (Fang et al., 2020).

Similar to FGF21, BHB directly regulates brain mitochondrial bioenergetics, biogenesis, content, and structure. In 2003, Tieu et al. (Tieu et al., 2003) demonstrated that in the 1-Methyl-4-phenyl-1,2,3,6-tetrahydropyridine (MPTP)-treated Parkinson's disease model, BHB increases mitochondrial oxygen consumption via a complex II-dependent manner. Specifically, suppression of complex II abrogates BHB-induced increases in mitochondrial oxygen respiration and abolishes BHB-mediated neuroprotective effects on substantia nigra pars compacta (SNpc) dopaminergic neurons. However, BHB had no effect on mitochondrial $\Delta\Psi_m$, and mitochondrial hydrogen peroxide (H_2O_2) production was increased after BHB treatment, suggesting that BHB may not be related to the amelioration of ROS and $\Delta\Psi_m$, perhaps, BHB would increase physiological levels of ROS, and/or cellular antioxidants may increase following BHB treatment. Using high levels of glutamate exposure to mimic metabolically injured neurons, BHB treatment of primary cultured rat cortical neurons increases mitochondrial respiratory capacity, suggesting that neuroprotection by exogenous BHB may partially be regulated by the preservation of mitochondrial respiratory capacity (Laird et al., 2013). In line with these studies, Marosi et al. (Marosi et al., 2016) found that neurons treated with BHB have an increase in mitochondrial respiration rate, ATP production, and NAD^+/NADH ratio, although mitochondrial biogenesis markers (e.g., PGC1α, NFR1 and 2, TFAM) and mtDNA copy number were not changed following BHB treatment; additionally, BHB increased mitochondrial ROS production, which is consistent with the previous study (Tieu et al., 2003).

The increases in ROS production were shown to underlie BHB-mediated *Bdnf* expression, supported by the evidence that reduced mitochondrial ROS production impeded

BHB-mediated *Bdnf* promoter activity (Marosi et al., 2016). In this study, paradoxically, antioxidant enzymes (e.g., superoxide dismutase 2 and heme oxygenase 1) were concurrently increased in neurons treated with BHB, suggesting that although mitochondrial ROS production was increased to promote *Bdnf* expression, simultaneously, enhanced antioxidant defenses after BHB treatment defend against the increased mitochondrial ROS production. Furthermore, in the oxygen-glucose deprivation/reoxygenation (OGD/R) treatment to SH-SY-5Y cells to mimic the ischemic injury model, BHB treatment confers against OGD/R-mediated reductions in ATP generation, increased ROS, and decreased $\Delta\Psi m$ (M. Guo et al., 2018). Furthermore, OGD/R-induced Drp1 mitochondrial recruitment promotes mitochondrial fission; however, mitochondrial Drp1 translocation is suppressed by BHB treatment, suggesting that BHB reduces mitochondrial fragmentation.

More recently, Dabke et al. (Dabke & Das, 2020) showed that BHB treatment to HT22 hippocampal murine neurons augments mitochondrial complexes (i.e., complex I+III) and citrate synthase enzyme activities. In the same cell line, BHB treatment increased mitochondrial complex I and IV enzyme activities (Majrashi et al., 2021). The findings suggest that BHB increases mitochondrial respiratory enzyme activity. Furthermore, the authors found that hippocampal neurons treated with BHB exhibited lower ROS production and improved antioxidants, such as glutathione and catalase, which is inconsistent with previous studies (Marosi et al., 2016; Tieu et al., 2003) showing an increase in ROS production following BHB treatment. These divergent findings may be attributed to timing, dose-dependent manner, and experimental type (*in vitro* vs *in vivo*). Lastly, using both an *in vivo* model using a mutated uracil-DNA glycosylase 1 that induces mitochondrial toxicity and an *in vitro* model where cultured hippocampal neurons and human fibroblasts were treated with H_2O_2 to cause oxidative

stress, BHB treatment improves mitochondrial biogenesis, structure, and function markers by upregulating PGC1α protein and gene expressions (*in vivo*) and increasing oxygen consumption rate and NAD^+/NADH ratio (*in vitro*) (Hasan-Olive et al., 2019). These findings suggest that BHB improves mitochondrial bioenergetics, biogenesis, and dynamics under normal and disease conditions.

Taken together, mitochondrial biogenesis and respiration markers are consistently improved by the hepatokines, (BHB and FGF21). However, while FGF21 ameliorated ROS production, ROS production following BHB treatment is more nuanced, with conflicting results. Future studies into these opposing findings are needed to establish the impact of hepatokines on ROS production in the brain and the relationship with mitochondrial function.

Adipokines

Adiponectin (ADN) is a protein that is secreted into the circulation from adipocytes and acts as a signaling molecule (adipokine). ADN has antidiabetic, insulin-sensitizing, antiatherogenic, anti-inflammatory, and neuroprotective effects (Yau et al., 2014), and is increased following exercise (García-Hermoso et al., 2017).

ADN can pass through the BBB and improve cell proliferation and reduce depression-like behavior (Yau et al., 2014). Specifically, exercise-mediated mitigation of depression-like behavior was offset in ADN-deficient mice via an impaired AMP-activated protein kinase signaling in the hippocampus. Interestingly, running increased BDNF protein levels in the isolated dentate gyrus of both WT and ADN KO mice, suggesting that ADN does not regulate BDNF in the dentate gyrus (Yau et al., 2014). Even if the role of ADN indicates a direct interplay

between adipose and brain tissues after exercise, the underlying mechanisms of how exercise-induced adipokines influence brain function need to be elucidated.

Adipokines and Brain Mitochondria

Similar to myokines and hepatokines, ADN augments brain mitochondrial bioenergetics, content, and dynamics in several brain disorders **(Table 1)**. For example, in 2018, a study found that ADN protects HT22 hippocampal neuronal cells from oxygen-glucose deprivation (OGD)-induced mitochondrial structural dysfunction and oxidative stress (B. Wang et al., 2018). In detail, using the OGD-induced neuronal injured *in vitro* model, ADN treatment ameliorates mitochondrial structural damages, including vanished cristae and mitochondrial swelling (B. Wang et al., 2018). Moreover, ADN treatment attenuated higher ROS and decreased $\Delta\Psi_m$ in OGD-treated cells (B. Wang et al., 2018). More recently, Wu et al. (Wu et al., 2020) demonstrated that in transcriptomic analysis, the expression of mitochondrial respiratory-related genes, such as *mt-Nd1*, *Nd4*, *mt-Atp8*, and *mt-cytb*, are increased after ADN peptide (ADNp) treatment in an intracerebral hemorrhage (ICH)-injured rodent model. In line with these findings, *in vivo* ADNp i.p. injection increases ATP levels following the ICH-injury (Wu et al., 2020), suggesting adiponectin improved mitochondrial respiratory factors. Using an *in vitro* ICH model, mitochondrial ROS and $\Delta\Psi_m$ are normalized following ADNp incubation in the primary astrocytes (Wu et al., 2020). Additionally, ADNp increased Drp1 (serine 637) phosphorylation, which suppresses the translocation of Drp1 to the mitochondria, and decreases mitochondrial fragmentation in the astrocytes, suggesting that ADNp regulates mitochondrial dynamics by suppressing mitochondrial fragmentation. In an *in vivo* model of ICH-induced injury, Yu et al. (Yu et al., 2019) activated ADN receptor 1 by intraperitoneally injecting AdipoRon, the agonist of the ADN

receptor and found that activation of the ADN receptor increased ATP levels and reduced ROS production in the brain, and further elevated mitochondrial biogenesis factors by enhancing the protein levels of PGC1α, NFR1, and TFAM. Furthermore, in the ICH model, activation of the ADN receptor increased overall mitochondrial mass and attenuated the hyperpolarized mitochondrial $\Delta\Psi_m$. These findings suggest that ADN improves mitochondrial bioenergetics, content, and dynamics in brain tissues under brain disease models.

CONCLUSIONS

In this mini-review, we describe how exerkines influence brain health by directly modulating mitochondrial bioenergetics, content, and dynamics **(Fig. 1)**. Since the initial findings that exercise increases BDNF levels in the brain, promoting neural plasticity and neurogenesis and improving cognitive function, researchers have been searching to identify factors mediating these beneficial actions of exercise on the brain. In the last two decades, several exerkines derived from muscle, liver, and adipose tissues have been shown to directly affect brain mitochondria, thereby showing the prevention or treatment of brain disorders. Apart from the exerkines covered in this mini-review, other peripherally derived exerkines have been shown to improve brain function [see the reviews (Chow et al., 2022; Matthews et al., 2009; Pedersen, 2019)]. However, whether these exerkines directly affect brain mitochondria is currently unknown. Thus, further studies are needed to shed light on the effects of these exerkines on brain health and/or disease via modulating mitochondrial bioenergetics, content, and dynamics under various disease conditions.

Recently, Schmidt et al. (Schmidt et al., 2021) proposed that in order to better appreciate mitochondrial bioenergetics and draw the conclusions that are physiologically relevant in the

mitochondrial environment, recent advances in comprehensive mitochondrial bioenergetics analyses (e.g., creatine-kinase clamp test, membrane potential, $NADH/NAD^+$ redox states) would be a proper approach. Current bioenergetics studies have been limited because they rely on the supra-physiological environment in the mitochondria and fail to recapitulate the free energies balance (e.g., ΔG_{redox}, $\Delta G_{\Delta\Psi}$, ΔG_{ATP}) and demand-driven environment. Therefore, future research exploring the link between exerkines and brain mitochondria needs to utilize comprehensive mitochondrial bioenergetics testing to better understand the mechanisms of how exerkines derived from peripheral tissues directly influence mitochondrial bioenergetics in a dynamic range of physiologically relevant conditions in the brain.

References:

Albrecht, E., Norheim, F., Thiede, B., Holen, T., Ohashi, T., Schering, L., Lee, S., Brenmoehl, J., Thomas, S., Drevon, C. A., Erickson, H. P., & Maak, S. (2015). Irisin—A myth rather than an exercise-inducible myokine. *Scientific Reports*, *5*, 8889. https://doi.org/10.1038/srep08889

Bookout, A. L., de Groot, M. H. M., Owen, B. M., Lee, S., Gautron, L., Lawrence, H. L., Ding, X., Elmquist, J. K., Takahashi, J. S., Mangelsdorf, D. J., & Kliewer, S. A. (2013). FGF21 regulates metabolism and circadian behavior by acting on the nervous system. *Nature Medicine*, *19*(9), 1147–1152. https://doi.org/10.1038/nm.3249

Brooks, G. A., Osmond, A. D., Arevalo, J. A., Curl, C. C., Duong, J. J., Horning, M. A., Moreno Santillan, D. D., & Leija, R. G. (2022). Lactate as a major myokine and exerkine. *Nature Reviews. Endocrinology*, *18*(11), 712. https://doi.org/10.1038/s41574-022-00724-0

Camandola, S., & Mattson, M. P. (2017). Brain metabolism in health, aging, and neurodegeneration. *The EMBO Journal*, *36*(11), 1474–1492. https://doi.org/10.15252/embj.201695810

Chen, X.-L., Wang, Y., Peng, W.-W., Zheng, Y.-J., Zhang, T.-N., Wang, P.-J., Huang, J.-D., & Zeng, Q.-Y. (2018). Effects of interleukin-6 and IL-6/AMPK signaling pathway on mitochondrial biogenesis and astrocytes viability under experimental septic condition. *International Immunopharmacology*, *59*, 287–294. https://doi.org/10.1016/j.intimp.2018.04.020

Cheng, A., Wan, R., Yang, J.-L., Kamimura, N., Son, T. G., Ouyang, X., Luo, Y., Okun, E., & Mattson, M. P. (2012). Involvement of PGC-1α in the formation and maintenance of

neuronal dendritic spines. *Nature Communications*, *3*, 1250. https://doi.org/10.1038/ncomms2238

Chow, L. S., Gerszten, R. E., Taylor, J. M., Pedersen, B. K., van Praag, H., Trappe, S., Febbraio, M. A., Galis, Z. S., Gao, Y., Haus, J. M., Lanza, I. R., Lavie, C. J., Lee, C.-H., Lucia, A., Moro, C., Pandey, A., Robbins, J. M., Stanford, K. I., Thackray, A. E., … Snyder, M. P. (2022). Exerkines in health, resilience and disease. *Nature Reviews. Endocrinology*, *18*(5), 273–289. https://doi.org/10.1038/s41574-022-00641-2

Dabke, P., & Das, A. M. (2020). Mechanism of Action of Ketogenic Diet Treatment: Impact of Decanoic Acid and Beta-Hydroxybutyrate on Sirtuins and Energy Metabolism in Hippocampal Murine Neurons. *Nutrients*, *12*(8), 2379. https://doi.org/10.3390/nu12082379

El Hayek, L., Khalifeh, M., Zibara, V., Abi Assaad, R., Emmanuel, N., Karnib, N., El-Ghandour, R., Nasrallah, P., Bilen, M., Ibrahim, P., Younes, J., Abou Haidar, E., Barmo, N., Jabre, V., Stephan, J. S., & Sleiman, S. F. (2019). Lactate Mediates the Effects of Exercise on Learning and Memory through SIRT1-Dependent Activation of Hippocampal Brain-Derived Neurotrophic Factor (BDNF). *The Journal of Neuroscience: The Official Journal of the Society for Neuroscience*, *39*(13), 2369–2382. https://doi.org/10.1523/JNEUROSCI.1661-18.2019

Fang, X., Ma, J., Mu, D., Li, B., Lian, B., & Sun, C. (2020). FGF21 Protects Dopaminergic Neurons in Parkinson's Disease Models Via Repression of Neuroinflammation. *Neurotoxicity Research*, *37*(3), 616–627. https://doi.org/10.1007/s12640-019-00151-6

Febbraio, M. A., & Pedersen, B. K. (2002). Muscle-derived interleukin-6: Mechanisms for activation and possible biological roles. *FASEB Journal: Official Publication of the*

Federation of American Societies for Experimental Biology, *16*(11), 1335–1347. https://doi.org/10.1096/fj.01-0876rev

Fix, D. K., VanderVeen, B. N., Counts, B. R., & Carson, J. A. (2019). Regulation of Skeletal Muscle DRP-1 and FIS-1 Protein Expression by IL-6 Signaling. *Oxidative Medicine and Cellular Longevity*, *2019*, 8908457. https://doi.org/10.1155/2019/8908457

Fonte, C., Smania, N., Pedrinolla, A., Munari, D., Gandolfi, M., Picelli, A., Varalta, V., Benetti, M. V., Brugnera, A., Federico, A., Muti, E., Tamburin, S., Schena, F., & Venturelli, M. (2019). Comparison between physical and cognitive treatment in patients with MCI and Alzheimer's disease. *Aging*, *11*(10), 3138–3155. https://doi.org/10.18632/aging.101970

García-Hermoso, A., Ceballos-Ceballos, R. J. M., Poblete-Aro, C. E., Hackney, A. C., Mota, J., & Ramírez-Vélez, R. (2017). Exercise, adipokines and pediatric obesity: A meta-analysis of randomized controlled trials. *International Journal of Obesity (2005)*, *41*(4), 475–482. https://doi.org/10.1038/ijo.2016.230

Guo, M., Wang, X., Zhao, Y., Yang, Q., Ding, H., Dong, Q., Chen, X., & Cui, M. (2018). Ketogenic Diet Improves Brain Ischemic Tolerance and Inhibits NLRP3 Inflammasome Activation by Preventing Drp1-Mediated Mitochondrial Fission and Endoplasmic Reticulum Stress. *Frontiers in Molecular Neuroscience*, *11*, 86. https://doi.org/10.3389/fnmol.2018.00086

Guo, P., Jin, Z., Wang, J., Sang, A., & Wu, H. (2021). Irisin Rescues Blood-Brain Barrier Permeability following Traumatic Brain Injury and Contributes to the Neuroprotection of Exercise in Traumatic Brain Injury. *Oxidative Medicine and Cellular Longevity*, *2021*, 1118981. https://doi.org/10.1155/2021/1118981

Hasan-Olive, M. M., Lauritzen, K. H., Ali, M., Rasmussen, L. J., Storm-Mathisen, J., & Bergersen, L. H. (2019). A Ketogenic Diet Improves Mitochondrial Biogenesis and Bioenergetics via the PGC1α-SIRT3-UCP2 Axis. *Neurochemical Research*, *44*(1), 22–37. https://doi.org/10.1007/s11064-018-2588-6

Hu, J., Cai, M., Shang, Q., Li, Z., Feng, Y., Liu, B., Xue, X., & Lou, S. (2021). Elevated Lactate by High-Intensity Interval Training Regulates the Hippocampal BDNF Expression and the Mitochondrial Quality Control System. *Frontiers in Physiology*, *12*, 629914. https://doi.org/10.3389/fphys.2021.629914

Islam, M. R., Valaris, S., Young, M. F., Haley, E. B., Luo, R., Bond, S. F., Mazuera, S., Kitchen, R. R., Caldarone, B. J., Bettio, L. E. B., Christie, B. R., Schmider, A. B., Soberman, R. J., Besnard, A., Jedrychowski, M. P., Kim, H., Tu, H., Kim, E., Choi, S. H., … Wrann, C. D. (2021). Exercise hormone irisin is a critical regulator of cognitive function. *Nature Metabolism*, *3*(8), 1058–1070. https://doi.org/10.1038/s42255-021-00438-z

Kang, K., Xu, P., Wang, M., Chunyu, J., Sun, X., Ren, G., Xiao, W., & Li, D. (2020). FGF21 attenuates neurodegeneration through modulating neuroinflammation and oxidant-stress. *Biomedicine & Pharmacotherapy = Biomedecine & Pharmacotherapie*, *129*, 110439. https://doi.org/10.1016/j.biopha.2020.110439

Kokorovic, A., Cheung, G. W. C., Rossetti, L., & Lam, T. K. T. (2009). Hypothalamic sensing of circulating lactate regulates glucose production. *Journal of Cellular and Molecular Medicine*, *13*(11–12), 4403–4408. https://doi.org/10.1111/j.1582-4934.2008.00596.x

Laird, M. D., Clerc, P., Polster, B. M., & Fiskum, G. (2013). Augmentation of normal and glutamate-impaired neuronal respiratory capacity by exogenous alternative biofuels.

Translational Stroke Research, *4*(6), 643–651. https://doi.org/10.1007/s12975-013-0275-0

Liang, J., Wang, C., Zhang, H., Huang, J., Xie, J., & Chen, N. (2021). Exercise-Induced Benefits for Alzheimer's Disease by Stimulating Mitophagy and Improving Mitochondrial Function. *Frontiers in Aging Neuroscience*, *13*, 755665. https://doi.org/10.3389/fnagi.2021.755665

Majrashi, M., Altukri, M., Ramesh, S., Govindarajulu, M., Schwartz, J., Almaghrabi, M., Smith, F., Thomas, T., Suppiramaniam, V., Moore, T., Reed, M., & Dhanasekaran, M. (2021). β-hydroxybutyric acid attenuates oxidative stress and improves markers of mitochondrial function in the HT-22 hippocampal cell line. *Journal of Integrative Neuroscience*, *20*(2), 321–329. https://doi.org/10.31083/j.jin2002031

Mäkelä, J., Tselykh, T. V., Maiorana, F., Eriksson, O., Do, H. T., Mudò, G., Korhonen, L. T., Belluardo, N., & Lindholm, D. (2014). Fibroblast growth factor-21 enhances mitochondrial functions and increases the activity of PGC-1α in human dopaminergic neurons via Sirtuin-1. *SpringerPlus*, *3*, 2. https://doi.org/10.1186/2193-1801-3-2

Markham, A., Cameron, I., Bains, R., Franklin, P., Kiss, J. P., Schwendimann, L., Gressens, P., & Spedding, M. (2012). Brain-derived neurotrophic factor-mediated effects on mitochondrial respiratory coupling and neuroprotection share the same molecular signalling pathways. *The European Journal of Neuroscience*, *35*(3), 366–374. https://doi.org/10.1111/j.1460-9568.2011.07965.x

Markham, A., Cameron, I., Franklin, P., & Spedding, M. (2004). BDNF increases rat brain mitochondrial respiratory coupling at complex I, but not complex II. *The European*

Journal of Neuroscience, *20*(5), 1189–1196. https://doi.org/10.1111/j.1460-9568.2004.03578.x

Marosi, K., Kim, S. W., Moehl, K., Scheibye-Knudsen, M., Cheng, A., Cutler, R., Camandola, S., & Mattson, M. P. (2016). 3-Hydroxybutyrate regulates energy metabolism and induces BDNF expression in cerebral cortical neurons. *Journal of Neurochemistry*, *139*(5), 769–781. https://doi.org/10.1111/jnc.13868

Marosi, K., & Mattson, M. P. (2014). BDNF mediates adaptive brain and body responses to energetic challenges. *Trends in Endocrinology and Metabolism: TEM*, *25*(2), 89–98. https://doi.org/10.1016/j.tem.2013.10.006

Martín-Maestro, P., Gargini, R., Perry, G., Avila, J., & García-Escudero, V. (2016). PARK2 enhancement is able to compensate mitophagy alterations found in sporadic Alzheimer's disease. *Human Molecular Genetics*, *25*(4), 792–806. https://doi.org/10.1093/hmg/ddv616

Matthews, V. B., Aström, M.-B., Chan, M. H. S., Bruce, C. R., Krabbe, K. S., Prelovsek, O., Akerström, T., Yfanti, C., Broholm, C., Mortensen, O. H., Penkowa, M., Hojman, P., Zankari, A., Watt, M. J., Bruunsgaard, H., Pedersen, B. K., & Febbraio, M. A. (2009). Brain-derived neurotrophic factor is produced by skeletal muscle cells in response to contraction and enhances fat oxidation via activation of AMP-activated protein kinase. *Diabetologia*, *52*(7), 1409–1418. https://doi.org/10.1007/s00125-009-1364-1

Mattson, M. P., Moehl, K., Ghena, N., Schmaedick, M., & Cheng, A. (2018). Intermittent metabolic switching, neuroplasticity and brain health. *Nature Reviews. Neuroscience*, *19*(2), 63–80. https://doi.org/10.1038/nrn.2017.156

Park, J., Kim, J., & Mikami, T. (2021). Exercise-Induced Lactate Release Mediates Mitochondrial Biogenesis in the Hippocampus of Mice via Monocarboxylate Transporters. *Frontiers in Physiology*, *12*, 736905. https://doi.org/10.3389/fphys.2021.736905

Pedersen, B. K. (2019). Physical activity and muscle-brain crosstalk. *Nature Reviews. Endocrinology*, *15*(7), 383–392. https://doi.org/10.1038/s41574-019-0174-x

Pedersen, B. K., Steensberg, A., Fischer, C., Keller, C., Keller, P., Plomgaard, P., Febbraio, M., & Saltin, B. (2003). Searching for the exercise factor: Is IL-6 a candidate? *Journal of Muscle Research and Cell Motility*, *24*(2–3), 113–119. https://doi.org/10.1023/a:1026070911202

Raefsky, S. M., & Mattson, M. P. (2017). Adaptive responses of neuronal mitochondria to bioenergetic challenges: Roles in neuroplasticity and disease resistance. *Free Radical Biology & Medicine*, *102*, 203–216. https://doi.org/10.1016/j.freeradbiomed.2016.11.045

Safdar, A., Saleem, A., & Tarnopolsky, M. A. (2016). The potential of endurance exercise-derived exosomes to treat metabolic diseases. *Nature Reviews. Endocrinology*, *12*(9), 504–517. https://doi.org/10.1038/nrendo.2016.76

Sa-Nguanmoo, P., Tanajak, P., Kerdphoo, S., Satjaritanun, P., Wang, X., Liang, G., Li, X., Jiang, C., Pratchayasakul, W., Chattipakorn, N., & Chattipakorn, S. C. (2016). FGF21 improves cognition by restored synaptic plasticity, dendritic spine density, brain mitochondrial function and cell apoptosis in obese-insulin resistant male rats. *Hormones and Behavior*, *85*, 86–95. https://doi.org/10.1016/j.yhbeh.2016.08.006

Schmidt, C. A., Fisher-Wellman, K. H., & Neufer, P. D. (2021). From OCR and ECAR to energy: Perspectives on the design and interpretation of bioenergetics studies. *The*

Journal of Biological Chemistry, *297*(4), 101140. https://doi.org/10.1016/j.jbc.2021.101140

Severinsen, M. C. K., & Pedersen, B. K. (2020). Muscle-Organ Crosstalk: The Emerging Roles of Myokines. *Endocrine Reviews*, *41*(4), 594–609. https://doi.org/10.1210/endrev/bnaa016

Shirazi, R., Palsdottir, V., Collander, J., Anesten, F., Vogel, H., Langlet, F., Jaschke, A., Schürmann, A., Prévot, V., Shao, R., Jansson, J.-O., & Skibicka, K. P. (2013). Glucagon-like peptide 1 receptor induced suppression of food intake, and body weight is mediated by central IL-1 and IL-6. *Proceedings of the National Academy of Sciences of the United States of America*, *110*(40), 16199–16204. https://doi.org/10.1073/pnas.1306799110

Sleiman, S. F., Henry, J., Al-Haddad, R., El Hayek, L., Abou Haidar, E., Stringer, T., Ulja, D., Karuppagounder, S. S., Holson, E. B., Ratan, R. R., Ninan, I., & Chao, M. V. (2016). Exercise promotes the expression of brain derived neurotrophic factor (BDNF) through the action of the ketone body β-hydroxybutyrate. *eLife*, *5*, e15092. https://doi.org/10.7554/eLife.15092

Steensberg, A., van Hall, G., Osada, T., Sacchetti, M., Saltin, B., & Klarlund Pedersen, B. (2000). Production of interleukin-6 in contracting human skeletal muscles can account for the exercise-induced increase in plasma interleukin-6. *The Journal of Physiology*, *529 Pt 1*(Pt 1), 237–242. https://doi.org/10.1111/j.1469-7793.2000.00237.x

Tieu, K., Perier, C., Caspersen, C., Teismann, P., Wu, D.-C., Yan, S.-D., Naini, A., Vila, M., Jackson-Lewis, V., Ramasamy, R., & Przedborski, S. (2003). D-beta-hydroxybutyrate rescues mitochondrial respiration and mitigates features of Parkinson disease. *The Journal of Clinical Investigation*, *112*(6), 892–901. https://doi.org/10.1172/JCI18797

Timper, K., Denson, J. L., Steculorum, S. M., Heilinger, C., Engström-Ruud, L., Wunderlich, C. M., Rose-John, S., Wunderlich, F. T., & Brüning, J. C. (2017). IL-6 Improves Energy and Glucose Homeostasis in Obesity via Enhanced Central IL-6 trans-Signaling. *Cell Reports*, *19*(2), 267–280. https://doi.org/10.1016/j.celrep.2017.03.043

Tu, T., Yin, S., Pang, J., Zhang, X., Zhang, L., Zhang, Y., Xie, Y., Guo, K., Chen, L., Peng, J., & Jiang, Y. (2021). Irisin Contributes to Neuroprotection by Promoting Mitochondrial Biogenesis After Experimental Subarachnoid Hemorrhage. *Frontiers in Aging Neuroscience*, *13*, 640215. https://doi.org/10.3389/fnagi.2021.640215

von Holstein-Rathlou, S., BonDurant, L. D., Peltekian, L., Naber, M. C., Yin, T. C., Claflin, K. E., Urizar, A. I., Madsen, A. N., Ratner, C., Holst, B., Karstoft, K., Vandenbeuch, A., Anderson, C. B., Cassell, M. D., Thompson, A. P., Solomon, T. P., Rahmouni, K., Kinnamon, S. C., Pieper, A. A., … Potthoff, M. J. (2016). FGF21 Mediates Endocrine Control of Simple Sugar Intake and Sweet Taste Preference by the Liver. *Cell Metabolism*, *23*(2), 335–343. https://doi.org/10.1016/j.cmet.2015.12.003

Wang, B., Guo, H., Li, X., Yue, L., Liu, H., Zhao, L., Bai, H., Liu, X., Wu, X., & Qu, Y. (2018). Adiponectin Attenuates Oxygen-Glucose Deprivation-Induced Mitochondrial Oxidative Injury and Apoptosis in Hippocampal HT22 Cells via the JAK2/STAT3 Pathway. *Cell Transplantation*, *27*(12), 1731–1743. https://doi.org/10.1177/0963689718779364

Wang, S., & Pan, J. (2016). Irisin ameliorates depressive-like behaviors in rats by regulating energy metabolism. *Biochemical and Biophysical Research Communications*, *474*(1), 22–28. https://doi.org/10.1016/j.bbrc.2016.04.047

Wrann, C. D., White, J. P., Salogiannnis, J., Laznik-Bogoslavski, D., Wu, J., Ma, D., Lin, J. D., Greenberg, M. E., & Spiegelman, B. M. (2013). Exercise induces hippocampal BDNF

through a PGC-1α/FNDC5 pathway. *Cell Metabolism*, *18*(5), 649–659. https://doi.org/10.1016/j.cmet.2013.09.008

Wu, X., Luo, J., Liu, H., Cui, W., Guo, K., Zhao, L., Bai, H., Guo, W., Guo, H., Feng, D., & Qu, Y. (2020). Recombinant Adiponectin Peptide Ameliorates Brain Injury Following Intracerebral Hemorrhage by Suppressing Astrocyte-Derived Inflammation via the Inhibition of Drp1-Mediated Mitochondrial Fission. *Translational Stroke Research*, *11*(5), 924–939. https://doi.org/10.1007/s12975-019-00768-x

Yau, S. Y., Li, A., Hoo, R. L. C., Ching, Y. P., Christie, B. R., Lee, T. M. C., Xu, A., & So, K.-F. (2014). Physical exercise-induced hippocampal neurogenesis and antidepressant effects are mediated by the adipocyte hormone adiponectin. *Proceedings of the National Academy of Sciences of the United States of America*, *111*(44), 15810–15815. https://doi.org/10.1073/pnas.1415219111

Yu, J., Zheng, J., Lu, J., Sun, Z., Wang, Z., & Zhang, J. (2019). AdipoRon Protects Against Secondary Brain Injury After Intracerebral Hemorrhage via Alleviating Mitochondrial Dysfunction: Possible Involvement of AdipoR1-AMPK-PGC1α Pathway. *Neurochemical Research*, *44*(7), 1678–1689. https://doi.org/10.1007/s11064-019-02794-5

Figure

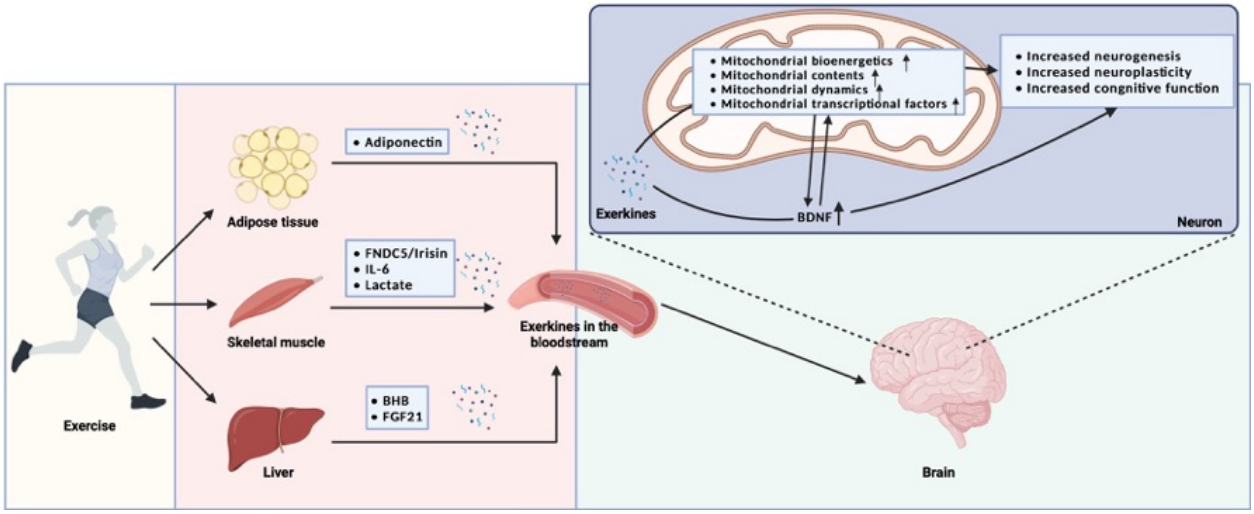

Figure 2.1. Effects of exerkines on brain mitochondrial bioenergetics, contents, dynamics, and transcriptional factors. Exercise-mediated secretion of peripheral factors (exerkines) derived from skeletal muscle (FNDC5/irisin, IL-6, lactate), adipose tissue (adiponectin), and liver (BHB, FGF21) are elevated in the bloodstream. These exerkines pass through the BBB and directly promote aspects of mitochondrial bioenergetics, content, dynamics, and transcriptional factors or indirectly enhance these parameters via elevating BDNF expression in the brain. Improved mitochondrial function results in increased neurogenesis, neuroplasticity, and cognitive function.

Table

Table 2.1. Role of exerkines on mitochondrial function, content, dynamics, and gene regulation.

Exerkine	Impact on Mitochondrial Health			
	Function	Content	Dynamics	Gene Regulation
BDNF	↑ complex I – induced respiration (Markham et al., 2004, 2012), no Δ complex II – induced respiration (Markham et al., 2004)	↑ mtDNA (Cheng et al., 2012) ↑ protein content (e.g., cytochrome c) (Cheng et al., 2012)		↑ transcription factors PGC1α, NFR1, TFAM (Cheng et al., 2012)
IL-6	↑ intercellular ATP levels (Chen et al., 2018)	↑ mtDNA (Chen et al., 2018), ↑ mitochondrial volume (EM) (Chen et al., 2018)		↑ transcription factors PGC1α, NFR1, TFAM (Chen et al., 2018)
Beta-hydroxybutyrate	↑ respiration (Hasan-Olive et al., 2019; Laird et al., 2013; Marosi et al., 2016), ↑ complex II – induced respiration (Tieu et al., 2003), ↑ intracellular ATP levels (M. Guo et al., 2018; Marosi et al., 2016), ↓ ROS production (M. Guo et al., 2018; Majrashi et al., 2021), ↓ ΔΨ (M. Guo et al., 2018), no Δ ΔΨ (Tieu et al., 2003), ↑ NAD:NADH redox (Marosi et al., 2016; Hasan-Olive et al., 2019)	↑ content (via CS activity (Dabke et al., 2016), no Δ mtDNA (Marosi et al., 2016)	↓ Drp1-related fission (M. Guo et al., 2018), ↑ Drp1-related fission (Hasan-Olive et al., 2019), ↓ Mfn1-related fusion (Hasan-Olive et al., 2019)	↑ transcription factors PGC1α (Hasan-Olive et al., 2019), no Δ transcription factors PGC1α, NRF1 and 2, TFAM (Marosi et al., 2016)

	↑ complex I-IV activities (Dabke et al., 2016, Majrashi et al., 2021), ↑ ROS production (Tieu et al., 2003; Marosi et al., 2016)			
Lactate	↑ intracellular ATP levels (Hu et al., 2021)		↓ Drp1-related fission (Hu et al., 2021) ↑ Mfn1/2-related fusion (Hu et al., 2021), no Δ Opa1-related fusion (Hu et al., 2021)	↑ transcription factors PGC1α, NRF2, TFAM (El Hayek et al., 2019; Hu et al., 2021; Park et al., 2021) ↑ mRNA levels of mitochondrial complex genes (Hu et al., 2021)
Adiponectin	↑ intracellular ATP levels (Wu et al., 2020; Yu et al., 2019), ↓ ROS production (B. Wang et al., 2018; Wu et al., 2020; Yu et al., 2019), ↓ ΔΨ (Yu et al., 2019), ↑ ΔΨ (B. Wang et al., 2018; Wu et al., 2020)		↓ Drp1-related fission (Wu et al., 2020), ↑ mitochondrial mass (Yu et al., 2019), ↓ mitochondrial swelling and damaged cristae (B. Wang et al., 2018)	↑ mRNA levels of mitochondrial complex genes (Wu et al., 2020), ↑ transcription factors PGC1α, NRF2, TFAM (Yu et al., 2019)
Irisin	↓ ROS production (P. Guo et al., 2021), ↓ ΔΨ (P. Guo et al., 2021), ↑ complex I, II, IV (S. Wang & Pan, 2016), ↑ intracellular ATP levels ((S. Wang & Pan, 2016)		↓ mitochondrial swelling and vacuolization (Tu et al., 2021)	↑ transcription factors PGC1α, NRF2, TFAM (P. Guo et al., 2021; Tu et al., 2021)
FGF21	↓ ROS production (Sa-Nguanmoo et al., 2016), ↓ ΔΨ (Sa-Nguanmoo et al., 2016), ↑ respiration (Mäkelä et al., 2014), ↑ NAD^+/NADH ratio	no Δ mtDNA (Mäkelä et al., 2014)	no Δ mitochondrial surface area (Mäkelä et al., 2014)	↑ transcription factors PGC1α (Fang et al., 2020; Mäkelä et al., 2014; Sa-Nguanmoo et al., 2016), ↑

	(Mäkelä et al., 2014), ↑ ΔΨ (Fang et al., 2020)			mitochondrial respiratory-related genes and proteins (Fang et al., 2020)

BDNF, brain-derived neurotrophic factor; IL-6, interleukin-6; PGC1α, peroxisome proliferator-activated receptor γ coactivator 1; NRF1 and 2, nuclear respiratory factor 1 and 2; TFAM, transcription factor A; ROS, reactive oxygen species; ATP, adenosine triphosphate; ΔΨ, membrane potential; Drp1, dynamin-related protein 1; Opa1, optic atrophy-1; Mfn 1 and 2, mitofusin-1 and 2; CS, citrate synthase; EM, electron microscope

CHAPTER 3

DIFFERENTIAL EFFECTS OF WESTERN DIET AND TRAUMATIC MUSCLE INJURY ON SKELETAL MUSCLE METABOLIC REGULATION IN MALE AND FEMALE MICE [2]

---

[2] Heo J, Schifino AG, McFaline-Figueroa J, Miller DL, Hoffman JR, Noble EE, Greising SM, Call JA. *Journal of Cachexia, Sarcopenia and Muscle*. 2023 Dec;14(6):2835-2850.

Abstract

This study was designed to develop an understanding of the pathophysiology of traumatic muscle injury in the context of Western diet (WD; high-fat, high-sugar) and obesity. The objective was to interrogate the combination of WD and injury on skeletal muscle mass, contractile and metabolic function.

Male and female C57BL/6J mice were randomized into four groups based on a two-factor study design: 1) injury (uninjured vs. volumetric muscle loss (VML)), and 2) diet (WD vs. normal chow (NC)). Electrophysiology was used to test muscle strength and metabolic function in cohorts of Uninjuried+NC, Uninjured+WD, VML+NC, and VML+WD at 8-wks of intervention.

VML-injured male and female mice both exhibited decrements in muscle mass (-17%, $p<0.001$) and muscle strength (-28%, $p<0.001$); however, VML+WD females had a 28% greater muscle mass compared to VML+NC females ($p=0.034$), a compensatory response not detected in males. VML-injured male and female mice both had lower carbohydrate- and fat-supported muscle mitochondrial respiration (JO_2) and less electron conductance through the electron transport system (ETS); however, male VML-WD had 48% lower carbohydrate-supported JO_2 ($p=0.014$) and 47% less carbohydrate-supported electron conductance ($p=0.026$) compared to male VML+NC, and this diet-injury phenotype was not present in females. ETS electron conductance starts with complex-I and complex-II dehydrogenase enzymes at the inner-mitochondrial membrane, and male VML+WD had 31% less complex-I activity ($p=0.004$) and 43% less complex-II activity ($p=0.005$) compared to male VML+NC. This was a diet-injury phenotype not present in females. Pyruvate dehydrogenase (PDH), β-hydroxyacyl-CoA dehydrogenase, citrate synthase, α-ketoglutarate dehydrogenase, and malate dehydrogenase metabolic enzyme activities were evaluated as potential drivers of impaired JO_2 in the context of diet and injury. There were

notable male and female differential effects in the enzyme activity and post-translational regulation of PDH. PDH enzyme activity was 24% less in VML-injured males, independent of diet ($p<0.001$); but PDH enzyme activity was not influenced by injury in females. PDH enzyme activity is inhibited by phosphorylation at serine-293 by pyruvate dehydrogenase kinase 4 (PDK4). In males, there was greater total PDH, phospho-PDH^{ser293}, and pPDH-to-total PDH ratio in WD mice compared to NC, independent of injury ($p\leq0.041$). In females, PDK4 was 51% greater in WD compared to NC, independent of injury ($p=0.025$) and was complemented by greater phospho-PDH^{ser293} ($p=0.001$).

Males are more susceptible to muscle metabolic dysfunction in the context of combined WD and traumatic injury compared to females, and this may be due to impaired metabolic enzyme functions.

Keywords:

mitochondrial bioenergetics, mitochondrial function, muscle contractility, musculoskeletal injury, metabolic flexibility, sex differences

Introduction

Extremity injuries are estimated at ~ 54% of all combat wounds sustained by injured active-duty U.S. military personnel (Owens et al., 2008). Among the numerous extremity injuries, volumetric muscle loss (VML) injury is a frank and irrecoverable loss of muscle mass due to surgical removal of skeletal muscle or traumatic injury that can occur in both military and general populations (Garg et al., 2015). The VML injury overwhelms the remaining muscle's endogenous regenerative and repair capacity (Corona et al., 2015, 2016), and is characterized by pathological fibrosis (Hoffman et al., 2022), metabolic dysfunction (Dalske et al., 2021; Southern et al., 2019), chronic inflammation (Larouche et al., 2023), and a permanent functional deficit (Mintz et al., 2020). Approximately 77% of military casualties are musculoskeletal injuries, many of which have a component of the VML injury (Cross et al., 2011; Owens et al., 2008).

Obesity has become a major health concern in our society, as well as among active-duty military personnel and veterans. Particularly, in a population of amputees secondary to military traumatic injuries, there was a higher likelihood of developing metabolic syndrome than in the general population (Ejtahed et al., 2017), suggesting that they are more likely to develop secondary comorbidities like type-2 diabetes. Indeed, although clinical evidence is rare, one study reported that 62% of wounded veterans were suffering from metabolic syndrome compared to 27% prevalence in the general population (Ejtahed et al., 2017). According to a recent warrior survey of approximately 19,000 wounded veterans, ~52% of wounded veterans were classified as obese (i.e., BMI >30 kg/m^2) in 2022, an increase from 43% in the 2014 survey (Marx, Mayara Fontes et al., 2022). It implies that their tissue pathology, rehabilitation, and regeneration are likely taking place in the context of obesity and/or poor diets, e.g., high-fat, high-sugar diets. In

contrast to wounded veterans, there is a paucity of clinical evidence regarding the general population and obesity rate following VML injury. Considering that obesity leads to skeletal muscle abnormalities, including perturbed protein turnover (Calonne et al., 2019), disrupted lipid metabolism (Koves et al., 2008), and mitochondrial dysfunction (Heo et al., 2021), prevention and management of obesity following injuries indicate one of the primary challenges for maintaining wounded veterans' and the general population' health.

Skeletal muscle is a critical metabolic tissue, which makes up about ~40% of the body mass and disposes of 80% of the insulin-stimulated glucose uptake in our body, contributing to whole-body metabolism. Notably, mitochondria play a critical role in the metabolic status of the skeletal muscle, regulating energy conversion between glucose and fat oxidation and largely maintaining the free energy for ATP hydrolysis (Gibb's free energy; ΔG_{ATP}) via oxidative phosphorylation (Muoio, 2014). Previously, deleterious impacts on the skeletal muscle (McFaline-Figueroa et al., 2022; Southern et al., 2019) and whole-body metabolism (Dalske et al., 2021) have been demonstrated with VML injury, which may disrupt the metabolic process in the skeletal muscle. For example, following VML injury, impaired mitochondrial respiration (McFaline-Figueroa et al., 2022; Southern et al., 2019), reduced enzyme activities in the electron transport system (ETS) (Aurora et al., 2014), and downregulated *PGC1α* gene and protein expression (Southern et al., 2019) were observed in the remaining muscle. Likewise, VML injury impairs whole-body metabolism, resulting in lower oxidation of carbohydrates during diurnal hours (Dalske et al., 2021).

Western diet (WD), high in saturated fat and sugar, alters skeletal muscle and whole-body metabolism, leading to insulin resistance, obesity, and type-2 diabetes. Recent studies have shown that oxidative capacity was impaired after WD in both *in vitro* (Gasier et al., 2020) and *in*

vivo (Bonnard et al., 2008; Chanseaume et al., 2006) models. For example, decreased mitochondrial respiration (Bonnard et al., 2008; Chanseaume et al., 2006; Gasier et al., 2020), increased reactive oxygen species (Bonnard et al., 2008; Gasier et al., 2020), reduced mitochondrial enzyme activities (Bonnard et al., 2008; Chanseaume et al., 2006; Gasier et al., 2020), ATP production (Chanseaume et al., 2006), abnormal mitochondrial dynamics (Gasier et al., 2020) and structure (Bonnard et al., 2008), were observed, resulting in insulin resistance. Collectively, either VML injury or WD, *per se*, altered mitochondrial function in skeletal muscle, thereby affecting systemic and whole-body metabolism.

In the past decades, there have been substantial efforts to understand the pathophysiology of the remaining muscle after VML injury; however, to date, the studies investigating the pathophysiology of VML in the context of WD on metabolic function have not been elucidated. The objective of this study was to investigate the extent to which WD affects skeletal muscle metabolic and contractile function following VML injury in both male and female mice. Studies were designed to explore the WD and VML injury interactions and to test the hypothesis wherein the excess dietary fuels would exacerbate susceptibility to VML-induced skeletal muscle bioenergetics and contractile dysfunction.

Methods

Animal protocol

All procedures and animal care guidelines were approved and conducted in accordance with the guidelines and regulations of the Institutional Animal Care and Use Committee at the University of Georgia. Procedures were carried out in compliance with the Animal Welfare Act,

and the Implementing Animal Welfare Regulations in compliance with the principles of the Guide for the Care and Use of Laboratory Animals. Male and female C57BL/6J mice that were the offspring of breeding pairs obtained from The Jackson Laboratory (stock: 000664) were used for this study. The mice (N=66, 12 weeks of age) were housed on a 12-hour light–dark cycle at 20-23 °C temperature with *ad libitum* access to water and chow. The mice were randomized into four groups (n=7-10): uninjured normal chow (Uninjured+NC), uninjured plus high-fat, high-sugar diet (Uninjured+WD), VML-injured normal chow control (VML+NC), and VML-injured plus high-fat, high-sugar diet (VML+WD). The WD groups (Uninjured+WD and VML+WD) were supplied 60% of high-fat chow plus 11% of high-fructose corn syrup water immediately following surgery *ad libitum* for 8 weeks. A more thorough description of the experimental design can be found in Supporting Information, ***Data* S1**.

Surgical creation of VML injury

VML injury was performed on the posterior compartment of anesthetized (isoflurane inhalation 1.5-3.0%) mice under aseptic surgical conditions as described previously (McFaline-Figueroa et al., 2022; Raymond-Pope et al., 2023). Mice received buprenorphine (Patterson Veterinary Supply, Inc.; 1.2mg/kg; s. q.) prior to surgery and again at 12- and 24-hours post-surgery for pain management. A single incision was made in the mid-gastrocnemius to expose posterior compartment muscles. A 4-mm biopsy punch was employed to induce VML (male; 24.09±5.58 mg, female; 19.25±3.94 mg) from the center of the plantar flexor muscles (gastrocnemius/plantaris/soleus) complex. The skin incision was closed using 6.0 silk suture (ETHICON, 668G S32), and mice were monitored through recovery.

Intraperitoneal glucose tolerance test (ipGTT)

One week before harvest, an intraperitoneal glucose tolerance test (ipGTT) was conducted following glucose injection (2.0g/kg body weight, i.p.) during the light-cycle in the animal facility. After 6 hours of fasting, blood glucose was evaluated before injection and again at 15, 30, 60, and 120 min after injection.

In vivo plantarflexion muscle function

Peak-isometric torque of hindlimb plantar flexor muscles was assessed *in vivo* as previously described (McFaline-Figueroa et al., 2022) using electrophysiological stimulation of the sciatic nerve and the Model 300C muscle lever system (Aurora Scientific, Aurora, Ontario, Canada). A full *in vivo* protocol can be found in ***Data* S1**.

Mitochondrial respiration

High-resolution oxygen respiration measurement was conducted on gastrocnemius permeabilized fiber bundles using an Oroboros Oxygraph-2K (Oroboros Instruments, Innsbruck, Austria) as previously described (Fisher-Wellman et al., 2018; McFaline-Figueroa et al., 2023) with minor adjustments. Experiments were carried out at 30°C in buffer Z (105 mM K-MES, 30 mM KCl, 1 mM EGTA, 10 mM K2HPO4, 5 mM MgCl, 0.5 mg/mL bovine serum albumin; pH 7.1) with 20 mM creatine monohydrate. To measure mitochondrial respiration (JO_2, or the rate of mitochondrial oxygen consumption) and electron conductance through the electron transport system (ETS) under a physiologically relevant environment, we used a CK clamp system wherein this assay relies on the enzymatic reaction of creatine kinase (CK) and phosphocreatine (PCr) to manipulate the levels of cellular energy demand (Gibbs-free energy; ΔG_{ATP}) (Fisher-Wellman et al., 2018). A full protocol can be found in ***Data* S1**.

Assessment of mitochondrial enzyme activities

Metabolic enzyme activities citrate synthase (CS), β-hydroxyacyl-CoA dehydrogenase (β-HAD), pyruvate dehydrogenase (PDH), malate dehydrogenase (MDH), α-ketoglutarate dehydrogenase (αKGDH), complex-I (CI), and complex-II (CII)] were assessed as previously described (McFaline-Figueroa et al., 2022) and using protocols thoroughly described in ***Data* S1**.

Immunoblotting

Immunoblotting to measure PDH regulatory proteins was conducted according to protocols previously described (Nichenko et al., 2021). A more complete description of the protocol, probes used, and limitations of primary antibody validation is found in ***Data* S1**.

Statistical analysis

All statistical analyses were completed using JMP Pro statistical software (version 16.0.0 SAS Institute, Cary, NC, USA), and figures were created using GraphPad Prism (version 9.4.1, GraphPad Software, San Diego, CA, USA). All data are represented as mean±standard deviation (SD). Group sample size was determined to be a minimal of 6 per group based on the standard deviation of permeabilized fiber bundle mitochondrial respiration using JMP. No animals were statistically excluded from the statistical analysis. The primary statistical test was to determine if the combination of diet and VML injury influenced the remaining muscle's physiology, and in the absence of a diet*injury interaction, if there were any main effects of diet or injury alone. There were detected sex differences in several statistical analyses, thus male and female data are shown independently, but were not statistically compared to one another (i.e., data are not evaluated by a three-way ANOVA with sex as an independent variable). A two-way ANOVA was used to analyze the data with diet and injury as independent variables. Statistical differences are

only reported where significant interactions are present (diet*injury) or in the absence of a significant interaction, when there was a Main Effect of diet or injury. A Tukey's HSD post-hoc test was used to determine group differences when appropriate. An α level of 0.05 was utilized for all analyses. A post-hoc multiple linear regression for variables (e.g., mitochondrial enzyme activities, pyruvate dehydrogenase relative protein content) that contributed to the variability in carbohydrate-supported mitochondrial respiration outcomes (carbohydrate-supported JO_2 and electron conductance) was conducted. All p-values for the main effects (diet and injury, respectively) and interaction effects (diet*injury) are displayed in ***Data* S2**.

Results

An expanded description of results can be found in ***Data* S3**.

Western diet establishes an obesity model in the context of VML injury

Eight weeks of WD significantly increased body mass in both males and females, independent of injury (**Figure 1A,D**; $p < 0.001$, respectively). Adiposity was greater with WD in both males and females (**Figure 1B,E**); however, male and female VML+WD had slightly less fat pad mass compared to VML+NC counterparts (**Figure 1B,E;** $p \leq 0.013$). Males demonstrated impaired glucose metabolism based on ipGTT, independent of injury (**Figure 1C**; $p < 0.001$); whereas only female Uninjured+WD had impaired glucose metabolism compared to Uninjured+NC (**Figure 1F**; $p = 0.016$).

Non-functional compensatory muscle mass adaptation in VML-injured females on WD

VML is defined by a non-recoverable loss of muscle mass and strength, and this was evident in both male and female mice. For example, independent of diet, VML-injured male mice had 17% less absolute gastrocnemius muscle mass (**Figure 2A**; $p < 0.001$), 28% less peak-isometric torque (**Figure 2D**; $p < 0.001$), and 16% less peak-isometric torque normalized to gastrocnemius muscle mass (a marker of muscle quality) (**Figure 2E**; $p = 0.006$). There was a significant interaction between diet and injury in female absolute gastrocnemius muscle mass and gastrocnemius mass normalized to tibia length, such that VML+WD females had 24% greater muscle mass compared to VML+NC females (**Figure 2F**; $p = 0.034$). This finding was mitigated when muscle mass was normalized to body mass (**Figure 2G**). Most importantly, the modest compensatory adaption in absolute gastrocnemius muscle mass in females did not

translate into functional differences in peak-isometric torque nor peak-isometric torque normalized to muscle mass (**Figure 2I,J**). Overall, there was no evidence of a combined effect of diet and injury on skeletal muscle contractile function in males or females.

WD exacerbates carbohydrate-supported mitochondrial respiration (JO_2) after VML injury in males

Mitochondrial oxygen consumption (JO_2) was assessed over a physiological range of ATP re-synthesis demands (**Figure 3A,D,G,J**) using the CK energetic clamp technique previously validated in VML-injured fiber bundles (McFaline-Figueroa et al., 2023). In general, VML injury negatively affected carbohydrate- and fat-supported mitochondrial JO_2 (**Figure 3B,E,H,K**) in agreement with a previous acute VML study (McFaline-Figueroa et al., 2023). This VML-induced phenotype was present in both males and females; however, in male mice there was evidence of a combined effect of diet and injury on carbohydrate-supported mitochondrial function. Notably, maximal JO_2 was 48% lower in VML+WD compared to VML+NC (**Figure 3B**; $p = 0.014$), and electron conductance was 47% less in VML-+WD compared to VML+NC (**Figure 3C**; $p = 0.026$).

For fat substrates, there were no statistically significant interactions between diet and injury in male or female mice ($p \geq 0.487$); however, there were notable independent effects of injury. In males, independent of diet, maximal JO_2 was 44% less in VML-injured compared to uninjured (**Figure 3H**; $p < 0.001$). Independent of diet, electron conductance was 39% less in VML-injured compared to uninjured (**Figure 3I**; $p < 0.001$). In females, there were only main effects of injury. Independent of diet, maximal JO_2 was 44% less in VML-injured compared to

uninjured (**Figure 3K**; $p < 0.001$), and electron conductance was 35% less in VML-injured compared to uninjured (**Figure 3L**; $p = 0.001$).

Impaired PDH activity contributes to lower carbohydrate-supported mitochondrial function after VML injury in males

NADH and $FADH_2$ accumulate from dehydrogenases in Krebs cycle, glycolysis, and β-oxidation. The activities of several metabolic enzymes were analyzed to explore mechanisms of altered carbohydrate- and fat-supported mitochondrial function in the context of diet and/or injury. PDH catalyzes the glycolysis end-product pyruvate into acetyl-CoA for Krebs cycle entry. There was no statistically significant interaction between diet and injury for PDH activity in both sexes (**Figure 4B,C;** $p \geq 0.209$). In males, there was an independent injury effect, showing PDH enzyme activity was ~24% less in VML-injured groups, independent of diet (**Figure 4B**; $p < 0.001$). In females, there was no independent effect of injury (**Figure 4C**).

β-HAD catalyzes the third step of β-oxidation that has a common end-product to PDH, i.e., acetyl-CoA. There was no significant interaction between diet and injury for β-HAD activity for males or females (**Figure 4J,K;** $p \geq 0.051$); however, independent of injury, WD groups had ~28% and ~97% greater β-HAD in males (**Figure 4J**; $p = 0.010$) and females (**Figure 4K**; $p < 0.001$), respectively. The greater β-HAD enzyme activity with WD in males and females is consistent with previous studies (Bruce et al., 2009).

CS catalyzes the first step of Krebs cycle by converting the acetyl-CoA from PDH or β-HAD into citrate. There was no statistically significant interaction between diet and injury for CS activity in males or females (**Figure 4D,E;** $p \geq 0.285$); however, there was an independent effect

of diet in males in which CS activity was 23% greater in WD compared to NC (**Figure 4D**; p = 0.005).

α-KGDH is a key rate-limiting step of Krebs cycle. There was an independent injury effect α-KGDH enzyme activity in males, indicating α-KGDH enzyme activity was ~32% less in VML-injured groups (**Figure 4F**; p = 0.005). In females, there is a significant interaction between diet and injury **(Figure 4G**; p = 0.001). Notably, α-KGDH enzyme activity was 44% lower in VML+NC compared to Uninjured+NC; however, VML+WD group had ~58% greater α-KGDH compared to VML+NC (**Figure 4G**), showing compensatory response in VML-injured females on WD.

Finally, MDH enzyme activity was investigated because it also is a key dehydrogenase in Krebs cycle and because malate is an important substrate for facilitating the shuttling electrons across the mitochondrial membrane via the malate-aspartate shuttle. There was no interaction between diet and injury for MDH activity in males or females (**Figure 4H,I;** $p \geq 0.120$). In females, there was an independent injury effect for MDH enzyme activity, showing that VML-injured groups have ~30% greater MDH activity compared to Uninjured groups (**Figure 4I**; p = 0.022).

Impaired complex-I and complex-II activities in VML-injured male mice on WD

Electron conductance starts with the oxidation of reduced metabolic equivalents (NADH and $FADH_2$) at CI and CII of the ETS. In male mice, there was a significant interaction between diet and injury for CI activity such that activity was 31% less in VML+WD compared to VML+NC (**Figure 5B**; p = 0.004). Similarly, there was a significant interaction for CII enzyme

activity in males, and VML+WD enzyme rates were 43% lower compared to VML+NC (**Figure 5D**; $p = 0.005$). In females, there was no significant interaction between diet and injury for CI nor CII activity (**Figure 5C,E;** $p \geq 0.102$); however, independent of diet, CI activity was 16% greater in VML-injured compared to uninjured (**Figure 5C**; $p < 0.001$).

Diet, but not VML injury, influences PDH inhibitory regulation at serine-293 in males and females

To further interrogate the relationship between PDH activity and carbohydrate-supported mitochondrial function in the context of diet and injury, the post-translational modifications to PDH that can influence its enzymatic function are analyzed. Post-translational phosphorylation (ser293) of PDH is inhibitory and facilitated by PDK4 in skeletal muscle. This inhibitory phosphorylation can be reversed by PDP. In male mice, there was a diet effect, independent of injury, for greater protein content of total PDH (**Figure 6A**; $p = 0.036$), $pPDH^{SER293}$ (**Figure 6B**; $p = 0.003$), and the ratio of pPDH-to-total PDH (**Figure 6C**; $p = 0.041$). However, we did not detect any statistically significant changes in the protein contents of PDK4 or PDP in males (**Figure 6E,F**; $p \geq 0.066$).

In female mice, there was a diet effect, independent of injury, for greater protein content of total PDH and $pPDH^{SER293}$ (**Figure 7A,B**; $p \leq 0.011$), but not the pPDH-to-total PDH ratio. There was a significant interaction between diet and injury for the relative protein content of PDP, with VML+NC and VML+WD all being significantly less than Uninjured+NC (**Figure 7E**; $p = 0.035$). Also, relative PDK4 protein content was 51% higher in WD groups, independent of

injury, in females (**Figure 7F,** $p = 0.025$). Both male and female datasets suggest WD, but not VML injury, is associated with changes in the post-translational states of PDH.

The relationship between carbohydrate metabolism, mitochondrial enzyme activities, and PDH post-translational modifications

Correlation assessment of continuous variables was conducted to better understand the potential contributing factors to carbohydrate-supported metabolism in male and female muscles (**Table 1**). Notably, both male and female JO_2 and conductance was strongly correlated with PDH enzyme activity. Interestingly, male mitochondrial respiration outcomes were not significantly correlated with complex-I or complex-II enzyme activities, despite there being an interaction between diet and injury for these variables. Next, a multiple linear regression model was built using the significant continuous outcomes from **Table 1** for male and female JO_2 and conductance. In males, PDH enzyme activity, total and pPDH protein levels explained 43% of the variability in carbohydrate-supported JO_2 (R^2=0.4311, $p = 0.002$) and 41% of the variability in carbohydrate-supported electron conductance (R^2=0.414, $p = 0.002$). In females, 64% of the variability in carbohydrate-supported JO_2 is explained by enzyme activities (CI, CII, PDH) and protein contents (total PDH, pPDH, PDK4) (R^2=0.640, $p = 0.001$); and ~52% of the variability in carbohydrate-supported electron conductance is explained by enzyme activities (CI, CII, PDH) and protein contents (total PDH, pPDH) (R^2=0.518, $p = 0.007$).

Discussion

Diet and obesity are independently associated with skeletal muscle and mitochondrial pathophysiology, and despite an increasing proportion of the general population and Servicemembers classified as obese, the influence of diet and obesity on the injury progression following a VML injury has not been explored. VML pathophysiology is associated with alteration in whole-body metabolism (Dalske et al., 2021; Raymond-Pope et al., 2023), i.e., there is an overt reduction in whole-body diurnal metabolism primarily driven by decreased carbohydrate oxidation during active hours (i.e., dark cycle) post-VML injury (Dalske et al., 2021). This aligns with findings of lower carbohydrate-supported mitochondrial respiration in permeabilized fiber bundles from VML-injured limbs (McFaline-Figueroa et al., 2023). The current study revealed that WD exacerbated the vulnerability to impaired carbohydrate-supported mitochondrial respiration caused by VML injury, particularly in male mice. Several, non-mutually exclusive mechanisms may contribute to this primary finding.

The proton motive force across the inner-mitochondrial membrane provides the potential energy to drive ATP re-synthesis at complex-V and is established through the proton-pumping complexes-I, -III, and -IV. These complexes pump protons against a concentration gradient and the energy to accomplish this task is provided by the redox reactions of the ETS. Specifically, as the electrons that are removed from NADH and $FADH_2$ (at complex-I and -II, respectively) are pulled through the ETS (i.e., electron conductance) by oxygen nearly 1-volt of reduction potential is generated to power proton movement across the inner-mitochondrial membrane. Tissues with a lower abundance of complex-I and -II proteins have slower ETS electron conductance (e.g., liver, (McLaughlin et al., 2020), and rotenone, which impairs complex-I function, also slows ETS electron conductance. The strongest complementary outcome to our

primary finding that diet and injury worsened JO_2 and conductance is a similar diet-injury interaction in male mice for complex-I and -II enzyme activity indicating that impairment in these enzyme activities contributes in part to impaired myofiber respiration. The framework that poor complex-I/II enzyme rates are associated with less electron conductance and JO_2 is also supported by findings from our female mice, although in females it is in the context of diet, independent of injury.

The mechanism of lower complex-I/II activity is not clear from the current study, but appears to be influenced by the combination of WD and VML injury. For example, complex-I/II activity was not negatively affected by VML injury in the absence of WD in a study of similar duration post-VML injury (Dalske et al., 2021). Moreover, in WD studies independent of VML injury, there is evidence of compensatory increases in complex-I/II mitochondrial respiration (Gonzalez-Armenta et al., 2019; McGowan et al., 2022; Stephenson et al., 2012) with no changes in complex-I/II relative protein content (McGowan et al., 2022) or enzyme activity (Hyatt et al., 2016). However, both WD and VML are independently associated with changes to the cellular environment, such as inflammatory responses (Larouche et al., 2023) and the presence of oxidative and reductive stress (Bonnard et al., 2008; Gortan Cappellari et al., 2016), and the combination of both stressors may be too great for the skeletal muscle to overcome with compensatory responses.

Complexes-I/II are not the only metabolic enzymes associated with causing changes to electron conductance and JO_2, specifically, an inability to convert pyruvate to acetyl-CoA can also slow electron conductance (McLaughlin et al., 2020). PDH plays a pivotal role in regulating glucose oxidation in the mitochondria by converting pyruvate into acetyl-CoA to activate glucose metabolism by entering the Krebs cycle (Patel et al., 2014). UK5099, which inhibits

mitochondrial pyruvate entry, impedes electron conductance (McLaughlin et al., 2020). Mitochondrial pyruvate entry is unclear in this study; however, PDH enzyme activities were negatively affected by VML injury in males.

It is interesting that in all of the Pearson correlation analyses, PDH enzyme activities were associated with JO_2 and conductance whereas complex-I/II enzyme activities were not (males) or were negatively correlated (females). PDH activation is determined through a balance of inhibitory phosphorylation at the serine residues (Ser232, 293, 300) by PDKs (PDK4 in skeletal muscle) and dephosphorylation by PDP (Patel et al., 2014). Unfortunately, our immunoblot analysis of PDH post-translational modification and protein contents of PDK and PDP were inconclusive in regard to a diet-injury interaction for males and females. However, in the context of diet alone, the relationship was clear. Both males and females on WD had greater pPDH protein content and lesser PDH enzyme activity, supporting the regulation of PDH activity by post-translational modification to PDH. Furthermore, the Pearson correlation analysis revealed that in both males and females there was a negative correlation between total and phospho-PDH protein content and mitochondrial respiration outcomes.

PDH activation is also reliant on the availability of numerous co-substrates, such as nicotinamide dinucleotide (NAD+), and in general, the NAD+ pool is important for sustaining glycolysis. For example, the NAD+ pool, required for the oxidation of glyceraldehyde 3-phosphate to 1,3-biphosphoglycerate by glyceraldehyde 3-phosphate dehydrogenase (step 5 of glycolysis), can be maintained by Complex-I oxidation of NADH (noting that electrons are shuttled across the mitochondrial membrane by the malate-aspartate shuttle) or by lactate dehydrogenase that oxidizes NADH while converting pyruvate to lactate. The enzymatic activity experiments for PDH were conducted at a saturation-levels of NAD+. Therefore, we can rule out

NAD+ limitation as a cause of low PDH enzyme rates for our results, but the extent to which electron carrier pools are affected by VML injury *in vivo* is an intriguing unknown.

Another plausible explanation is that fatty-acids not completely metabolized (i.e., incomplete fatty-acid oxidation) lead to PDH enzyme activity inhibition. Koves et al. (Koves et al., 2023) demonstrated that incomplete fatty-acid oxidation is detrimental to pyruvate oxidation, and that restricted PDH activity can reduce fatty-acid oxidation. The conceptual framework proposed by the authors is that a crucial co-factor (i.e., free CoA) required for long-chain fatty-acid oxidation is maintained by reverse flux of pyruvate-mediated acetyl-CoA via the medium-chain ketothiolase (MCK) and that this reverse flux process is permissible in the presence of short-chain carbons. However, the short-chain carbon circuit for proper MCK function is only possible with efficient long-chain fatty acid oxidation, which underscores the significant cooperative relationship that exists between the fat and carbohydrate oxidation pathways.

Our data showed that β-HAD activity (i.e., increased β-oxidation induced by WD) increased, and conversely, the fat-supported mitochondrial JO_2 and conductance were compromised by VML and WD, independently. Consequently, we can surmise incomplete long-chain fatty acids by WD could suppress PDH activity, thereby downregulating the free CoA production via MCK to contribute to incomplete/inefficient fat oxidation. However, there are notable limitations in this study that should be acknowledged regarding this line of reasoning. First, we were unable to analyze the specific substrate levels of acetyl-CoA, NADH, and NAD+, for example, due to tissue availability and therefore cannot comment on the extent to which diet and injury influence incomplete fatty-acid oxidation or the availability of crucial enzymatic co-factors. Second, we assessed PDK4 protein content and not PDK4 enzyme activity, and the latter may have provided deeper insight into PDH enzyme regulation.

In the current study, there were several differential outcomes in males and females. Females, for example, demonstrated some compensatory WD adaptations (e.g., absolute muscle mass), which is consistent with previous studies reporting female protection against high-fat diet-derived obesity (Ingvorsen et al., 2017; McGowan et al., 2022). To date, numerous studies have revealed that females have greater mitochondrial content and mitochondrial biogenesis-related gene responses compared to males; notably, quantifying sex differences was outside the statistical model for our study (Montero et al., 2018; Moriggi et al., 2021). We posit that one of the potential mechanisms may be associated with ovarian hormones because ovarian hormones are known to modulate mitochondrial function and biogenesis (Ikeda et al., 2019). Particularly, 17-β estradiol is the most crucial female sex hormone, and it is believed that increased 17-β estradiol in females activates the mitochondrial bioenergetics (Torres et al., 2018) and lipid metabolism (Roepstorff et al., 2006). For example, compared to males, females have greater intramuscular lipid stores and hormone-dependent lipase activity (Roepstorff et al., 2006), fatty acid-related gene expression, such as a cluster of differentiation-36 and fatty acid binding proteins (Kiens et al., 2004), greater carnitine palmitoyl transferase-1, and CS activity (Maher et al., 2009). Taken together, this difference in mitochondrial quality between males and females may contribute inherently to the differential progression of mitochondrial-relevant pathologies after WD and VML injury. Future studies are necessary to determine the mechanisms by which sex hormones (i.e., ovarian hormones) are directly associated with metabolic function following WD and VML injury.

Conclusions

In conclusion, this study provides novel evidence that the metabolic consequences of VML injury combined with a WD exhibit more pronounced effects in males compared to females. The findings reveal that WD exerts detrimental effects on carbohydrate-supported mitochondrial metabolism in males following VML injury, as evidenced by dysregulation of PDH and a significant decrease in the complex-I/II enzyme activities. However, females demonstrate compensatory responses to the combined effects of injury and diets, suggesting potential protective mechanisms. Given the susceptibility of wounded veterans and individuals with traumatic injuries to metabolic syndrome and its long-term comorbidities, it is crucial to develop pre- and clinical approaches targeting the pathophysiology resulting from the interaction of diets and injury. These insights underscore the importance of addressing the sex-specific metabolic responses and implementing strategies to prevent or treat the harmful impacts of this combined effect.

References

Aurora, A., Garg, K., Corona, B. T., & Walters, T. J. (2014). Physical rehabilitation improves muscle function following volumetric muscle loss injury. *BMC Sports Science, Medicine & Rehabilitation*, *6*(1), 41. https://doi.org/10.1186/2052-1847-6-41

Bonnard, C., Durand, A., Peyrol, S., Chanseaume, E., Chauvin, M.-A., Morio, B., Vidal, H., & Rieusset, J. (2008). Mitochondrial dysfunction results from oxidative stress in the skeletal muscle of diet-induced insulin-resistant mice. *The Journal of Clinical Investigation*, *118*(2), 789–800. https://doi.org/10.1172/JCI32601

Bruce, C. R., Hoy, A. J., Turner, N., Watt, M. J., Allen, T. L., Carpenter, K., Cooney, G. J., Febbraio, M. A., & Kraegen, E. W. (2009). Overexpression of carnitine palmitoyltransferase-1 in skeletal muscle is sufficient to enhance fatty acid oxidation and improve high-fat diet-induced insulin resistance. *Diabetes*, *58*(3), 550–558. https://doi.org/10.2337/db08-1078

Calonne, J., Isacco, L., Miles-Chan, J., Arsenijevic, D., Montani, J.-P., Guillet, C., Boirie, Y., & Dulloo, A. G. (2019). Reduced Skeletal Muscle Protein Turnover and Thyroid Hormone Metabolism in Adaptive Thermogenesis That Facilitates Body Fat Recovery During Weight Regain. *Frontiers in Endocrinology*, *10*, 119. https://doi.org/10.3389/fendo.2019.00119

Chanseaume, E., Malpuech-Brugère, C., Patrac, V., Bielicki, G., Rousset, P., Couturier, K., Salles, J., Renou, J.-P., Boirie, Y., & Morio, B. (2006). Diets high in sugar, fat, and energy induce muscle type-specific adaptations in mitochondrial functions in rats. *The Journal of Nutrition*, *136*(8), 2194–2200. https://doi.org/10.1093/jn/136.8.2194

Corona, B. T., Rivera, J. C., Owens, J. G., Wenke, J. C., & Rathbone, C. R. (2015). Volumetric muscle loss leads to permanent disability following extremity trauma. *Journal of Rehabilitation Research and Development*, *52*(7), 785–792. https://doi.org/10.1682/JRRD.2014.07.0165

Corona, B. T., Wenke, J. C., & Ward, C. L. (2016). Pathophysiology of Volumetric Muscle Loss Injury. *Cells, Tissues, Organs*, *202*(3–4), 180–188. https://doi.org/10.1159/000443925

Cross, J. D., Ficke, J. R., Hsu, J. R., Masini, B. D., & Wenke, J. C. (2011). Battlefield orthopaedic injuries cause the majority of long-term disabilities. *The Journal of the American Academy of Orthopaedic Surgeons*, *19 Suppl 1*, S1-7. https://doi.org/10.5435/00124635-201102001-00002

Dalske, K. A., Raymond-Pope, C. J., McFaline-Figueroa, J., Basten, A. M., Call, J. A., & Greising, S. M. (2021). Independent of physical activity, volumetric muscle loss injury in a murine model impairs whole-body metabolism. *PloS One*, *16*(6), e0253629. https://doi.org/10.1371/journal.pone.0253629

Ejtahed, H.-S., Soroush, M.-R., Hasani-Ranjbar, S., Angoorani, P., Mousavi, B., Masumi, M., Edjtehadi, F., & Soveid, M. (2017). Prevalence of metabolic syndrome and health-related quality of life in war-related bilateral lower limb amputees. *Journal of Diabetes and Metabolic Disorders*, *16*, 17. https://doi.org/10.1186/s40200-017-0298-2

Fisher-Wellman, K. H., Davidson, M. T., Narowski, T. M., Lin, C.-T., Koves, T. R., & Muoio, D. M. (2018). Mitochondrial Diagnostics: A Multiplexed Assay Platform for Comprehensive Assessment of Mitochondrial Energy Fluxes. *Cell Reports*, *24*(13), 3593-3606.e10. https://doi.org/10.1016/j.celrep.2018.08.091

Garg, K., Ward, C. L., Hurtgen, B. J., Wilken, J. M., Stinner, D. J., Wenke, J. C., Owens, J. G., & Corona, B. T. (2015). Volumetric muscle loss: Persistent functional deficits beyond frank loss of tissue. *Journal of Orthopaedic Research: Official Publication of the Orthopaedic Research Society*, *33*(1), 40–46. https://doi.org/10.1002/jor.22730

Gasier, H. G., Dohl, J., Suliman, H. B., Piantadosi, C. A., & Yu, T. (2020). Skeletal muscle mitochondrial fragmentation and impaired bioenergetics from nutrient overload are prevented by carbon monoxide. *American Journal of Physiology. Cell Physiology*, *319*(4), C746–C756. https://doi.org/10.1152/ajpcell.00016.2020

Gonzalez-Armenta, J. L., Gao, Z., Appt, S. E., Vitolins, M. Z., Michalson, K. T., Register, T. C., Shively, C. A., & Molina, A. J. A. (2019). Skeletal Muscle Mitochondrial Respiration Is Elevated in Female Cynomolgus Macaques Fed a Western Compared with a Mediterranean Diet. *The Journal of Nutrition*, *149*(9), 1493–1502. https://doi.org/10.1093/jn/nxz092

Gortan Cappellari, G., Zanetti, M., Semolic, A., Vinci, P., Ruozi, G., Falcione, A., Filigheddu, N., Guarnieri, G., Graziani, A., Giacca, M., & Barazzoni, R. (2016). Unacylated Ghrelin Reduces Skeletal Muscle Reactive Oxygen Species Generation and Inflammation and Prevents High-Fat Diet-Induced Hyperglycemia and Whole-Body Insulin Resistance in Rodents. *Diabetes*, *65*(4), 874–886. https://doi.org/10.2337/db15-1019

Heo, J.-W., No, M.-H., Cho, J., Choi, Y., Cho, E.-J., Park, D.-H., Kim, T.-W., Kim, C.-J., Seo, D. Y., Han, J., Jang, Y. C., Jung, S.-J., Kang, J.-H., & Kwak, H.-B. (2021). Moderate aerobic exercise training ameliorates impairment of mitochondrial function and dynamics in skeletal muscle of high-fat diet-induced obese mice. *FASEB Journal: Official*

Publication of the Federation of American Societies for Experimental Biology, *35*(2), e21340. https://doi.org/10.1096/fj.202002394R

Hoffman, D. B., Raymond-Pope, C. J., Sorensen, J. R., Corona, B. T., & Greising, S. M. (2022). Temporal changes in the muscle extracellular matrix due to volumetric muscle loss injury. *Connective Tissue Research*, *63*(2), 124–137. https://doi.org/10.1080/03008207.2021.1886285

Hyatt, H. W., Kephart, W. C., Holland, A. M., Mumford, P., Mobley, C. B., Lowery, R. P., Roberts, M. D., Wilson, J. M., & Kavazis, A. N. (2016). A Ketogenic Diet in Rodents Elicits Improved Mitochondrial Adaptations in Response to Resistance Exercise Training Compared to an Isocaloric Western Diet. *Frontiers in Physiology*, *7*, 533. https://doi.org/10.3389/fphys.2016.00533

Ikeda, K., Horie-Inoue, K., & Inoue, S. (2019). Functions of estrogen and estrogen receptor signaling on skeletal muscle. *The Journal of Steroid Biochemistry and Molecular Biology*, *191*, 105375. https://doi.org/10.1016/j.jsbmb.2019.105375

Ingvorsen, C., Karp, N. A., & Lelliott, C. J. (2017). The role of sex and body weight on the metabolic effects of high-fat diet in C57BL/6N mice. *Nutrition & Diabetes*, *7*(4), e261. https://doi.org/10.1038/nutd.2017.6

Kiens, B., Roepstorff, C., Glatz, J. F. C., Bonen, A., Schjerling, P., Knudsen, J., & Nielsen, J. N. (2004). Lipid-binding proteins and lipoprotein lipase activity in human skeletal muscle: Influence of physical activity and gender. *Journal of Applied Physiology (Bethesda, Md.: 1985)*, *97*(4), 1209–1218. https://doi.org/10.1152/japplphysiol.01278.2003

Koves, T. R., Ussher, J. R., Noland, R. C., Slentz, D., Mosedale, M., Ilkayeva, O., Bain, J., Stevens, R., Dyck, J. R. B., Newgard, C. B., Lopaschuk, G. D., & Muoio, D. M. (2008).

Mitochondrial overload and incomplete fatty acid oxidation contribute to skeletal muscle insulin resistance. *Cell Metabolism*, *7*(1), 45–56. https://doi.org/10.1016/j.cmet.2007.10.013

Koves, T. R., Zhang, G.-F., Davidson, M. T., Chaves, A. B., Crown, S. B., Johnson, J. M., Slentz, D. H., Grimsrud, P. A., & Muoio, D. M. (2023). Pyruvate-supported flux through medium-chain ketothiolase promotes mitochondrial lipid tolerance in cardiac and skeletal muscles. *Cell Metabolism*, *35*(6), 1038-1056.e8. https://doi.org/10.1016/j.cmet.2023.03.016

Larouche, J. A., Wallace, E. C., Spence, B. D., Buras, E., & Aguilar, C. A. (2023). Spatiotemporal mapping of immune and stem cell dysregulation after volumetric muscle loss. *JCI Insight*, *8*(7), e162835. https://doi.org/10.1172/jci.insight.162835

Larsen, S., Nielsen, J., Hansen, C. N., Nielsen, L. B., Wibrand, F., Stride, N., Schroder, H. D., Boushel, R., Helge, J. W., Dela, F., & Hey-Mogensen, M. (2012). Biomarkers of mitochondrial content in skeletal muscle of healthy young human subjects. *The Journal of Physiology*, *590*(14), 3349–3360. https://doi.org/10.1113/jphysiol.2012.230185

Maher, A. C., Fu, M. H., Isfort, R. J., Varbanov, A. R., Qu, X. A., & Tarnopolsky, M. A. (2009). Sex differences in global mRNA content of human skeletal muscle. *PloS One*, *4*(7), e6335. https://doi.org/10.1371/journal.pone.0006335

Marx, Mayara Fontes, Evans, Sarah, Odom, Elizabeth, Berghammer, Lara, & Chisolm, Nicole. (2022). *Annual warrior survey 2022*. https://www.woundedwarriorproject.org/media/ylwhpx4h/wwp-2022-annual-warrior-survey-full-report.pdf

McFaline-Figueroa, J., Hunda, E. T., Heo, J., Winders, E. A., Greising, S. M., & Call, J. A. (2023). The bioenergetic “CK Clamp” technique detects substrate-specific changes in mitochondrial respiration and membrane potential during early VML injury pathology. *Frontiers in Physiology*, *14*, 1178213. https://doi.org/10.3389/fphys.2023.1178213

McFaline-Figueroa, J., Schifino, A. G., Nichenko, A. S., Lord, M. N., Hunda, E. T., Winders, E. A., Noble, E. E., Greising, S. M., & Call, J. A. (2022). Pharmaceutical Agents for Contractile-Metabolic Dysfunction After Volumetric Muscle Loss. *Tissue Engineering. Part A*, *28*(17–18), 795–806. https://doi.org/10.1089/ten.TEA.2022.0036

McGowan, E. M., Ehrlicher, S. E., Stierwalt, H. D., Robinson, M. M., & Newsom, S. A. (2022). Impact of 4 weeks of western diet and aerobic exercise training on whole-body phenotype and skeletal muscle mitochondrial respiration in male and female mice. *Physiological Reports*, *10*(24), e15543. https://doi.org/10.14814/phy2.15543

McLaughlin, K. L., Hagen, J. T., Coalson, H. S., Nelson, M. A. M., Kew, K. A., Wooten, A. R., & Fisher-Wellman, K. H. (2020). Novel approach to quantify mitochondrial content and intrinsic bioenergetic efficiency across organs. *Scientific Reports*, *10*(1), 17599. https://doi.org/10.1038/s41598-020-74718-1

Mintz, E. L., Passipieri, J. A., Franklin, I. R., Toscano, V. M., Afferton, E. C., Sharma, P. R., & Christ, G. J. (2020). Long-Term Evaluation of Functional Outcomes Following Rat Volumetric Muscle Loss Injury and Repair. *Tissue Engineering. Part A*, *26*(3–4), 140–156. https://doi.org/10.1089/ten.TEA.2019.0126

Montero, D., Madsen, K., Meinild-Lundby, A.-K., Edin, F., & Lundby, C. (2018). Sexual dimorphism of substrate utilization: Differences in skeletal muscle mitochondrial volume

density and function. *Experimental Physiology*, *103*(6), 851–859. https://doi.org/10.1113/EP087007

Moriggi, M., Belloli, S., Barbacini, P., Murtaj, V., Torretta, E., Chaabane, L., Canu, T., Penati, S., Malosio, M. L., Esposito, A., Gelfi, C., Moresco, R. M., & Capitanio, D. (2021). Skeletal Muscle Proteomic Profile Revealed Gender-Related Metabolic Responses in a Diet-Induced Obesity Animal Model. *International Journal of Molecular Sciences*, *22*(9), 4680. https://doi.org/10.3390/ijms22094680

Muoio, D. M. (2014). Metabolic inflexibility: When mitochondrial indecision leads to metabolic gridlock. *Cell*, *159*(6), 1253–1262. https://doi.org/10.1016/j.cell.2014.11.034

Nichenko, A. S., Sorensen, J. R., Southern, W. M., Qualls, A. E., Schifino, A. G., McFaline-Figueroa, J., Blum, J. E., Tehrani, K. F., Yin, H., Mortensen, L. J., Thalacker-Mercer, A. E., Greising, S. M., & Call, J. A. (2021). Lifelong Ulk1-Mediated Autophagy Deficiency in Muscle Induces Mitochondrial Dysfunction and Contractile Weakness. *International Journal of Molecular Sciences*, *22*(4), 1937. https://doi.org/10.3390/ijms22041937

Nichenko, A. S., Southern, W. M., Atuan, M., Luan, J., Peissig, K. B., Foltz, S. J., Beedle, A. M., Warren, G. L., & Call, J. A. (2016). Mitochondrial maintenance via autophagy contributes to functional skeletal muscle regeneration and remodeling. *American Journal of Physiology. Cell Physiology*, *311*(2), C190-200. https://doi.org/10.1152/ajpcell.00066.2016

Owens, B. D., Kragh, J. F., Wenke, J. C., Macaitis, J., Wade, C. E., & Holcomb, J. B. (2008). Combat wounds in operation Iraqi Freedom and operation Enduring Freedom. *The Journal of Trauma*, *64*(2), 295–299. https://doi.org/10.1097/TA.0b013e318163b875

Patel, M. S., Nemeria, N. S., Furey, W., & Jordan, F. (2014). The pyruvate dehydrogenase complexes: Structure-based function and regulation. *The Journal of Biological Chemistry*, *289*(24), 16615–16623. https://doi.org/10.1074/jbc.R114.563148

Raymond-Pope, C. J., Basten, A. M., Bruzina, A. S., McFaline-Figueroa, J., Lillquist, T. J., Call, J. A., & Greising, S. M. (2023). Restricted physical activity after volumetric muscle loss alters whole-body and local muscle metabolism. *The Journal of Physiology*, *601*(4), 743–761. https://doi.org/10.1113/JP283959

Roepstorff, C., Donsmark, M., Thiele, M., Vistisen, B., Stewart, G., Vissing, K., Schjerling, P., Hardie, D. G., Galbo, H., & Kiens, B. (2006). Sex differences in hormone-sensitive lipase expression, activity, and phosphorylation in skeletal muscle at rest and during exercise. *American Journal of Physiology. Endocrinology and Metabolism*, *291*(5), E1106-1114. https://doi.org/10.1152/ajpendo.00097.2006

Schifino, A. G., Cooley, M. A., Zhong, R. X., Heo, J., Hoffman, D. B., Warren, G. L., Greising, S. M., & Call, J. A. (2024). Tibial bone strength is negatively affected by volumetric muscle loss injury to the adjacent muscle in male mice. *Journal of Orthopaedic Research: Official Publication of the Orthopaedic Research Society*, *42*(1), 123–133. https://doi.org/10.1002/jor.25643

Southern, W. M., Nichenko, A. S., Tehrani, K. F., McGranahan, M. J., Krishnan, L., Qualls, A. E., Jenkins, N. T., Mortensen, L. J., Yin, H., Yin, A., Guldberg, R. E., Greising, S. M., & Call, J. A. (2019). PGC-1α overexpression partially rescues impaired oxidative and contractile pathophysiology following volumetric muscle loss injury. *Scientific Reports*, *9*(1), 4079. https://doi.org/10.1038/s41598-019-40606-6

Stephenson, E. J., Camera, D. M., Jenkins, T. A., Kosari, S., Lee, J. S., Hawley, J. A., & Stepto, N. K. (2012). Skeletal muscle respiratory capacity is enhanced in rats consuming an obesogenic Western diet. *American Journal of Physiology. Endocrinology and Metabolism*, *302*(12), E1541-1549. https://doi.org/10.1152/ajpendo.00590.2011

Thome, T., Kumar, R. A., Burke, S. K., Khattri, R. B., Salyers, Z. R., Kelley, R. C., Coleman, M. D., Christou, D. D., Hepple, R. T., Scali, S. T., Ferreira, L. F., & Ryan, T. E. (2020). Impaired muscle mitochondrial energetics is associated with uremic metabolite accumulation in chronic kidney disease. *JCI Insight*, *6*(1), e139826, 139826. https://doi.org/10.1172/jci.insight.139826

Torres, M. J., Kew, K. A., Ryan, T. E., Pennington, E. R., Lin, C.-T., Buddo, K. A., Fix, A. M., Smith, C. A., Gilliam, L. A., Karvinen, S., Lowe, D. A., Spangenburg, E. E., Zeczycki, T. N., Shaikh, S. R., & Neufer, P. D. (2018). 17β-Estradiol Directly Lowers Mitochondrial Membrane Microviscosity and Improves Bioenergetic Function in Skeletal Muscle. *Cell Metabolism*, *27*(1), 167-179.e7. https://doi.org/10.1016/j.cmet.2017.10.003

Table

Table 3.1

Pearson's correlation matrix between investigated continuous variables

	CI	CII	PDH	tPDH	pPDH	pPDH:tPDH	PDP	PDK4
Males								
Carb JO_2	0.196	0.355	**0.613****	**-0.449***	**-0.4924***	-0.308	-0.014	-0.305
Carb conduct	-0.011	0.238	**0.632****	**-0.473***	**-0.442***	-0.250	-0.166	-0.127
CI activity		**0.862***	0.199	0.080	-0.162	-0.396	-0.725	-0.684
CII activity			0.332	0.043	-0.181	-0.408	-0.692	-0.516
PDH activity				-0.214	-0.270	-0.204	0.126	-0.022
PDH					**0.786****	0.209	-0.396	0.059
pPDH						**0.482***	-0.172	0.304
pPDH:PDH							0.194	0.357
PDP								**0.465****
Females								
Carb JO_2	**-0.591****	**-0.713****	**0.436****	**-0.550****	**0.554****	-0.049	0.194	**-0.376***
Carb conduct	**-0.624****	**-0534***	**0.443****	**-0.568****	**-0.494****	-0.002	0.260	-0.271
CI activity		**0.449***	-0.183	0.369	0.384	-0.008	-0.332	**0.484***
CII activity			-0.401	0.280	0.252	-0.122	-0.376	0.199
PDH activity				-0.309	**-0.452***	-0.345	0.329	**-0.378***
PDH					**0.752****	-0.104	**-0.376***	0.126
pPDH						**0.518****	-0.336	**0.550****
pPDH:PDH							0.009	**0.612****
PDP								-0.053

Correlations are reported as Pearson correlation coefficient. *$p<0.05$* are highlighted in bold. CI, complex-I activity; CII, complex-II activity; PDH, pyruvate dehydrogenase activity; tPDH, pyruvate dehydrogenase protein content; pPDH, phospho-pyruvate dehydrogenase protein content; pPDH:tPDH, phospho-to-total pyruvate dehydrogenase protein content ration; PDP, pyruvate dehydrogenase phosphatase protein content; PDK4, pyruvate dehydrogenase kinase 4 protein content. * *$p<0.05$*. ** *$p<0.01$*.

Figure Legends

Figure 3.1. High-fat, high-sugar diet establishes an obesity model in the context of VML injury. Body mass was measured every two weeks. (A) Male bi-weekly body mass and total body mass change from Week 0 to Week 8. (B) Male terminal fat pad mass, and (C) Male glucose tolerance test and calculated AUC (area under the curve). (D) Female bi-weekly body mass and total body mass change from Week 0 to Week 8. (E) Female terminal fat pad mass, and (F) Male glucose tolerance test and calculated AUC (area under the curve). The data shows that obesity was induced by 8 weeks of a high-fat, high-sugar diet. Body mass in WD groups was greater than NC groups in both males (A; $p < 0.001$) and females (D: $p < 0.001$), independent of injury. Blood glucose levels were tested at 7 weeks. The AUC from blood glucose levels has a diet main effect in males (C; $p < 0.001$). In females, there was a diet and injury interaction effect (F; $p = 0.016$) where Uninjured+WD groups have significantly a greater AUC compared to Uninjured+NC. There were diet and injury interaction effects in fat pad mass in both sexes (B; $p = 0.013$ and E; $p = 0.011$, respectively). The study design is two-way ANOVA to determine an interaction effect between diet and injury. For bar graphs, the left two bars represent Uninjured groups (Uninjured+NC and Uninjured+WD), and the right two bars represent VML-injured groups (VML+NC and VML+WD), whereas the NC groups are represented by grey bars (Uninjured+NC and VML+NC), and the WD groups (Uninjured+WD and VML+WD) are represented by either blue (male) or red (female). For linear graphs, the black lines represent data from NC groups (Uninjured+NC and VML+NC), and the color bars represent data from WD groups (Uninjured+WD and VML+WD). The normal lines indicate Uninjured groups (Uninjured+NC and Uninjured+WD), and the dotted lines represent VML-injured groups (VML+NC and VML+WD). Values are mean±SD, and each data point represents a single mouse. Significant differences among groups are denoted (*) when there was a significant interaction between diet and injury. Statistically significant Main Effects are noted in boxes in the absence of a significant interaction. All p-values are shown in **Supplemental Material, *Data* S2**.

Figure 3.2. Skeletal muscle mass and in vivo contractile function in the context of diet and injury. (A) Male gastrocnemius muscle mass, (B) muscle mass normalized to body mass, and (C) muscle mass normalized tibial length. (D) Male peak-isometric torque and peak-isometric torque normalized to muscle mass. (F) Female gastrocnemius muscle mass, (G) muscle mass normalized to body mass, and (H) muscle mass normalized by tibial length. (I) Female peak-isometric torque and (J) peak-isometric torque normalized to muscle mass. Peak-isometric torque was normalized to either muscle mass or body mass to compare muscle contractility while also negating the diet-induced differences in body mass, which may exaggerate the degree of contractile functional loss. The data indicate that VML injury impaired muscle mass and contractile function in both males and females, independent of diet. The study design is two-way ANOVA to find an interaction effect between diet and injury. For bar graphs, the left two bars are Uninjured groups (Uninjured+NC and Uninjured+WD), and the right two bars are VML-injured groups (VML+NC and VML+WD). The NC groups are represented by grey bars (Uninjured+NC and VML+NC), and the WD groups (Uninjured+WD and VML+WD) are represented by either blue (male) or red (female). Values are mean±SD, and each data point represents a single mouse. Significant differences among groups are denoted (*) when there was a significant interaction between diet and injury. Statistically significant Main Effects are noted in boxes in the absence of a significant interaction. All p-values are shown in **Supplemental Material, *Data* S2.**

Figure 3.3. Permeabilized fiber bundle carbohydrate- or fat-supported mitochondrial respiration and electron conductance in the context of diet and injury. The relationship between ATP re-synthesis demand (ΔG_{ATP}) and mitochondrial oxygen consumption (JO_2) normalized to citrate synthase activity (CS) in males (A and G) and females (D and J). Maximal JO_2 (ΔG_{ATP} = -12.87 kcal/mol) and electron conductance in males (B and H) and females (E and K). Electron conductance in males (C and I) and females (F and L). The creatine kinase clamp assay was used to determine mitochondrial maximal JO_2 and electron conductance under physiologically relevant conditions. Electron conductance was calculated by the slope between JO_2 and energy demand (ΔG_{ATP}), allowing for an estimation of mitochondrial sensitivity (respiratory conductance) to altering energetic demands (a steeper slope shows greater sensitivity and kinetics). All data were normalized by citrate synthase activity (an indirect marker of mitochondrial content). The data shows that in males, there was an interaction between diet and injury in carbohydrate-supported mitochondrial respiration and electron conductance (B; $p = 0.014$ and C; $p = 0.026$, respectively) where carbohydrate-mediated mitochondrial respiration and electron conductance were significantly disrupted in VML+WD compared to VML+NC (B,C). In females, there was no significant interaction for maximal JO_2 nor electron conductance; however, there were diet and injury main effects (maximal JO_2; injury, $p = 0.003$ and diet, $p < 0.001$ and electron conductance; injury, $p = 0.004$ and diet, $p < 0.001$). For fat substrates, there is no significant interaction between diet and injury in both males and females. In males, there were diet and injury main effects in both maximal JO_2 (injury; $p < 0.001$ and diet; $p = 0.001$) and electron conductance (injury; $p < 0.001$ and diet; $p = 0.016$). In females, irrespective of diet, there was an injury main effect in both maximal JO_2 ($p < 0.001$) and electron conductance ($p < 0.001$). The study design is two-way ANOVA to find an interaction effect between diet and injury. For bar graphs, the left two bars are Uninjured groups (Uninjured+NC and Uninjured+WD), and the right two bars are VML-injured groups (VML+NC and VML+WD). The NC groups are represented by grey bars (Uninjured+NC and VML+NC), and the WD groups (Uninjured+WD and VML+WD) are shaded by either blue (male) or red (female). For linear graphs, the black lines represent data from NC groups (Uninjured+NC and VML+NC), and the color bars represent data from WD groups (Uninjured+WD and VML+WD). The normal lines indicate Uninjured groups (Uninjured+NC and Uninjured+WD), and the dotted lines represent VML-injured groups (VML+NC and VML+WD). Values are mean±SD, and each data point represents a permeabilized fiber bundle (≥3 per mouse). Significant differences among groups are denoted (*) when there was a significant interaction between diet and injury. Statistically significant Main Effects are noted in boxes in the absence of a significant interaction. All p-values are shown in **Supplemental Material, *Data* S2.**

Figure 3.4. Mitochondrial enzyme kinetics. (A) Cartoon depicting glucose and fat oxidation and matrix dehydrogenase activity. Pyruvate dehydrogenase enzyme activity in males (B) and females (C), respectively. Citrate synthase (CS) enzyme activity in males (D) and females (E), respectively. alpha-ketoglutarate enzyme activity in males (F) and females (G), respectively. Malate dehydrogenase enzyme activity in males (H) and females (I), respectively. β-hydroxyacyl-CoA dehydrogenase (β-HAD) activity in males (J) and females (K), respectively. All enzymatic assays were determined by either a spectrophotometer (CS activity and β-HAD) or spectrofluorometer (PDH, MDH, and αKGDH) and were normalized to CS activity (an indirect marker of mitochondrial content). The data shows that an interaction effect of diet and injury for PDH in both sexes was not shown; however, there were diet (B, $p < 0.001$) and injury (B, $p < 0.001$) main effects in males, and diet (C, $p < 0.001$) main effects in females. For CS activity, WD Groups have a greater CS enzyme activity compared to NC groups (D, $p = 0.005$) in males. The αKGDH enzyme activity was lower in VML-injured groups compared to the Uninjured groups (main effect of injury; F, $p = 0.005$). In females, there was a significant interaction effect in αKGDH enzyme activity (G, $p = 0.005$). Notably, Uninjured+NC had a higher αKGDH compared to VML+NC; however, VML+WD had greater α-KGDH compared to VML+NC (G). For MDH, there is only injury main effect in females, independent of diet (I, $p = 0.022$). The NC groups are represented by grey bars, and the WD groups are shaded by either blue (male) or red (female). In both sexes, β-HAD was greater in WD groups compared to NC groups, irrespective of injury (main effect of diet; male, $p = 0.010$ and $p < 0.001$). The study design is two-way ANOVA to find an interaction effect between diet and injury. For bar graphs, the left two bars are Uninjured groups (Uninjured+NC and Uninjured+WD), and the right two bars are VML-injured groups (VML+NC and VML+WD). The NC groups are represented by grey bars (Uninjured+NC and VML+NC), and the WD groups (Uninjured+WD and VML+WD) are shaded by either blue (male) or red (female). For linear graphs, the black lines represent data from NC groups (Uninjured+NC and VML+NC), and the color bars represent data from WD groups (Uninjured+WD and VML+WD). The normal lines indicate Uninjured groups (Uninjured+NC and Uninjured+WD), and the dotted lines represent VML-injured groups (VML+NC and VML+WD). Values are mean±SD, and each data point represents a single mouse. Significant differences among groups are denoted (*) when there was a significant interaction between diet and injury. Statistically significant Main Effects are noted in boxes in the absence of a significant interaction. All p-values are shown in **Supplemental Material, *Data* S2.**

Figure 3.5. Mitochondrial complex-I and -II enzyme activities. (A) Cartoon depicting electron transport chain. Complex-I (CI) enzyme activity in males (B) and females (C), respectively. Complex-II (CII) enzyme activity in males (D) and females (E), respectively. All enzymatic rates are normalized to citrate synthase activity (CS). Complex-I/II enzyme activities were measured using a spectrophotometer to indirectly monitor the oxidation of NADH to NAD+ by observing the reduction of the colorimetric indicator, 6-dichlorophenolindophenol, at 600 nm of wavelength. The data indicate that there were significant interaction effects in complex-I (B; $p = 0.004$) and II (D; $p = 0.004$) enzyme activity in male mice where the VML+WD had lower complex-I/II activities compared to VML+NC. The study design is two-way ANOVA to find an interaction effect between diet and injury. For bar graphs, the left two bars are Uninjured groups (Uninjured+NC and Uninjured+WD), and the right two bars are VML-injured groups (VML+NC and VML+WD). The NC groups are represented by grey bars (Uninjured+NC and VML+NC), and the WD groups (Uninjured+WD and VML+WD) are shaded by either blue (male) or red (female). For linear graphs, the black lines represent data from NC groups (Uninjured+NC and VML+NC), and the color bars represent data from WD groups (Uninjured+WD and VML+WD). The normal lines indicate Uninjured groups (Uninjured+NC and Uninjured+WD), and the dotted lines represent VML-injured groups (VML+NC and VML+WD). Values are mean±SD, and each data point represents a single mouse. Significant differences among groups are denoted (*****) when there was a significant interaction between diet and injury. Statistically significant Main Effects are noted in boxes in the absence of a significant interaction. All p-values are shown in **Supplemental Material, *Data* S2.**

Figure. 3.6. Immunoblot analysis of PDH, PDK4, and PDP protein content in males. **(**A) Total pyruvate dehydrogenase (PDH) protein content, (B) phospho-PDH^{SER293} protein content, and (C) the ratio of phospho-to-total PDH protein content. (D) Representative immunoblots and total protein for total-PDH and phospho-PDH ^{SER293} analysis. (E) Pyruvate dehydrogenase phosphatase (PDP) protein content and pyruvate dehydrogenase kinase 4 (PDK4) protein content (F). (G) Representative immunoblots and total protein for PDP and PDK4 analysis. All immunoblots were normalized to total protein in the lane of the transferred PVDF membrane. The data shows that WD influenced PDH regulation, independent of injury, in males. For all PDH data, there were diet main effects, independent of injury (A; $p = 0.036$, B; $p = 0.003$, and C; $p = 0.041$, respectively). There is no group difference in PDP and PDK4 protein content. The study design is two-way ANOVA to find an interaction effect between diet and injury. For bar graphs, the left two bars are Uninjured groups (Uninjured+NC and Uninjured+WD), and the right two bars are VML-injured groups (VML+NC and VML+WD). The NC groups are represented by grey bars (Uninjured+NC and VML+NC), and the WD groups (Uninjured+WD and VML+WD) are represented by blue color. Values are mean±SD, and each data point represents a single mouse. Statistically significant Main Effects are noted in boxes in the absence of a significant interaction. All p-values are shown in **Supplemental Material, *Data* S2.**

Figure 3.7. Immunoblot analysis of PDH, PDK4, and PDP protein content in females. **(**A) Total pyruvate dehydrogenase (PDH) protein content, (B) phospho-PDH^{SER293} protein content, and (C) the ratio of phospho-to-total PDH protein content. (D) Representative immunoblots and total protein for total-PDH and phospho-PDH ^{SER293} analysis. (E) Pyruvate dehydrogenase phosphatase (PDP) protein content and pyruvate dehydrogenase kinase 4 protein content (F). (G) Representative immunoblots and total protein for PDP and PDK4 analysis. All immunoblots were normalized to total protein in the lane of the transferred PVDF membrane. The WD groups had a greater total-PDH and phospho-PDH protein content, regardless of injury, (A; $p = 0.011$ and B;$p = 0.001$, respectively). For PDP protein content, there was an interaction effect of diet and injury, showing that Uninjured+NC had a greater PDP compared to VML+NC and VML+WD groups. The PDK was higher in WD groups compared to NC groups (main effect of diet; $p = 0.025$), regardless of injury. For bar graphs, the left two bars are Uninjured groups (Uninjured+NC and Uninjured+WD), and the right two bars are VML-injured groups (VML+NC and VML+WD). The NC groups are represented by grey bars (Uninjured+NC and VML+NC), and the WD groups (Uninjured+WD and VML+WD) are shaded by red color. Values are mean±SD, and each data point represents a single mouse. Significant differences among groups are denoted (*) when there was a significant interaction between diet and injury. Statistically significant Main Effects are noted in boxes in the absence of a significant interaction. All p-values are shown in **Supplemental Material, *Data* S2.**

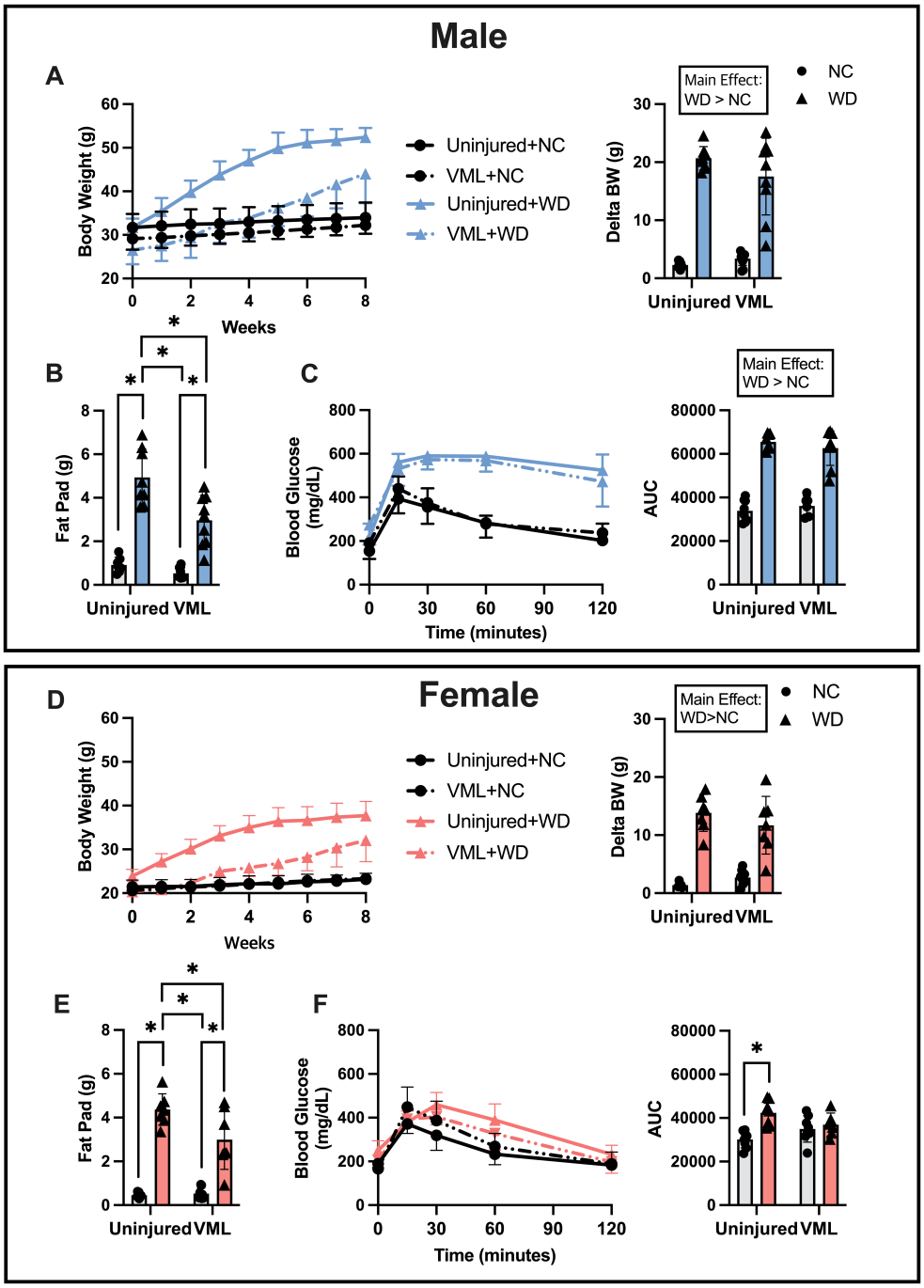
Male
A
Body Weight (g)
Weeks
Uninjured+NC
VML+NC
Uninjured+WD
VML+WD
Main Effect:
WD > NC
NC
WD
Delta BW (g)
Uninjured VML
B
Fat Pad (g)
Uninjured VML
C
Blood Glucose (mg/dL)
Time (minutes)
Main Effect:
WD > NC
AUC
Uninjured VML
Female
D
Body Weight (g)
Weeks
Uninjured+NC
VML+NC
Uninjured+WD
VML+WD
Main Effect:
WD>NC
NC
WD
Delta BW (g)
Uninjured VML
E
Fat Pad (g)
Uninjured VML
F
Blood Glucose (mg/dL)
Time (minutes)
AUC
Uninjured VML

Figure 3.1

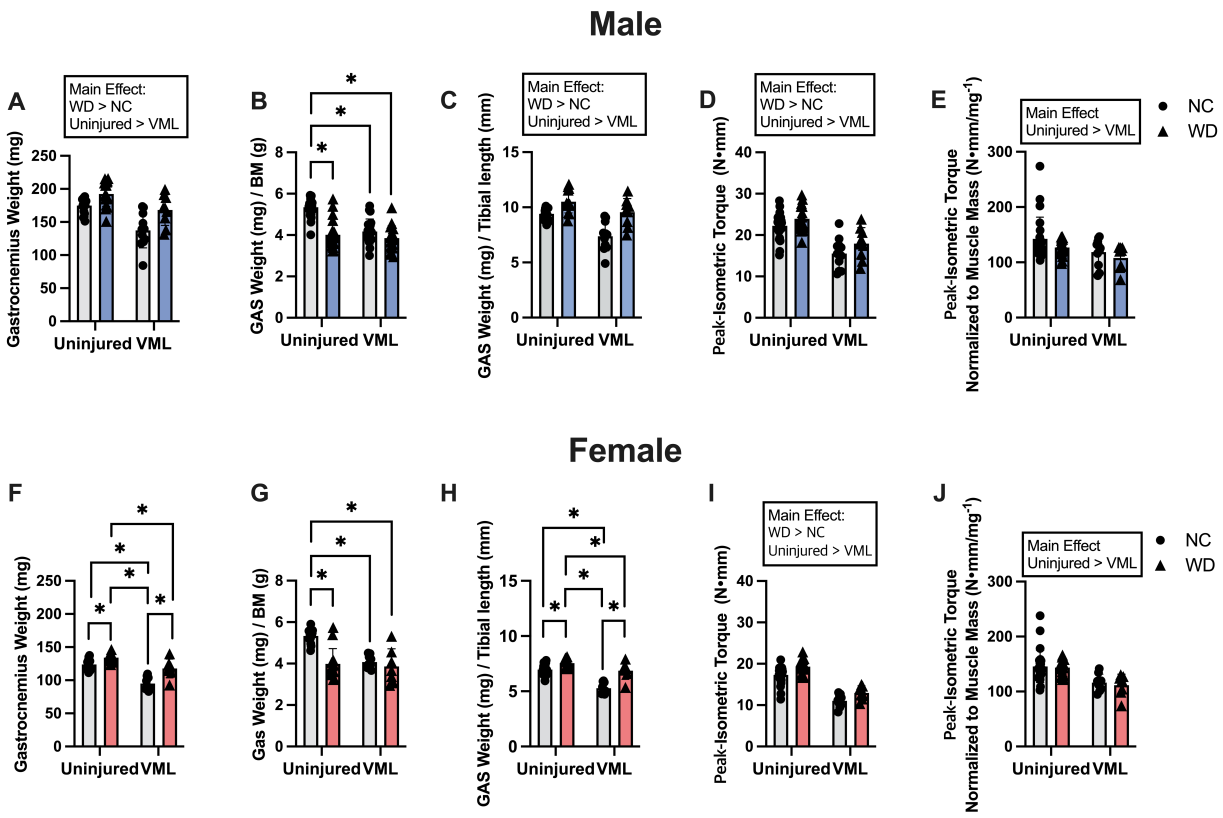
Male
A
Main Effect:
WD > NC
Uninjured > VML
Gastrocnemius Weight (mg)
Uninjured VML
B
GAS Weight (mg) / BM (g)
Uninjured VML
C
Main Effect:
WD > NC
Uninjured > VML
GAS Weight (mg) / Tibial length (mm)
Uninjured VML
D
Main Effect:
WD > NC
Uninjured > VML
Peak-Isometric Torque (N•mm)
Uninjured VML
E
Main Effect
Uninjured > VML
NC
WD
Peak-Isometric Torque
Normalized to Muscle Mass (N•mm/mg-1)
Uninjured VML
Female
F
Gastrocnemius Weight (mg)
Uninjured VML
G
Gas Weight (mg) / BM (g)
Uninjured VML
H
GAS Weight (mg) / Tibial length (mm)
Uninjured VML
I
Main Effect:
WD > NC
Uninjured > VML
Peak-Isometric Torque (N•mm)
Uninjured VML
J
Main Effect
Uninjured > VML
NC
WD
Peak-Isometric Torque
Normalized to Muscle Mass (N•mm/mg-1)
Uninjured VML

Figure 3.2

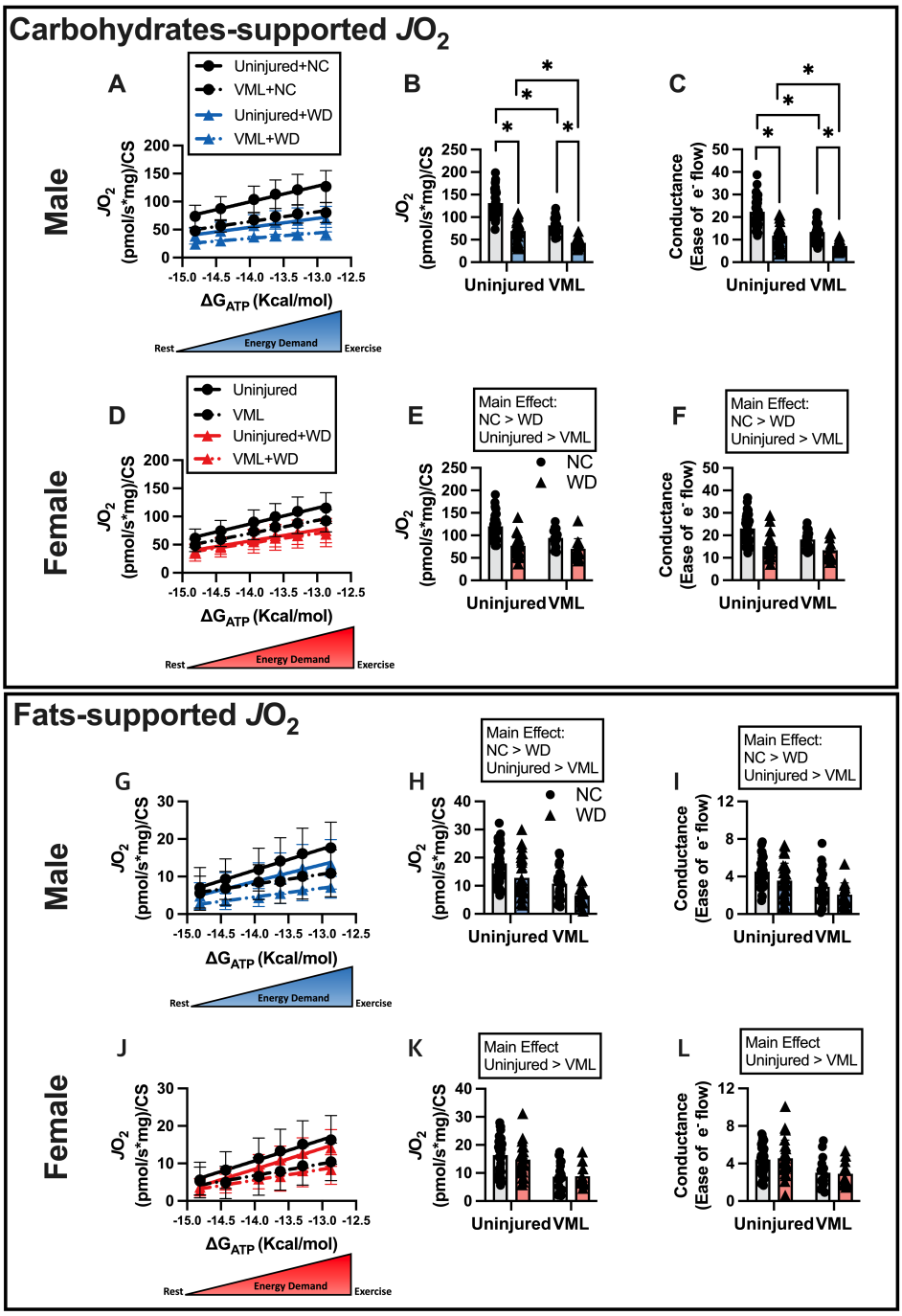
Carbohydrates-supported JO2
Male
Female
A
B
C
D
E
F
Uninjured+NC
VML+NC
Uninjured+WD
VML+WD
Uninjured
VML
JO2 (pmol/s*mg)/CS
ΔGATP (Kcal/mol)
-15.0 -14.5 -14.0 -13.5 -13.0 -12.5
Rest
Energy Demand
Exercise
Conductance (Ease of e- flow)
Uninjured VML
Main Effect:
NC > WD
Uninjured > VML
NC
WD
Fats-supported JO2
G
H
I
J
K
L
Main Effect
Uninjured > VML

Figure 3.3

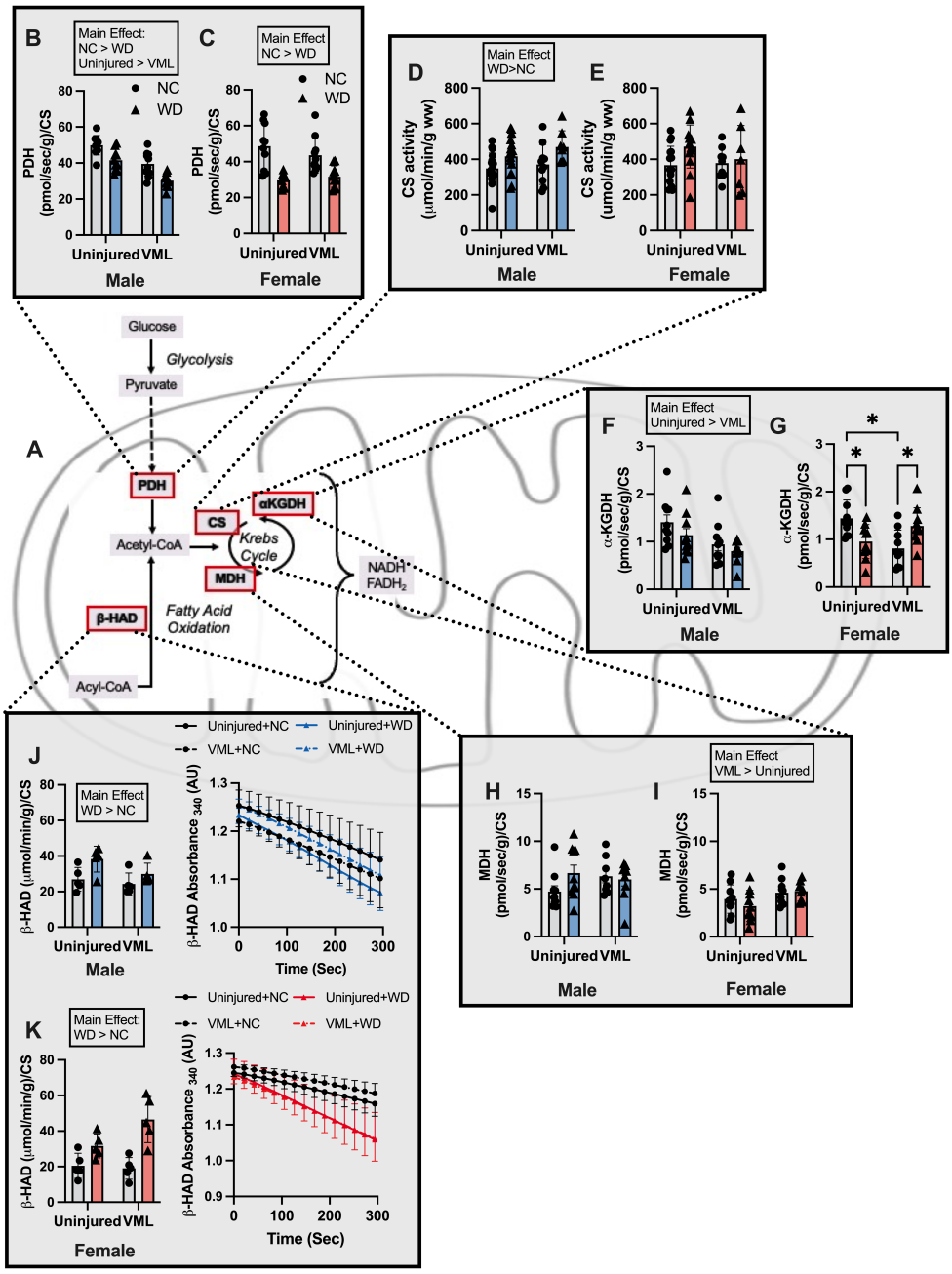
B
Main Effect:
NC > WD
Uninjured > VML
NC
WD
PDH (pmol/sec/g)/CS
Uninjured VML
Male
C
Main Effect
NC > WD
Female
D
Main Effect
WD>NC
CS activity (µmol/min/g ww)
E
A
Glucose
Glycolysis
Pyruvate
PDH
CS
αKGDH
Acetyl-CoA
Krebs Cycle
MDH
NADH
FADH2
β-HAD
Fatty Acid Oxidation
Acyl-CoA
F
Main Effect
Uninjured > VML
α-KGDH (pmol/sec/g)/CS
G
J
Main Effect
WD > NC
β-HAD (µmol/min/g)/CS
Uninjured+NC
Uninjured+WD
VML+NC
VML+WD
β-HAD Absorbance 340 (AU)
Time (Sec)
K
Main Effect:
WD > NC
H
MDH (pmol/sec/g)/CS
I
Main Effect
VML > Uninjured

Figure 3.4

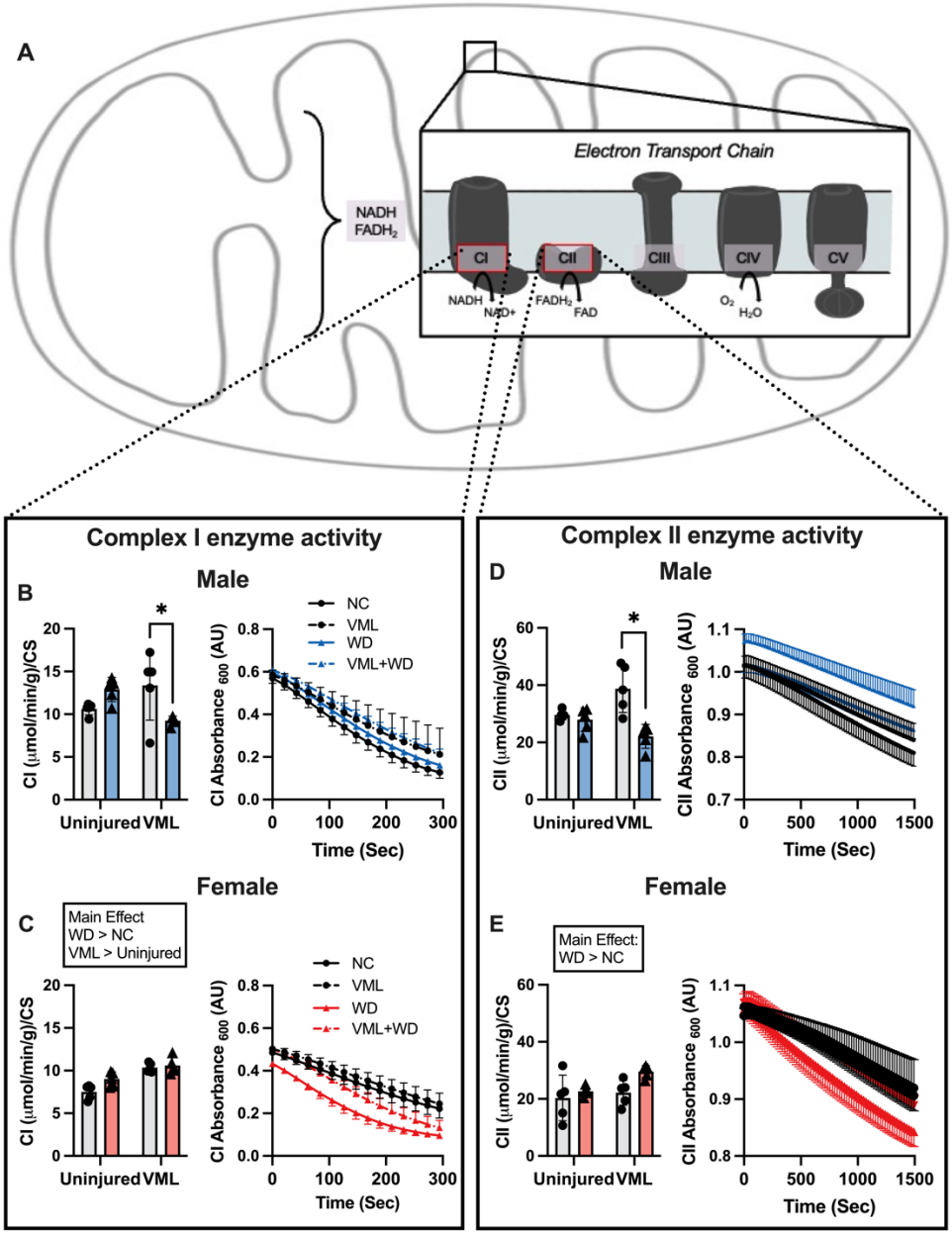
A
Electron Transport Chain
NADH
FADH2
CI
CII
CIII
CIV
CV
NADH
NAD+
FADH2
FAD
O2
H2O
Complex I enzyme activity
Male
B
CI (µmol/min/g)/CS
CI Absorbance 600 (AU)
Uninjured
VML
Time (Sec)
NC
VML
WD
VML+WD
Female
C
Main Effect
WD > NC
VML > Uninjured
Complex II enzyme activity
Male
D
CII (µmol/min/g)/CS
CII Absorbance 600 (AU)
Female
E
Main Effect:
WD > NC

Figure 3.5

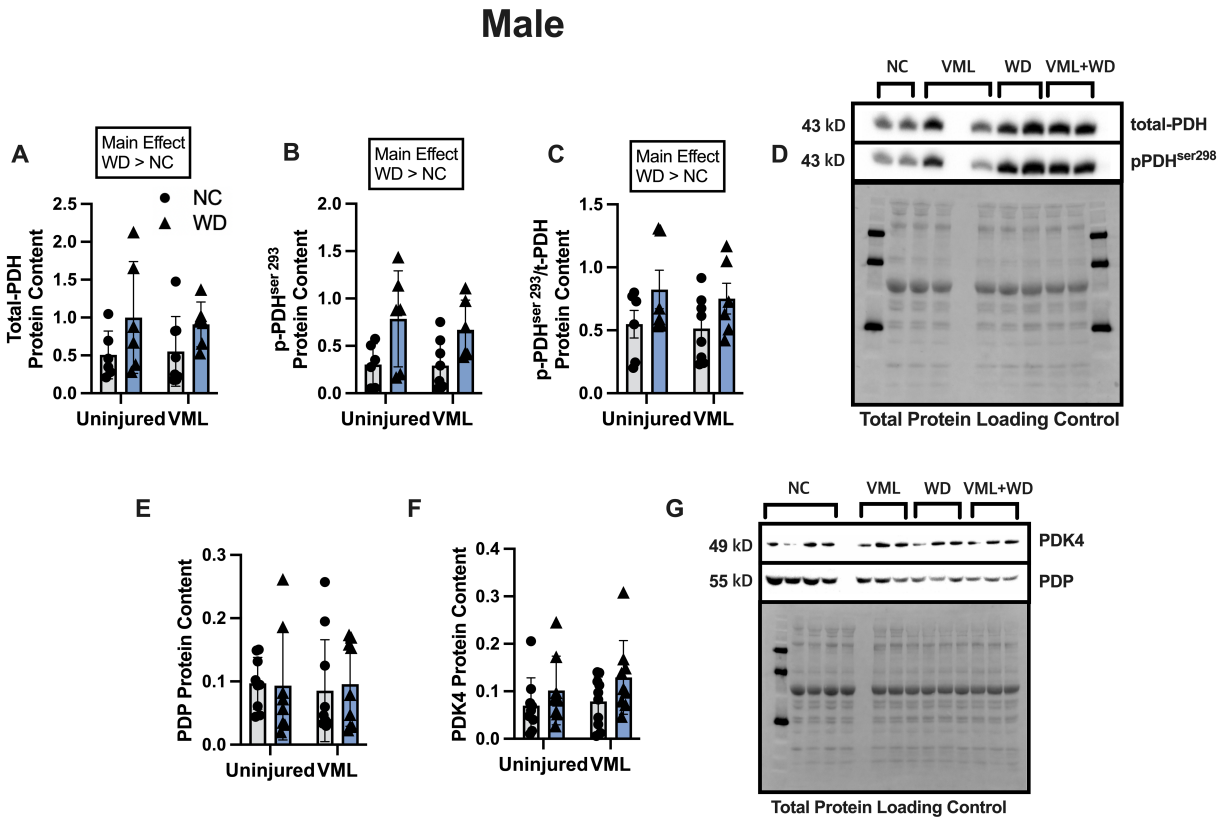
Male
A
Main Effect
WD > NC
NC
WD
Total-PDH
Protein Content
Uninjured
VML
B
Main Effect
WD > NC
p-PDH ser 293
Protein Content
Uninjured
VML
C
Main Effect
WD > NC
p-PDH ser 293/t-PDH
Protein Content
Uninjured
VML
D
NC
VML
WD
VML+WD
43 kD
total-PDH
43 kD
pPDH ser298
Total Protein Loading Control
E
PDP Protein Content
Uninjured
VML
F
PDK4 Protein Content
Uninjured
VML
G
NC
VML
WD
VML+WD
49 kD
PDK4
55 kD
PDP
Total Protein Loading Control

Figure 3.6

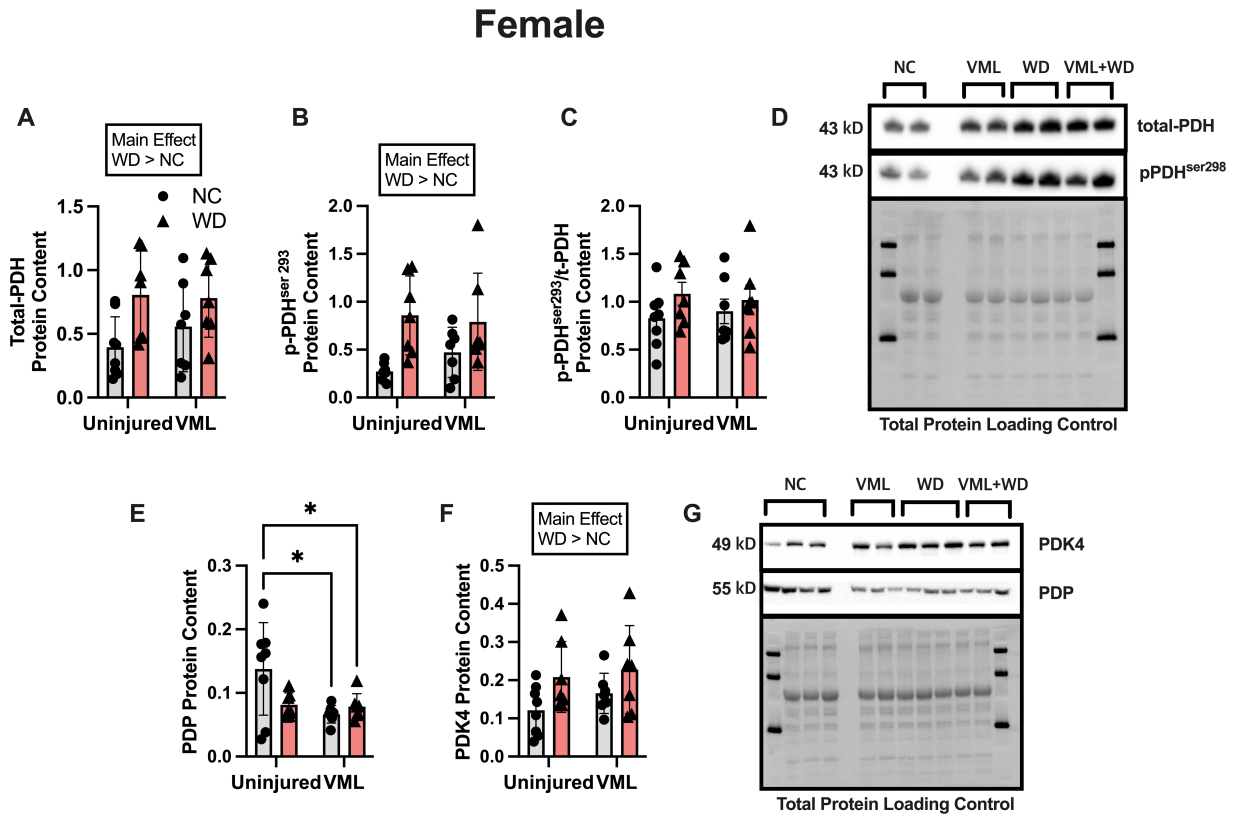
Female
A
Main Effect
WD > NC
NC
WD
Total-PDH
Protein Content
Uninjured
VML
B
Main Effect
WD > NC
p-PDH ser 293
Protein Content
C
p-PDH ser293/t-PDH
Protein Content
D
NC
VML
WD
VML+WD
43 kD
total-PDH
43 kD
pPDH ser298
Total Protein Loading Control
E
PDP Protein Content
F
Main Effect
WD > NC
PDK4 Protein Content
G
49 kD
PDK4
55 kD
PDP
Total Protein Loading Control

Figure 3.7

Supplemental Materials

Supplemental Material, *Data* S1

Methods

Experimental design

The mice were randomized into four groups (n=7-10): uninjured normal chow (Uninjured+NC), uninjured plus high-fat, high-sugar diet (Uninjured+WD), VML-injured normal chow control (VML+NC), and VML-injured plus high-fat, high-sugar diet (VML+WD). VML injured mice underwent unilateral VML injury to the posterior compartment of the left hindlimb. The WD groups (Uninjured+WD and VML+WD) were supplied 60% of high-fat chow plus 11% of high-fructose corn syrup water immediately following surgery *ad libitum* for 8 weeks. At the 7 weeks, fasting blood glucose levels were evaluated. Terminally, 8 weeks post-randomization, morphological measurement (body weight, fat pad, and muscle mass), *in vivo* muscle function (plantar flexor peak-isometric strength), metabolic function (carbohydrate- and fat-mediated mitochondrial oxygen consumption), enzyme kinetic assays (pyruvate dehydrogenase; PDH, beta-hydroxy acyl CoA dehydrogenase; β-HAD, malate dehydrogenase; MDH, alpha-ketoglutarate dehydrogenase; α-KGDH, complex-I, and complex-II), and immunoblotting (PDH regulations) were assessed.

Muscle and Fat pads dissection

After conducting *in vivo* muscle function tests, mice were humanely euthanized using CO_2 inhalation followed by cervical dislocation. The gastrocnemius muscle was then extracted and

weighed. It was subsequently prepared for mitochondrial respiration testing, homogenized for enzyme kinetic assays, and rapidly frozen in liquid nitrogen for additional analyses. After the muscle dissection, anterior, inguinal, and visceral fat pads were collected and measured.

In vivo plantarflexion muscle function

Peak-isometric torque of hindlimb plantar flexor muscles (gastrocnemius/plantaris/soleus) was assessed *in vivo* as previously described (McFaline-Figueroa et al., 2022; Schifino et al., 2024). Briefly, mice were anesthetized using 1.5-3.0% inhaled isoflurane at an oxygen flow rate of 0.4L/min. Both limbs were depilated and aseptically prepared before the peroneal nerve was severed to avoid recruitment of the dorsiflexor muscles. The sciatic nerve was stimulated using platinum-iridium needle electrodes (Model E2-12; Grass Technologies, West Warwick, RI) to obtain isolated contraction of the hindlimb plantar flexors. Peak-isometric torque was determined as the greatest torque assessed during a 250-ms stimulation utilizing 1-ms square-wave pulses at a frequency of 120 Hz and increasing amperage 0.6 to 3.0 mA (Model 701C; Aurora Scientific, Aurora, Ontario, Canada) on the body temperature-controlled platform (37°C). Peak-isometric torque was normalized to either muscle mass or body mass to compare muscle contractility while also negating the diet-induced differences in body mass, which may exaggerate the degree of contractile functional loss.

Mitochondrial respiration

High-resolution oxygen respiration measurement was conducted on gastrocnemius permeabilized fiber bundles using an Oroboros Oxygraph-2K (Oroboros Instruments, Innsbruck, Austria) as

previously described (Fisher-Wellman et al., 2018; McFaline-Figueroa et al., 2023) with minor adjustments. Experiments were carried out at 30°C in buffer Z (105 mM K-MES, 30 mM KCl, 1 mM EGTA, 10 mM K2HPO4, 5 mM MgCl, 0.5 mg/mL bovine serum albumin; pH 7.1) with 20 mM creatine monohydrate. To measure mitochondrial respiration (JO_2) and electron conductance through the electron transport system (ETS) under a physiologically relevant environment, we used a CK clamp system wherein this assay relies on the enzymatic reaction of creatine kinase (CK) and phosphocreatine (PCr) to manipulate the levels of cellular energy demand (Gibbs-free energy; ΔG_{ATP}) (Fisher-Wellman et al., 2018). For the experiment, permeabilized fiber bundles from gastrocnemius muscle energized using either carbohydrate (10 mM glutamate, 5 mM malate, and 10 mM succinate) or fat (40 μM palmitoyl-carnitine and 5 mM malate) substrates with 20 U/mL CK and 5 mM ATP to mimic near exercise conditions (maximal JO_2), followed by sequential PCr titrations (1, 1, 2, 3, 9, 15 mM) to reduce ΔG_{ATP} to resting conditions. The rates were normalized to the wet weight of tissue loaded into each respiration chamber and citrate synthase (CS) activity to account for differences in the mitochondrial content (Larsen et al., 2012).

Assessment of mitochondrial enzyme activities

Mitochondrial enzyme activities, citrate synthase (CS) and complex-I/II enzyme activities, were determined using a spectrophotometer (Molecular Devices, San Jose, CA, USA) with a protocol from McFaline-Figueroa. et al (McFaline-Figueroa et al., 2022). Mitochondrial content was assessed by CS activity as previously described (Southern et al., 2019). Complex-I activity was assessed in 50 mM potassium phosphate buffer, 3 mg/mL BSA, 0.4 μM antimycin A, 240 μM

potassium cyanide, 50 μM decyl-ubiquinone, and 80 μM 2, 6- dichlorophenolindophenol (DCPIP). The oxidation of NADH was measured via the reduction of DCPIP at 600 nm. Complex-II activity was determined in a buffer (10 mM KH_2PO_4, 2 mM EDTA, 1 mg/mL BSA at pH 7.8 and added with 200 μM ATP, 10 mM succinate, and 80 μM DCPIP. Following incubating the buffer for 10 minutes at 37C, the assay was initiated by adding oxidized 80 μM decyl-ubiquinone, and reduction of DCPIP followed at 600 nm. β-hydroxyacyl-CoA dehydrogenase (β-HAD) activity was determined by incubating homogenate in a buffer containing 100 mM triethanolamine, 451 μM β-nicotinamide adenine dinucleotide and 5 mM ethylenediaminetetraacetic acid (EDTA), as previously described (Nichenko et al., 2016). The dehydrogenase activities of pyruvate (PDH), alpha-ketoglutarate (αKGDH), and malate (MDH) were measured using a spectrofluorometer (FluoroMax Plus-C; Horiba Instruments Inc., Irvine, CA, USA) in the 50 mM phosphate buffer with 10 mM $CaCl_2$, 200 mM $MgCl_2$, 2 mM Rotenone, 8 mM NAD+, 100 mM coenzyme A, and 300 mM thiamine pyrophosphate. This buffer was supplemented with the respective substrate, 10 mM alpha-ketoglutarate, 10 mM pyruvate, or 5 mM malate. All enzyme activities were normalized to mitochondrial content (CS enzyme activity).

Immunoblotting

For relative protein content analysis, the protein concentration of muscle homogenates was determined by analyzing absorbance at 562 nm via a Spectrophotometer. 20 □g of total protein was loaded and separated by SDS-PAGE, transferred to a PVDF membrane, and immunoblotted as described previously (Nichenko et al., 2021). For pyruvate dehydrogenase-related protein

levels analysis, PVDF membranes were probed for the proteins at a dilution of 1:1000: Total pyruvate dehydrogenase (tPDH, RRID:AB_2162928), phospho-pyruvate dehydrogenase (ser293) (pPDH, RRID:AB_2799014), pyruvate dehydrogenase phosphatase (PDP, RRID:AB_2938792), pyruvate dehydrogenase kinase-4 (PDK4, RRID:AB_1625831). Although the antibodies used in the study were not robustly validated by negative controls (e.g., PDK4 knockout), providing these data enhances and supports the transparency and reliability of the research findings. Immunoblots were normalized to total protein in the lane and quantified via Bio-Rad Laboratories Image Lab software (Hercules, CA, USA).

Supplemental Material, *Data* S2

Supplemental Table 3.1. All statistical results of variables.

Variables		Sex	Main effect of injury	Main effect of diet	Interaction (Injury X Diet)
Delta Body weight	Figure 1B	Male	$p = 0.404$	$\mathbf{p < 0.001}$	$p = 0.087$
	Figure 1G	Female	$p = 0.732$	$\mathbf{p < 0.001}$	$p = 0.157$
Blood Glucose levels AUC	Figure 1D	Male	$p = 0.874$	$\mathbf{p < 0.001}$	$p = 0.232$
	Figure 1I	Female	$p = 0.876$	$p = 0.001$	$\mathbf{p = 0.016}$
Fat pad mass	Figure 1E	Male	$p = 0.001$	$p < 0.001$	$\mathbf{p = 0.013}$
	Figure 1J	Female	$p = 0.021$	$p < 0.001$	$\mathbf{p = 0.011}$
Absolute GAS mass	Figure 2A	Male	$\mathbf{p < 0.001}$	$\mathbf{p < 0.001}$	$p = 0.219$
	Figure 2F	Female	$p < 0.001$	$p < 0.001$	$\mathbf{p = 0.034}$
GAS weight/Body Mass	Figure 2B	Male	$p < 0.001$	$p < 0.001$	$\mathbf{p < 0.001}$
	Figure 2G	Female	$p = 0.001$	$p < 0.001$	$\mathbf{p = 0.002}$
GAS weight/Tibial Length	Figure 2C	Male	$\mathbf{p < 0.001}$	$\mathbf{p < 0.001}$	$p = 0.081$
	Figure 2H	Female	$p < 0.001$	$p < 0.001$	$\mathbf{p = 0.003}$
Peak-Isometric Torque	Figure 2D	Male	$\mathbf{p < 0.001}$	$\mathbf{p = 0.024}$	$p = 0.673$
	Figure 2I	Female	$\mathbf{p < 0.001}$	$\mathbf{p = 0.001}$	$p = 0.901$
Peak-Isometric Torque/Muscle Mass	Figure 2E	Male	$\mathbf{p = 0.006}$	$p = 0.080$	$p = 0.755$
	Figure 2J	Female	$\mathbf{p < 0.001}$	$p = 0.578$	$p = 0.836$
Carbohydrate-mediated JO_2	Figure 3B	Male	$p < 0.001$	$p < 0.001$	$\mathbf{p = 0.014}$
	Figure 3E	Female	$\mathbf{p = 0.003}$	$\mathbf{p < 0.001}$	$p = 0.083$
Carbohydrates Conductance	Figure 3C	Male	$p < 0.001$	$p < 0.001$	$\mathbf{p = 0.026}$
	Figure 3F	Female	$\mathbf{p = 0.004}$	$\mathbf{p < 0.001}$	$p = 0.178$
Fat-mediated JO_2	Figure 3H	Male	$\mathbf{p < 0.001}$	$\mathbf{p = 0.001}$	$p = 0.761$
	Figure 3K	Female	$\mathbf{p < 0.001}$	$p = 0.561$	$p = 0.487$
Fat Conductance	Figure 3I	Male	$\mathbf{p < 0.001}$	$\mathbf{p = 0.016}$	$p = 0.859$
	Figure 3L	Female	$\mathbf{p = 0.001}$	$p = 0.970$	$p = 0.743$
PDH Enzyme Activity	Figure 4B	Male	$\mathbf{p < 0.001}$	$\mathbf{p < 0.001}$	$p = 0.776$
	Figure 4C	Female	$p = 0.599$	$\mathbf{p < 0.001}$	$p = 0.209$
	Figure 4D	Male	$p = 0.191$	$\mathbf{p = 0.005}$	$p = 0.598$

CS Enzyme Activity	Figure 4E	Female	$p = 0.440$	$p = 0.099$	$p = 0.285$
α-KGDH Enzyme Activity	Figure 4F	Male	$\mathbf{p = 0.005}$	$p = 0.123$	$p = 0.624$
	Figure 4G	Female	$p = 0.209$	$p = 0.953$	$\mathbf{p = 0.001}$
MDH Enzyme Activity	Figure 4H	Male	$p = 0.517$	$p = 0.277$	$p = 0.120$
	Figure 4I	Female	$\mathbf{p = 0.022}$	$p = 0.538$	$p = 0.344$
β-HAD Enzyme Activity	Figure 4J	Male	$p = 0.080$	$\mathbf{p = 0.010}$	$p = 0.344$
	Figure 4K	Female	$p = 0.103$	$\mathbf{p < 0.001}$	$p = 0.051$
Complex-I Enzyme Activity	Figure 5B	Male	$p = 0.645$	$p = 0.359$	$\mathbf{p = 0.004}$
	Figure 5C	Female	$\mathbf{p < 0.001}$	$\mathbf{p = 0.028}$	$p = 0.102$
Complex-II Enzyme Activity	Figure 5D	Male	$p = 0.477$	$p = 0.001$	$\mathbf{p = 0.005}$
	Figure 5E	Female	$p = 0.054$	$\mathbf{p = 0.035}$	$p = 0.246$
Total-PDH Protein Contents	Figure 6A	Male	$p = 0.911$	$\mathbf{p = 0.036}$	$p = 0.723$
	Figure 7A	Female	$p = 0.561$	$\mathbf{p = 0.011}$	$p = 0.426$
Phospho-PDH Protein Contents	Figure 6B	Male	$p = 0.638$	$\mathbf{p = 0.003}$	$p = 0.697$
	Figure 7B	Female	$p = 0.611$	$\mathbf{p = 0.001}$	$p = 0.309$
p-PDH/t-PDH Relative Value	Figure 6C	Male	$p = 0.654$	$\mathbf{p = 0.041}$	$p = 0.878$
	Figure 7C	Female	$p = 0.972$	$p = 0.156$	$p = 0.600$
PDP Protein Contents	Figure 6E	Male	$p = 0.850$	$p = 0.887$	$p = 0.767$
	Figure 7E	Female	$p = 0.023$	$p = 0.161$	$\mathbf{p = 0.035}$
PDK4 Protein Contents	Figure 6F	Male	$p = 0.414$	$p = 0.066$	$p = 0.672$
	Figure 7F	Female	$p = 0.320$	$\mathbf{p = 0.025}$	$p = 0.692$

GAS, gastrocnemius; PDH, pyruvate dehydrogenase; CS, citrate synthase; α-KGDH, alpha-ketoglutarate dehydrogenase; MDH, malate dehydrogenase; β-HAD, beta-hydroxyacyl-CoA dehydrogenase; PDP, pyruvate dehydrogenase phosphatase; PDK4, pyruvate dehydrogenase kinase 4.

Supplemental Material, *Data* S3

Results

Western diet establishes an obesity model in the context of VML injury

Eight weeks of WD significantly increased body mass in both males and females, independent of injury (**Figure 1A,B,F,G**), and males on WD had worse blood glucose regulation as blood glucose AUC was 83% greater, independent of injury (**Figure 1D**). In females, there was a significant interaction between diet and injury (**Figure 1I**), and the AUC was higher to ~40% in Uninjured+WD compared to Uninjured+NC, but there was no significant difference between VML+NC and VML+WD. There was a significant interaction between diet and injury in fat pad mass for both males (**Figure 1E**) and females (**Figure 1F**), as the Uninjured+WD and VML+WD groups had higher fat pad mass than the Uninjured+NC and VML+NC groups. These results collectively indicate that it is possible to establish an obesity model in the context of a VML-injury with eight weeks of WD.

Non-functional compensatory muscle mass adaptation in VML-injured females on WD

VML is defined by a non-recoverable loss of muscle mass and function, and this was evident in both male and female mice. Independent of diet, VML-injured male mice had 17% less absolute gastrocnemius muscle mass (**Figure 2A**), 28% less peak-isometric torque (**Figure 2D**), and 16% less peak-isometric torque normalized to gastrocnemius muscle mass (a marker of muscle quality) (**Figure 2E**). There was a significant interaction between diet and injury for muscle mass normalized to body mass in which Uninjured+WD, VML+NC, and VML+WD were all significantly less than Uninjured+NC (**Figure 2B**). Peak-isometric torque and normalized peak-

isometric torque were also significantly less in VML-injured females compared to uninjured controls, independent of diet (**Figure 2I and J**). There was a significant interaction between diet and injury in absolute gastrocnemius muscle mass, and interestingly, VML+WD females had 24% greater muscle mass compared to VML+NC females (**Figure 2F**). This finding was mitigated when muscle mass was normalized to body mass (**Figure 2G**). Overall, there was no evidence of a combined effect of diet and injury on skeletal muscle contractile function in males or females.

WD exacerbates carbohydrate-supported mitochondrial respiration after VML injury in males

Mitochondrial respiration was assessed over a physiological range of ATP re-synthesis demands using the CK energetic clamp technique (Fisher-Wellman et al., 2018; Koves et al., 2023; Thome et al., 2020) previously validated in VML-injured fiber bundles (McFaline-Figueroa et al., 2023). Briefly, extramitochondrial ATP-free energy (ΔG_{ATP}) was energetically clamped between maximal ATP demand (ΔG_{ATP} = -12.87 kcal/mol) and minimal demand (ΔG_{ATP} =-14.81kcal/mol) by leveraging the enzymatic activity of CK and titrating in PCr (**Figure 3A and D**). Moreover, the slope of the linear line between JO_2 and ΔG_{ATP} (dotted lines, **Figures 3A and D**) was used to calculate the electron conductance, which indicates how dynamically mitochondria can adapt to changing energy demands. All maximal JO_2 and electron conductance were normalized to CS activity, a marker of the mitochondrial content (Larsen et al., 2012).

In male mice, there was evidence of a combined effect of diet and injury on mitochondrial function. There was a significant interaction between diet and injury for both maximal JO_2 (**Figure 3B**) and electron conductance (**Figure 3B**) when mitochondria were

saturated with carbohydrate-mediated carbon fuels. Notably, maximal JO_2 was 48% lower in VML+WD compared to VML+NC (**Figure 3B**), and electron conductance was 47% less in VML-+WD compared to VML+NC (**Figure 3C**).

There was no interaction between diet and injury for maximal JO_2 nor electron conductance in females; however, there was evidence of injury and diet independently having a negative effect on mitochondrial function. Independent of diet, maximal JO_2 was 17% less in VML-injured compared to uninjured (**Figure 3E**); and independent of injury, maximal JO_2 was 32% less in WD compared to NC (**Figure 3E**). Independent of diet, electron conductance was 18% less in VML-injured compared to uninjured (**Figure 3F**); and independent of injury, electron conductance was 31% less in WD compared to NC (**Figure 3F**).

Skeletal muscle is a dynamic tissue that can readily transition between metabolizing carbohydrates and fats. For fat substrates, there were no statistically significant interactions between diet and injury in male or female mice; however, there were notable independent effects of diet or injury. In males, independent of diet, maximal JO_2 was 44% less in VML-injured compared to uninjured (**Figure 3H**); and independent of injury, maximal JO_2 was 33% less in WD compared to NC (**Figure 3H**). Independent of diet, electron conductance was 39% less in VML-injured compared to uninjured (**Figure 3I**); and independent of injury, electron conductance was 24% less in WD compared to NC (**Figure 3I**). In females, there were only main effects of injury. Independent of diet, maximal JO_2 was 44% less in VML-injured compared to uninjured (**Figure 3K**), and electron conductance was 35% less in VML-injured compared to uninjured (**Figure 3L**).

Impaired complex-I and complex-II activities in VML-injured male mice on WD

In male mice, there was a significant interaction between diet and injury for complex-I activity and activity was 31% less in VML+WD compared to VML+NC (**Figure 5B**). Similarly, there was a significant interaction (**Figure 5D**) for complex-II enzyme activity in males, and VML+WD enzyme rates were 43% lower compared to VML+NC (**Figure 5D**; $p = 0.020$). In females, there was no significant interaction between diet and injury of complex-I nor complex-II activity; however, there were independent diet and injury main effects. Independent of injury, complex-I enzyme activity was 10% greater in WD compared to NC groups and independent of diet, complex-I activity was 16% greater in VML-injured compared to uninjured (**Figure 5C**). Complex-II enzyme activity was ~22% higher in WD groups compared to NC groups, independent of injury (**Figure 5E**).

CHAPTER 4

ACUTE MITOCHONDRIAL REACTIVE OXYGEN SPECIES EMISSIONS DRIVE MITOCHONDRIAL DYSFUNCTION AFTER TRAUMATIC MUSCLE INJURY IN MALE MICE [3]

---

[3] Junwon Heo, David L. Miller, Jessica R. Hoffman, Emma Oberholtzer, Kateyln Castelli, Genevieve Sparagna, Kelsey Fisher-Wellman, Sarah M. Greising, Jarrod A. Call

Submitted to *Redox Biology*, March 7th 2025

Abstract

Volumetric muscle loss (VML) injury results in irreversible muscle loss, impaired regeneration, and mitochondrial dysfunction that is characterized by hyperpolarized membrane potential, reduced respiration, and excessive reactive oxygen species (ROS) emission. This study investigated mitochondrial bioenergetics, ROS emissions, and antioxidant buffering capacity (AoxBC) in a murine VML model and evaluated SS-31, a mitochondrial-targeted antioxidant, as a therapeutic intervention. VML injury impaired mitochondrial bioenergetics, increased ROS, and reduced AoxBC. However, SS-31 improved mitochondrial bioenergetic efficiency, reduced ROS, and enhanced AoxBC but had a limited impact on muscle function (i.e., muscle mass and contractile function). In addition, while SS-31 partially enhanced metabolic adaptation to rehabilitation, it did not significantly improve contractile function, suggesting that oxidative stress would not be the primary driver of poor muscle adaptation post-VML. Future studies are needed to explore specific mechanisms and optimize the therapeutic strategies in remaining muscle following VML injury.

Keywords

Traumatic Injury, Metabolism, Mitochondrial Bioenergetic, Reactive Oxygen Species, Antioxidants, Rehabilitation

List of Abbreviations

VML: Volumetric Muscle Loss, JO_2: Mitochondrial Respiration, JH_2O_2: Hydrogen Peroxide, ROS: Reactive Oxygen Species, ADP: Adenosine Diphosphate, ATP: Adenosine Triphosphate AoxBC: Antioxidant Buffering Capacity, $\Delta\psi m$: Mitochondrial Membrane Potential, Δp: Proton Motive Force, NADPH: Nicotinamide adenine dinucleotide phosphate, ETC: Electron Transport Chain,

1. Introduction

Volumetric muscle loss (VML) injury results in a permeant loss in muscle mass and contractile strength. The injury overwhelms the remaining muscle's endogenous regenerative and repair capacity and is characterized by altered peripheral nerve innervation, pathological fibrosis, and chronic inflammation. There are no standards for rehabilitation following VML injury leaving patients on a trajectory toward limb amputation and lifelong disability. Efforts to establish evidence-based rehabilitation protocols have failed in part due to the remaining muscle tissue being resistant to rehabilitation because of a decreased capability to adapt.

The lack of adaptive capability of the remaining muscle after a VML injury is multifaceted as there are nerve, vascular, and cellular conditions to consider. One such cellular condition is a population of dysfunctional mitochondria within the remaining muscle tissue. Specifically, the remaining muscle after VML injury is marked by alterations in mitochondrial respiration (JO_2) and network organization (Heo et al., 2023; McFaline-Figueroa et al., 2022; Southern et al., 2019), mitochondrial membrane potential ($\Delta\psi m$) (McFaline-Figueroa et al., 2023), and mitochondrial enzyme activities (Heo et al., 2023; McFaline-Figueroa et al., 2022; Southern et al., 2019). Importantly, genetic and pharmaceutical approaches to rescue the oxidative capacity of the remaining muscle after VML injury have yielded associated improvements in contractile strength (McFaline-Figueroa et al., 2022; Raymond-Pope et al., 2023; Southern et al., 2019), suggesting a connection between mitochondrial function and the overall quality of the muscle tissue.

A cellular mechanism that may link mitochondrial function to muscle quality in the context of VML is the production and buffering of reactive oxygen species (ROS). Mitochondrial ROS production in skeletal muscle is linked to $\Delta\psi m$. When $\Delta\psi m$ is

hyperpolarized (i.e., more negative) in concert with a reduced ATP re-synthesis capacity (a phenomenon detected in VML-injured myofibers) (Brand & Nicholls, 2011), the high proton motive force (Δp) equilibrates with an elevated NADH/NAD, FADH2/FAD, and coenzyme-Q redox state. This shift increases the reduction potential of various redox centers, promoting electron leak to O_2 and enhancing ROS production at complexes I and III (Murphy, 2009). Mitochondrial ROS production is buffered in part by antioxidant proteins (e.g., thioredoxin and glutathione reductase) that contribute to a redox circuit in the mitochondrial matrix (Smith et al., 2020). When mitochondrial ROS emissions are too high due to greater ROS production, impaired buffering capacity, or a combination of the two, the associated oxidative stress can damage proteins and lipids critical to cellular function (Murphy, 2009).

To date, there is only circumstantial evidence of mitochondrial ROS-associated oxidative stress following VML injury, primarily a hyperpolarized Δψm with lower JO_2 (McFaline-Figueroa et al., 2023). The primary objective of the current study was to investigate the role of mitochondrial ROS in the context of VML injury and to test the primary hypothesis that VML injury is associated with greater mitochondrial ROS production. The secondary objective of the current study was to test the extent to which improving the antioxidant buffering capacity (AoxBC) of VML-injured muscle yields greater adaptive capability of the remaining muscle. The secondary hypothesis was that an exogenous antioxidant agent would improve the contractile and metabolic function of the remaining muscle after rehabilitation. To test these hypotheses, this study leveraged an established murine multi-muscle VML injury model (Heo et al., 2023; McFaline-Figueroa et al., 2023; Raymond-Pope et al., 2023; Schifino et al., 2024) and electrophysiological approaches to detect mitochondrial complex-specific ROS production, AoxBC, mitochondrial bioenergetics, skeletal muscle contractile strength and adaptation to

combined voluntary wheel running (i.e., rehabilitation) and exogenous antioxidant treatment. By addressing these goals, this study provides insights into the therapeutic potential of mitochondrial-targeted interventions combined with physical rehabilitation to augment muscle physiology following traumatic injury.

2. Materials and methods

2.1 Animals and ethical approval

Adult male, age 12 weeks, C57BL/6J mice were purchased from Jackson Laboratories (Stock #000664) and were group-housed with food and water provided *ad libitum*. Housing temperature was maintained at 20–23°C on a 12-h light-dark cycle. After arrival, mice were acclimated to the colony for 1-week before being enrolled into control and experimental groups. All procedures and animal care guidelines were approved and conducted in accordance with the guidelines and regulations of the Institutional Animal Care and Use Committee at the University of Georgia. Procedures were carried out in compliance with the Animal Welfare Act and the Implementing Animal Welfare Regulations, in compliance with the principles of the Guide for the Care and Use of Laboratory Animals.

2.2 Experimental designs

2.2.1 Experiment 1: Time course of ROS emission and association with mitochondrial dysfunction after VML injury

Permeabilized gastrocnemius muscle fiber bundles from VML-injured mice were assessed at 7-, 14-, 30-, and 60-day post-injury for ROS emission, ROS production, AoxBC, and mitochondrial function (n=4 per time point). Results were compared to gastrocnemius fiber bundles from uninjured mice (**Figure 1A**).

2.2.2 *Experiment 2: Effect of SS-31 on ROS emissions and mitochondrial function*

Based on the results from experiment 1, the first 14-days post-injury is a critical time to address excess ROS emissions. SS-31, also known as Elamipretide or Bendavia, is a

mitochondrial-targeted antioxidant currently in clinical trials for various conditions, such as Barth syndrome (Reid Thompson et al., 2021), Friedreich's ataxia (J. Johnson et al., 2021; Lynch & Farmer, 2021; H. Zhao et al., 2017), dry age-relevant macular degeneration (Mettu et al., 2022), and primary mitochondrial myopathy (Karaa et al., 2018, 2020, 2023). SS-31 accumulates up to 1000-fold in mitochondria while indicating favorable pharmacokinetics and minimal toxicity (Karaa et al., 2018, 2020, 2023; Mettu et al., 2022; Reid Thompson et al., 2021). SS-31 not only protects against excessive oxidative stress but also enhances mitochondrial bioenergetics in aging and mitochondrial myopathies (Campbell et al., 2019; Pharaoh et al., 2023; Reid Thompson et al., 2021) by interacting with cardiolipin and mitochondrial proteins (Chavez et al., 2020; Mitchell et al., 2020). Previously, preclinical and clinical studies have shown that chronic treatment with SS-31 augments exercise tolerance, muscle function, and ADP sensitivity (Pharaoh et al., 2023; Reid Thompson et al., 2021). In addition, another *in vitro* study demonstrated the endogenous therapeutic ability of SS-31 to protect against excessive oxidative stress, reducing lipid peroxidation and maintaining mitochondrial membrane potential (K. Zhao et al., 2004, 2005).

To determine the extent to which SS-31 had efficacy in VML-injured muscle, mice were randomized into two groups: VML+Saline and VML+SS-31. Saline or SS-31(8 mg/kg body mass/day) was administered subcutaneously for 14-days consecutive days after VML injury and outcomes were assessed at 14- or 28-days post-injury in separate cohorts (n=6-8 per group cohort) (**Figure 1B**). Permeabilized gastrocnemius muscle fiber bundles were assessed for ROS emissions, ROS production, AoxBC, and mitochondrial function. Lipidomic analysis was conducted for cardiolipin species from remaining muscle samples.

2.2.3 Experiment 3: Effect of SS-31 on the site of ROS emission after VML

To determine the site within the electron transport chain of ROS emission after VML injury, mice were randomized into two groups (n=5 per group): VML+Saline and VML+SS-31. Separate cohorts were assessed at 7- and 14-days post-injury, therefore mice were administered saline or SS-31 subcutaneously for 7- or 14-days, respectively. Site-specific ROS emissions were determined from permeabilized gastrocnemius muscle fiber bundles and compared to muscle fiber bundles from uninjured mice (**Figure 1C**). Mitochondrial-enriched proteomic analysis was conducted for remaining muscle samples of the 14-day VML+Saline, 14-day VML+SS-31, and uninjured groups.

2.2.4 Experiment 4: Effect of SS-31 on rehabilitation adaptive capability post-injury

To determine if SS-31 treatment improves the adaptive capability to rehabilitation after VML injury, mice were randomized into three groups (n=8 per group): VML+Saline, VML+Saline+Rehabilitation, and VML+SS-31+Rehabiliation. Rehabilitation consisted of 6-weeks of voluntary wheel running starting at 2-weeks post-injury. SS-31 or saline were administered daily for the first 14-days post-injury. At 8-weeks post-injury, muscle adaptations were assessed via *in vivo* peak-isometric torque of the hindlimb plantar flexors and permeabilized muscle fiber bundle mitochondrial function. ROS emission, ROS production, and AoxBC (**Figure 1D**).

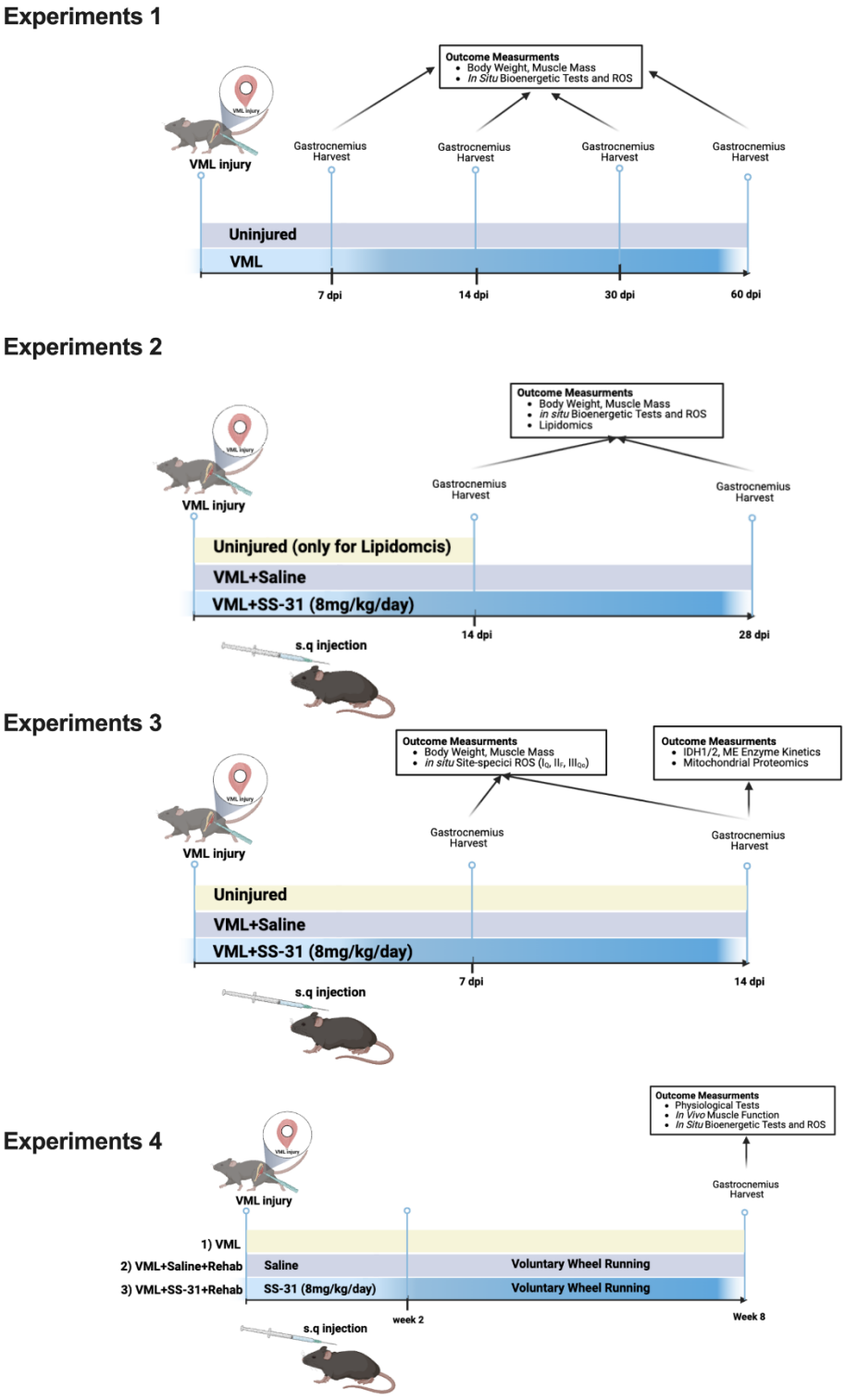

Figure 4.1. Schematic of experimental designs 1-4 and dependent variables. Volumetric muscle loss, VML; reactive oxygen species, ROS; subcutaneous, s.q.

2.3 Surgical creation of VML injury

VML injury was carried out on the posterior muscle compartment of anesthetized (isoflurane inhalation 1.5-3.0%) mice under aseptic surgical conditions as described previously (Heo et al., 2023; McFaline-Figueroa et al., 2022). Before surgery, mice received buprenorphine (1.2mg/kg; s. q.) for pain management. A 4-mm biopsy punch was utilized to create a VML defect in the plantar flexor muscles (gastrocnemius/plantaris/soleus). The skin incision was closed using 6.0 silk sutures, and mice were monitored throughout recovery.

2.4 Intraperitoneal glucose tolerance test (ipGTT)

One week before harvest, an intraperitoneal glucose tolerance test (ipGTT) was carried out following a glucose injection (2.0g/kg body weight, i.p.). After 6 hours of fasting, blood glucose was evaluated before glucose injection and again at 15, 30, 60, and 120 minutes after injection.

2.5 *In vivo* plantarflexion muscle function

Peak-isometric torque of hindlimb plantar flexor muscles was assessed *in vivo* as previously described (Heo et al., 2023; McFaline-Figueroa et al., 2022; Schifino et al., 2024) using electrophysiological stimulation of the sciatic nerve and the Model 300C muscle lever system (Aurora Scientific, Aurora, Ontario, Canada). Peak-isometric torque was normalized to body mass and mice were euthanized immediately afterward and tissue harvested for metabolic assays.

2.6 Mitochondrial respiration

High-resolution oxygen respiration measurement was conducted on permeabilized gastrocnemius fiber bundles using an Oroboros Oxygraph-2K (Oroboros Instruments, Innsbruck, Austria) as previously described (Fisher-Wellman et al., 2018; Heo et al., 2023) with minor adjustments. To measure JO_2 and electron conductance through the electron transport chain (ETC) under a physiologically relevant environment, we employed a creatine kinase (CK) clamp system where this assay depends on the enzymatic reaction of CK and phosphocreatine (PCr) to manipulate the levels of cellular energy demand (Gibbs-free energy; ΔG_{ATP}) (Fisher-Wellman et al., 2018). After recording the basal rate, permeabilized fiber bundles from gastrocnemius muscle energized using either carbohydrate (5 mM Pyruvate and 2 mM malate) or fat (40 μM palmitoyl-carnitine and 2 mM malate) substrates with 20 U/mL CK, 1 mM PCr, and 5 mM ATP to mimic near exercise conditions (maximal JO_2), followed by adding cytochrome c (10 μM) to check mitochondrial integrity. Subsequently, sequential PCr titrations (6, 12, 15 mM) to reduce ΔG_{ATP} to resting conditions. In addition to recording absolute JO_2, the changes in JO_2 relative to the change in ΔG_{ATP} were also evaluated. The $JO_2/\Delta G_{ATP}$ relationship is referred to as the respiratory conductance and reflects the sensitivity of mitochondria to changes in energy demand (Fisher-Wellman et al., 2018). The rates were normalized to the wet weight of tissue in the chamber of the machines and citrate synthase (CS) activity to account for differences in the mitochondrial content (Larsen et al., 2012). CS activity for samples from each study are reported in **Supplemental Figure 1**.

2.7 Mitochondrial membrane potential

The Δψm was measured fluorometrically in buffer Z containing 5 mM creatine, using a spectrofluorometer (FluoroMax Plus-C; Horiba Instruments Inc., Irvine, CA, USA) (Fisher-Wellman et al., 2018; McFaline-Figueroa et al., 2023). The membrane potential was assessed with tetramethylrhodamine methyl ester (TMRM) at 30°C, in accordance with the CK clamp assay protocol and with constant stirring. TMRM excitation/emission [(572/590 nm)/(551/590 nm)] fluorescence is quenched, meaning the 572/551 ratio increases with greater mitochondrial membrane polarization. To our knowledge, the 572/551 ratio is represented here as there has been no report validating the conversion of the 572/551 ratio to millivolts in permeabilized muscle fiber.

2.8 ROS emission, ROS production, Antioxidants buffering capacity and site-specific ROS

The ROS emission and production were measured in buffer Z supplemented with Amplex Ultrared (5 μM), Cu-Zn superoxide dismutase (25 units/ml), and horseradish peroxidase (1 U/mL) detection system of H_2O_2 (Ex:Em 565:600), as previously described (Smith et al., 2020) with a minor modification. After recording the basal rate, ROS emission was assessed by adding 5 mM pyruvate and 2 mM malate (carbohydrate substrates), or 40 μM palmitoyl-carnitine and 5 mM malate (fat substrates). ROS production was assessed by the addition of 1 μM auranofin, an inhibitor of thioredoxin, and 100 μM carmustine (BCNU), an inhibitor of glutathione reductase. The AoxBC (percentage of ROS buffered by antioxidant enzymes thioredoxin and glutathione reductase) reflects the percentage of ROS produced but not emitted (i.e., (ROS production – ROS emission) / ROS production) x 100) (Smith et al., 2020).

Site-specific ROS production was determined fluorometrically by stimulating each site while inhibiting others, with slight modifications as previously described (Quinlan, Perevoschikova, et al., 2013; Quinlan, Perevoshchikova, et al., 2013). The capacity for superoxide/hydrogen peroxide production at site I_Q was measured in permeabilized muscle fibers by driving reverse electron transport using succinate at a high concentration (5 mM) (Brand, 2016). Then, rotenone (4 uM) was added to inhibit site I_Q, and the rate was corrected for the rotenone-sensitive rate to accurately determine superoxide/hydrogen peroxide production at site I_Q. The ROS from site II_F can be assessed by adding a low concentration of succinate (500 uM), rotenone (4 μM), myxothiazol (2 μM), and antimycin A (2 μM) to inhibit IQ, III_{Qo}, and III_{Qi}, respectively. Subsequently, malonate (1 mM) was added to inhibit site II_F directly, and the rate was corrected for the malonate-sensitive rate to analyze II_F -specific ROS production. Lastly, the ROS at site III_{Qo} can be quantified by adding succinate (5 mM), antimycin A (2 μM), and rotenone (4 μM), and then, the rate was accounted for the myxothiazol (2 μM)-sensitive rate to determine site III_{Qo}-specific ROS.

2.9 Assessment of mitochondrial enzyme activities

CS activity, complex I, and complex II were measured using a spectrophotometer (Molecular Devices, San Jose, CA, USA) as previously described (Heo et al., 2023; McFaline-Figueroa et al., 2022). CoA-SH, a byproduct generated by the CS-catalyzed reaction between oxaloacetate and acetyl-CoA, reacts with 5′, 5′-Dithiobis 2-nitrobenzoic acid (DTNB) to produce TNB, which is detected by absorbance at 412 nm. Complex-I activity was assessed in 50 mM potassium phosphate buffer, 3 mg/mL BSA, 0.4 μM antimycin A, 240 μM potassium cyanide, 50 μM decyl-ubiquinone, and 80 μM 2, 6- dichlorophenolindophenol (DCPIP). The oxidation of

NADH was measured via the reduction of DCPIP at 600 nm. Complex-II activity was determined in a buffer (10 mM KH2PO4, 2 mM EDTA, 1 mg/mL BSA at pH 7.8 and added with 200 μM ATP, 10 mM succinate, and 80 μM DCPIP. Following incubating the buffer for 10 minutes at 30C, the assay was initiated by adding oxidized 80 μM decyl-ubiquinone, and reduction of DCPIP followed at 600 nm.

The dehydrogenase activities of isocitrate dehydrogenase (IDH1/2) and malic enzyme (ME2) were measured via the NADPH autofluorescence using a spectrophotometer in buffer Z, as previously described (Fisher-Wellman et al., 2018; McLaughlin et al., 2020). This buffer was supplemented with the respective substrate, 10 mM iso-citrate, 10 mM pyruvate, or 5 mM malate. Enzymatic rates were determined using a standard curve performed with NADPH standards. All enzyme activities were normalized to mitochondrial content (CS enzyme activity). Although IDH2 is the principal mitochondrial isoform that maintains redox homeostasis, IDH1 in the cytosol also contributes to NADPH production, influencing mitochondrial redox states by affecting glutathione and thioredoxin levels (Gelman et al., 2018). Since we used whole muscle homogenates to measure IDH activity rather than isolated mitochondria, we did not distinguish between IDH1 and IDH2. Measuring total NADPH-dependent IDH 1/2 activity, therefore, captures the overall NADPH-producing capacity pertinent to oxidative stress regulation in muscle tissues.

2.10 Cardiolipin quantification

Cardiolipin was quantified using previously published methods, including liquid chromatography coupled to electrospray ionization mass spectrometry in an API 4000 mass spectrometer (Sciex, Framingham, MA, USA) (Sparagna et al., 2005). For sample preparation,

the muscle was homogenized using a glass-on-glass homogenizer in PBS. Lipids were extracted from 0.25 mg of protein per sample using a modified Bligh and Dyer method, with 1,000 moles of tetra myristyl cardiolipin added as an internal standard (Avanti Polar Lipids) (Sparagna et al., 2005).

2.11 LC-MS/MS Analysis (mitochondrial proteomics)

Samples were analyzed on a LC-MS/MS system consisted of an Orbitrap Eclipse Mass Spectrometer and a Vanquish Neo nano-UPLC system (Thermo Scientific, Waltham, MA). Peptide mixture was injected via trap-and-elute procedure using a Thermo Scientific Acclaim PepMap 100 trap column (cat# 164946) and a Thermo Scientific DNV PepMap Neo (cat# DNV75500PN) analytical column. Peptides were separated employing linear gradient elution consisted of water (A) and 80% acetonitrile (B) both of which contained 0.1% formic acid. Data were acquired by top speed data dependent mode where maximum MS/MS scans were acquired per cycle time of 1 second between adjacent survey spectra. Dynamic exclusion option was enabled which duration was set to 60 seconds. To identify proteins, spectra were searched against the UniProtmouse protein FASTA database (17,082 annotated entries, Oct 2021) using the Sequest HT search engine with the Proteome Discoverer v2.5 (Thermo Scientific, Waltham, MA). Search parameters were as follows: FT-trap instrument; parent mass error tolerance, 10 ppm; fragment mass error tolerance, 0.6 Da (monoisotopic); enzyme, trypsin (full); # maximum missed cleavages, 2; variable modifications, +15.995 Da (oxidation) on methionine; static modifications, +57.021 Da (carbamidomethyl) on cysteine.

2.12 Statistical analysis

All statistical analyses were determined using JMP Pro statistical software (version 16.0.0 SAS Institute, Cary, NC, USA), and figures were created using GraphPad Prism (version 9.4.1, GraphPad Software, San Diego, CA, USA). All data are represented as mean±standard deviation (SD). Experiment 1 data were analyzed by one-way ANOVA. Experiment 2 data were analyzed by student's t-test. Experiment 3 data were analyzed by one-way ANOVA. Experimental 4 data were analyzed by one-way ANOVA. A Tukey's HSD post-hoc test was used to determine differences among independent groups if there was a statistical significance ANOVA p-value (alpha level of 0.05). Proteomic data was analyzed by one-way ANOVA using a Bonferroni adjusted p-value. Lipidomic data was analyzed by one-way ANOVA.

3. Results

3.1 Time course of ROS emission and association with mitochondrial dysfunction after VML injury

Consistent with previous reports utilizing the CK clamp to investigate mitochondrial function after VML injury (Heo et al., 2023; McFaline-Figueroa et al., 2023), there is robust evidence supporting an immediate and lasting change in both carbohydrate- and fat-mediated JO_2 from 7- to 60-days post-VML (**Figure 2A, B, F, G**, carbohydrate; $p \leq 0.004$ and fat; $p \leq 0.007$). Notably, respiratory conductance was significantly impaired in VML-injured fiber bundles compared to uninjured fiber bundles for both substrates (**Figure 2C, H**, carbohydrate; $p \leq 0.015$ and fat; $p \leq 0.037$), and this was associated with a hyperpolarized $\Delta\psi m$ (**Figure 2D, I**, carbohydrate; $p = 0.001$ and fat; $p = 0.001$). To further assess the mitochondrial bioenergetic relationships, JO_2 values were plotted against their corresponding $\Delta\psi m$ at each ΔG_{ATP} (**Figure 2E, J**). This relationship is crucial as, *in vivo*, the energy generated from the Δp driven by $\Delta\psi m$ determines the extent to which ATP synthase can displace the ATP/ADP ratio away from equilibrium. Thus, the ability of mitochondria to control the relationship between JO_2 and $\Delta\psi m$ serves as a crucial indicator of respiratory efficiency and mitochondrial readiness in response to energy demand (referred to as *bioenergetic efficiency* in this paper). These data showed that VML-injured groups exhibit a right- and downward shift compared to uninjured in the relationship between JO_2 and $\Delta\psi m$, suggesting that VML-injured mitochondria have a less bioenergetic efficiency compared to the Uninjured mitochondria (Fisher-Wellman et al., 2018; Koves et al., 2023; Williams et al., 2024).

To determine the extent to which the hyperpolarized $\Delta\psi m$ from VML-injured muscle fiber bundles was associated with ROS, the rate of H_2O_2 (JH_2O_2) was assessed using

carbohydrate- or fat-substrates in the presence of endogenous antioxidant buffering systems (ROS emission) and when endogenous antioxidants were inhibited (ROS production) (**Figure 2K**). Compared to uninjured, carbohydrate-mediated ROS emission (**Figure 2L,** $p \leq 0.001$) and production (**Figure 2L,** $p < 0.030$) were significantly higher in VML-injured fiber bundles until 14-days post-injury, and AoxBC was less at both 7- and14-days post-injury (**Figure 2L**, $p \leq 0.001$). Similarly, fat-mediated ROS emission **(Figure 2M**, $p \leq 0.033$) was greater through 14-days post-injury, and ROS production was significantly greater at 30- and 60-days post-injury **(Figure 2M**, $p \leq 0.026$). Fat-mediated Aox BC for VML-injured muscle fiber bundles was less out to 14-days post-injury compared to uninjured **(Figure 2M**, $p < 0.001$).

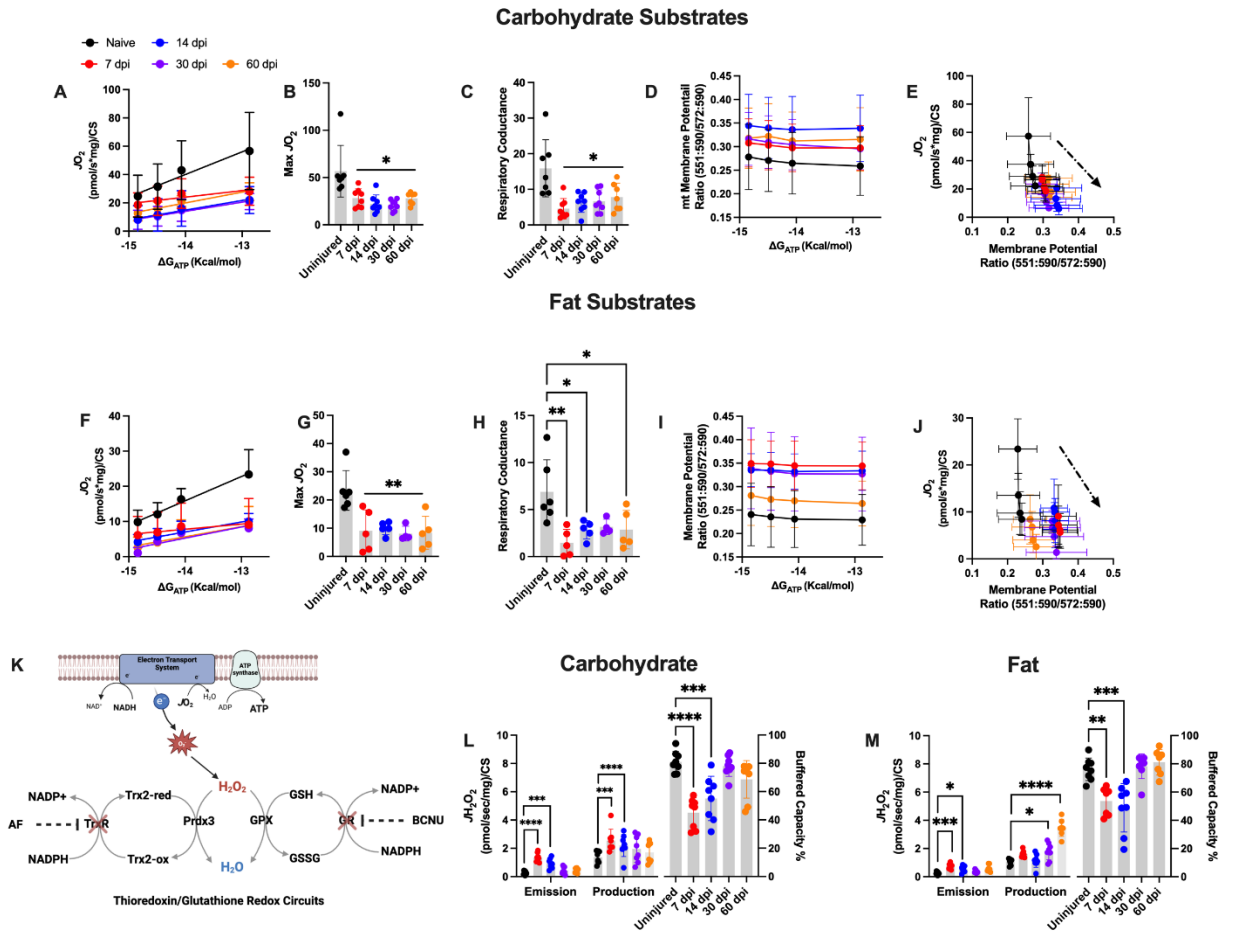

Figure 4.2. Time course of permeabilized muscle fiber bundle mitochondrial bioenergetics and reactive oxygen species after volumetric muscle loss injury. **A,F:** The relationship between ATP re-synthesis demand (ΔG_{ATP}) and mitochondrial oxygen consumption (JO_2) normalized to citrate synthase (CS) activity for carbohydrate and fat substrates, respectively. **B,G:** Maximal JO_2 for carbohydrate and fat substrates, respectively. **C,H:** Respiratory conductance for carbohydrate and fat substrates, respectively. **D,I:** The relationship between ΔG_{ATP} and mitochondrial membrane potential for carbohydrate and fat substrates, respectively. **E,J:** The relationship between JO_2 and mitochondrial membrane potential (i.e., bioenergetic efficiency) for carbohydrate and fat substrates, respectively. The arrows indicate the down, rightward shift with VML injury. **K:** Schematic of endogenous H_2O_2 buffering circuits within mitochondria with inhibitors against those circuits indicated. **L,M:** reactive oxygen species emission, production, and antioxidant buffer capacity for carbohydrate and fat substrates, respectively. Statistical significance was determined by one-way ANOVA with Tukey's HSD post-hoc test. Data are expressed as mean ± SD. *p < 0.05, **p < 0.01, ***p < 0.001, and ****p < 0.0001. dpi, days post-injury.

3.2 Effect of SS-31 on ROS emissions and mitochondrial function

To more definitely link ROS emissions to mitochondrial dysfunction in the context of VML injury, we sought to buffer ROS using the mitochondrial-targeted antioxidant SS-31. Body mass, gastrocnemius muscle mass, and body mass-normalized muscle mass were not affected by SS-31 intervention (**Supplemental Figure 2**). At 14-days post-injury, carbohydrate-mediated maximal JO_2 and respiratory conductance were 68% and 60% greater, respectively, in VML+SS-31 muscle fiber bundles compared to VML+Saline (**Figure 3A-C,** $p \leq 0.001$). Similarly, fat-mediated maximal JO_2 and respiratory conductance were 102% and 105% greater, respectively, in VML+SS-31 muscle fiber bundles compared to VML+Saline (**Figure 3F-H,** $p \leq 0.005$). SS-31 intervention also influenced the JO_2- $\Delta\psi m$ relationship as there was a left and upward shift in the bioenergetic efficiency for both carbohydrate- and fat-mediated metabolism compared to VML+Saline (**Figure 3E, J**). This improved mitochondrial bioenergetic efficiency could be related to the modest improvement of complex-I and -II enzyme kinetics after SS-31 intervention (**Supplemental Figure 3**). Overall, the discernable shift suggests that permeabilized fiber bundles from VML+SS-31 mice utilized $\Delta\psi m$-driven Δp more effectively for ATP synthesis and could shift the cellular environment that influences ROS production and emissions.

To test this, ROS emission, ROS production, and AoxBC were assessed (**Figure 3K, L**). ROS emissions from permeabilized fiber bundles from VML+SS-31 mice were 70% and 68% less (carbohydrate and fat substrates, respectively) compared to VML+Saline (**Figure 3K, L**, $p \leq 0.001$). There was no significant difference in ROS production between VML+SS-31 and VML+Saline; however, the AoxBC was 41% and 43% greater (carbohydrate and fat substrates, respectively) at 14-days post-injury for VML+SS-31 (**Figure 3K, L**, $p \leq 0.001$). All outcomes were repeated in a cohort of VML-Saline and VML-SS-31 mice at 28-days post-injury

(**Supplemental Figure 3**). The goal was to determine the extent to which the beneficial effects of SS-31 on mitochondrial function and AoxBC lasted after the 14-day intervention period. Although the magnitude of difference between VML+Saline and VML+SS-31 was less at 28-days post-injury, the primary findings held such that VML+SS-31 had greater $\dot{V}O_2$, respiratory conductance, a left and upward shift in bioenergetic efficiency, less ROS emission, and greater AoxBC compared to VML+Saline (**Supplemental Figure 3**).

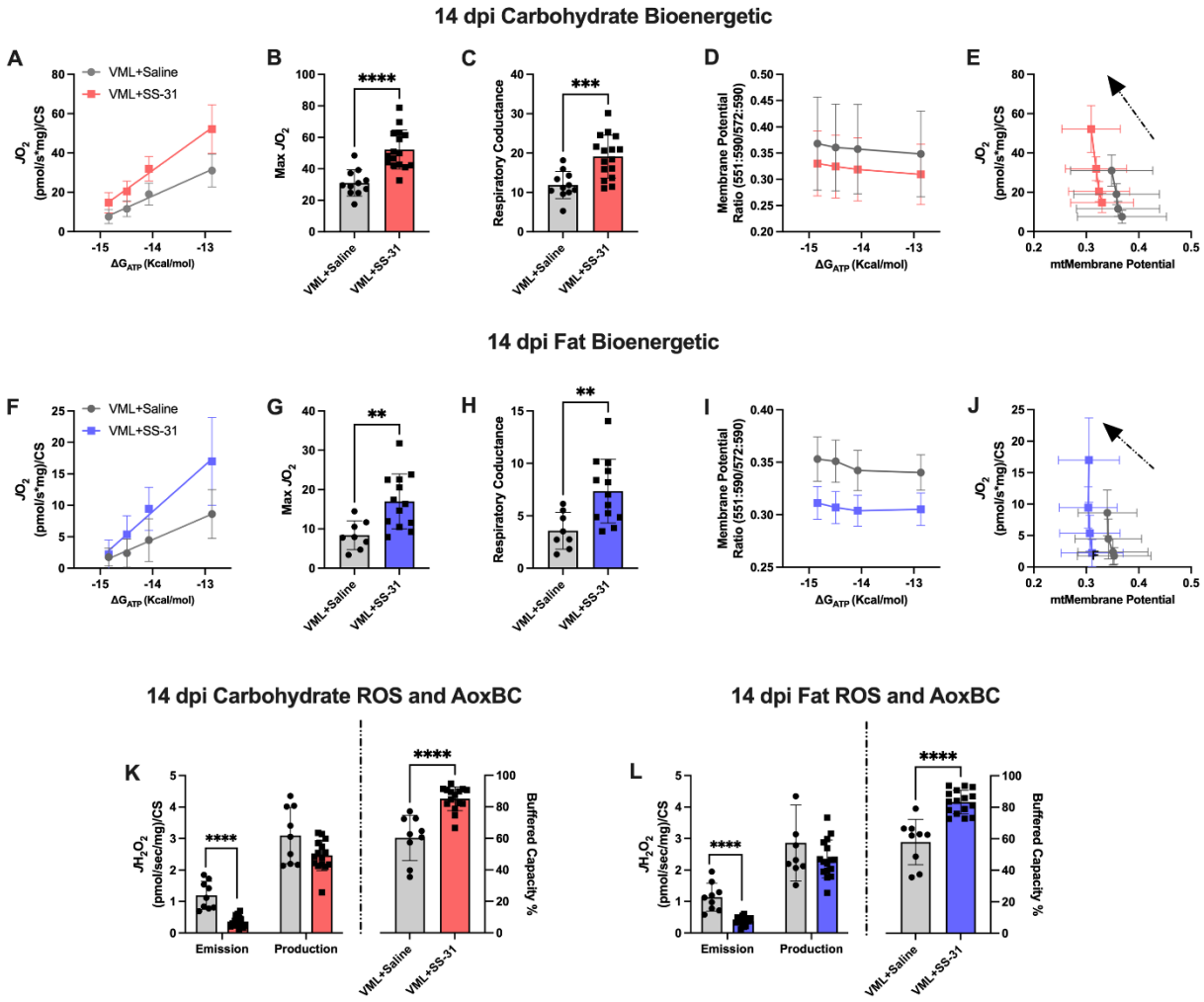

Figure 4.3. Effect of SS-31 on permeabilized muscle fiber bundle mitochondrial bioenergetics and reactive oxygen species after VML injury. **A,F:** The relationship between ATP re-synthesis demand (ΔG_{ATP}) and mitochondrial oxygen consumption (JO_2) normalized to citrate synthase (CS) activity for carbohydrate and fat substrates, respectively, at 14-days post-injury. **B,G:** Maximal JO_2 for carbohydrate and fat substrates, respectively, at 14-days post-injury. **C,H:** Respiratory conductance for carbohydrate and fat substrates, respectively, at 14-days post-injury. **D,I:** The relationship between ΔG_{ATP} and mitochondrial membrane potential for carbohydrate and fat substrates, respectively, at 14-days post-injury. **E,J:** The relationship between JO_2 and mitochondrial membrane potential (i.e., bioenergetic efficiency) for carbohydrate and fat substrates, respectively, at 14-days post-injury. The arrows indicate the up, leftward shift with SS-31 intervention. **K,L:** Reactive oxygen species emission, production, and antioxidant buffer capacity for carbohydrate and fat substrates, respectively, at 14-days post-injury. Statistical significance was determined by student's t-test. Data are expressed as mean ± SD. *$p < 0.05$, **$p < 0.01$, ***$p < 0.001$, and ****$p < 0.0001$. dpi, days post-injury. AoxBC, antioxidant buffering capacity. ROS, reactive oxygen species.

3.3 Effect of SS-31 on the site of ROS emission after VML

To better interrogate the specific sources of ROS emission from the electron transport chain following VML injury and SS-31 intervention, we assessed three different site-specific ROS sites at 7- and 14-days post-injury, aligning with the time course of the highest production and emission rates (**Figure 1L-M**). Electron leak from the following complex sites was investigated: complex-I_Q, complex-II_F, and complex-III_{Qo} (**Figure 4A**) (Brand, 2016; Quinlan, Perevoschikova, et al., 2013).

At 14-days post-injury, I_Q, II_F, and III_{Qo} sites had 146%, 109%, and 125% greater ROS emission in muscle fiber bundles from VML+Saline compared to uninjured (**Figure 4B**, $p \leq 0.002$), and the stacked ROS production across all three sites was 126% greater (**Figure 4C**, $p \leq 0.001$). Muscle fiber bundles from VML+SS-31 mice had significantly less ROS emissions in I_Q and III_{Qo}, individually and collectively (**Figure 4B-C**, $p \leq 0.001$). The outcomes were similar at 7-days post-injury, with the exception that there was no statistical difference between VML+Saline and uninjured for ROS emission from complex-II_F at 7-days post-injury (**Supplemental Figure 4**).

These findings suggest that ROS was emitted regardless of the mitochondrial complex within the electron transport chain following two weeks of VML injury, contributing to greater oxidative stress. In contrast, SS-31 demonstrates a protective effect, reducing ROS emission across multiple sites, which may play a crucial role in alleviating oxidative stress and supporting mitochondrial function.

The thioredoxin/glutathione-dependent reductase antioxidant buffering systems explored here rely on NADPH as an electron donor to regenerate thioredoxin and glutathione substrates (Munro et al., 2016). In mitochondria, NADPH can be generated through multiple enzymes,

particularly isocitrate dehydrogenase 2 (IDH2) and malic enzyme (ME), thereby coupling the oxidation of respiratory substrates to the replenishment of NADPH pools. Additionally, nucleotide transhydrogenase (NNT) leverages the Δp to facilitate electron transfer from NADH to $NADP^+$, thereby producing NADPH and NAD^+. However, as the C57BL/6J mouse line carries an NNT gene mutation, we ruled out the possibility of NADPH production via NNT in this model. IDH1/2 and ME2 enzymatic rates were 37% and 31% less, respectively (**Figure 4D, E,** $p \leq 0.008$), for VML+Saline compared to uninjured, and these rates were rescued for VML+SS-31 (**Figure 4D, E,** $p \leq 0.038$). The mechanism of SS-31 effect on these NADPH maintaining enzymes is unclear, but the results of greater enzyme activity to support the thioredoxin/glutathione reductase antioxidant buffering systems helps explain the overall benefit of SS-31 in VML-injured muscle.

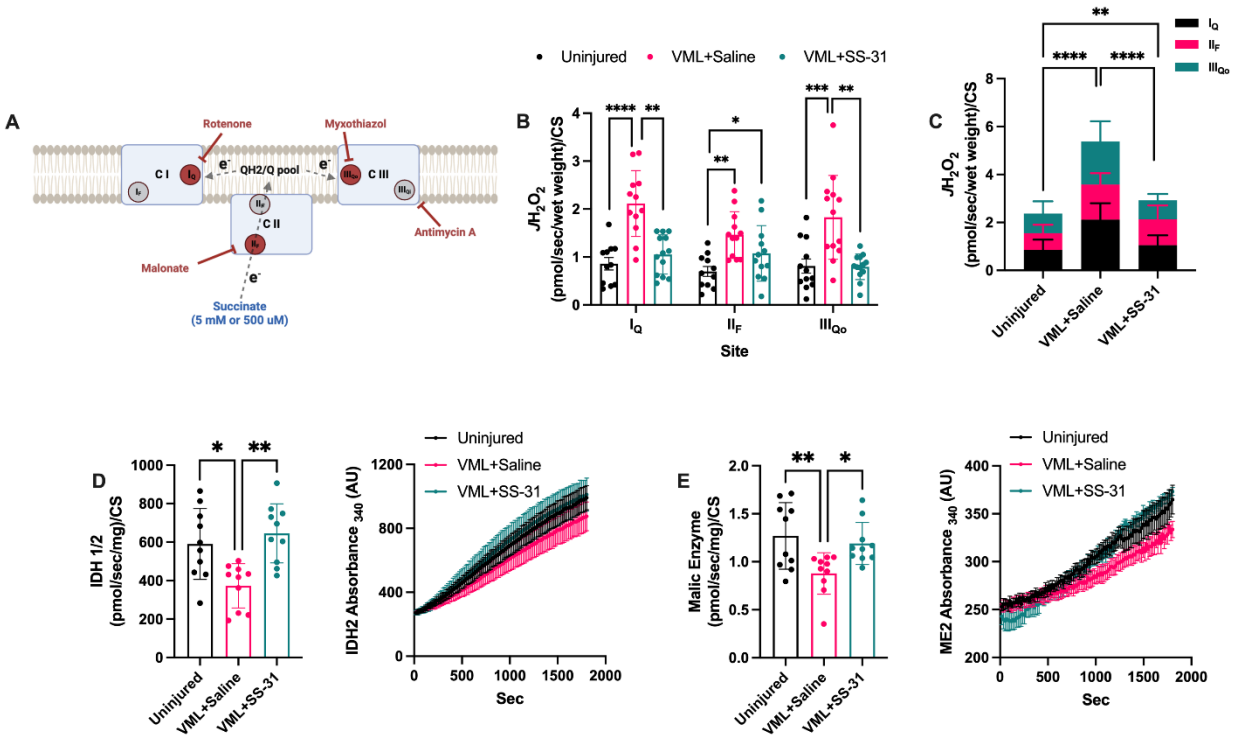

Figure 4.4. Site-specific reactive oxygen species emission after VML injury. **A:** Schematic of specific sites of reactive oxygen species emission within the electron transport chain investigated with substrate (blue) and inhibitors (red) indicated. **B:** Rate of H_2O_2 emission (JH_2O_2) across complexes –I through -III in permeabilized muscle fiber bundles at 14-days post-injury. **C:** Cumulative JH_2O_2 for complex -I through -III in permeabilized muscle fiber bundles at 14-days post-injury. **D:** Isocitrate dehydrogenase enzyme activity from muscle homogenates at 14-days post-injury. **E:** Malic enzyme enzyme activity from muscle homogenates at 14-days post-injury. Statistical significance was determined by one-way ANOVA with Tukey's HSD post-hoc test. Data are expressed as mean ± SD. *p < 0.05, **p < 0.01, ***p < 0.001, and ****p < 0.0001.

In order to better understand how SS-31 influences mitochondrial bioenergetic and ROS, we had the tissue samples from Experimental 2 analyzed the quantification of mitochondrial cardiolipin using mass spectrometry (**Figure 5**). Cardiolipin, which constitutes 10-20% of mitochondrial lipids, is known to bind to oxidative phosphorylation proteins, affecting their function (J. M. Johnson et al., 2018; Pennington et al., 2019; Prola et al., 2021). Also, SS-31 accumulates in the inner-mitochondrial membrane by selectively binding to cardiolipin (Szeto & Birk, 2014; Szeto & Liu, 2018). This interaction enhances the curvature of mitochondrial cristae, thereby supporting the structural integrity of the inner-mitochondrial membrane and organizing respiratory chain super-complexes for improved mitochondrial bioenergetics (Szeto & Birk, 2014; Szeto & Liu, 2018).

Cardiolipin comprises two phosphatidic acid units connected by a central glycerol backbone. It is predominantly located within the inner mitochondrial membrane, where it is synthesized through a series of enzymatic reactions involving cardiolipin synthase and various transacylation enzymes, which are also localized in this membrane. Cardiolipin molecules initially produced by cardiolipin synthase often have uneven acyl chains, rendering them partially functional and referred to as nascent cardiolipin. These nascent cardiolipin molecules undergo transacylation, primarily mediated by the enzyme cardiolipin transacylase tafazzin, to form tetralinoleoyl-CL (L_4CL), a more functionally mature form (J. M. Johnson et al., 2018; Pennington et al., 2019). There were no statistical differences between uninjured and VML saline for total cardiolipin, total L4CL, nor L_4CL/tetrazolyl cardiolipin (O_4CL; nascent cardiolipin) ratio (**Figure 5A-C,** $p \leq 0.997$). Analysis of the dominant 72-carbon cardiolipin species showed no significant differences for each individual species (**Figure 5D,** $p \leq 0.995$); however, a chi-squared analysis revealed a shift in the predominant cardiolipin species toward a nascent form

(L_3O), with a relative greater percentage of L_3O (36.62%) and a lower percentage of L_4CL (29.72%) compared to uninjured (**Figure 5D**). These findings suggest a shift towards less mature cardiolipin species post-VML injury.

SS-31 had no significant effect on cardiolipin abundance nor species compared to VML saline and uninjured **Figure 5D,** $p \leq 0.999$). SS-31 treated muscle showed the same shift toward less mature cardiolipin species as the VML saline using a chi-squared analysis. These results indicate that SS-31 treatment does not significantly influence the remodeling of cardiolipin species post-VML injury.

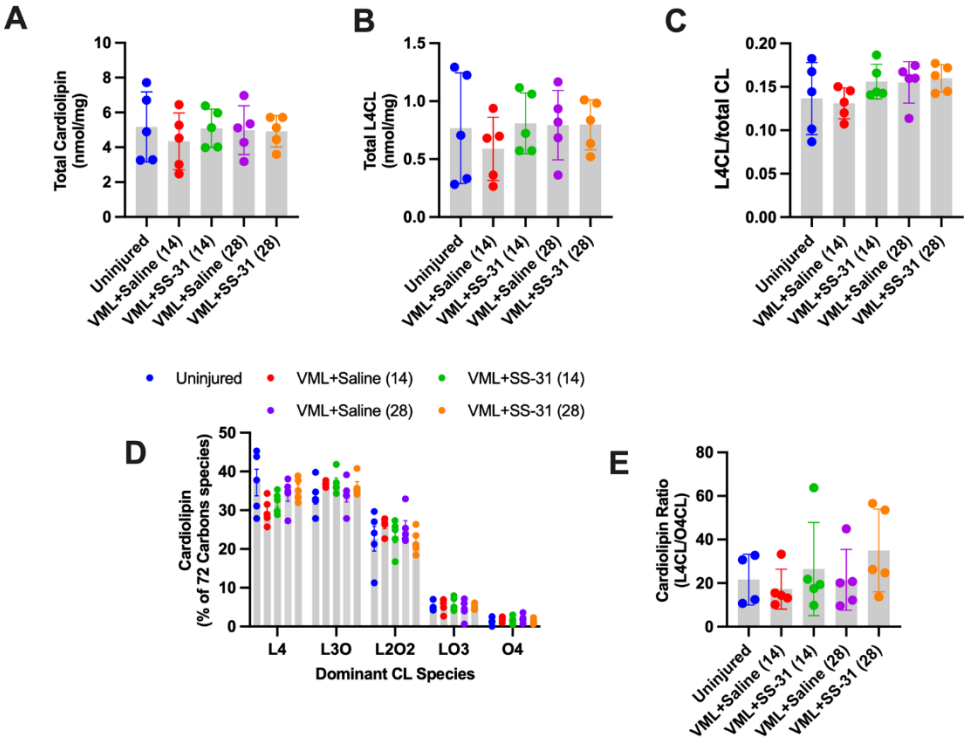

Figure 4.5. Total cardiolipin and cardiolipin species following VML injury. **A:** Total cardiolipin (CL) species content. **B:** Tetralinoleoyl cardiolipin (L_4CL) content. **C:** L_4CL-to-total CL content ratio. **D:** Analysis of 72-carbon CL species. **E:** Ratio of L_4CL-to-O_4CL species. **S**tatistical significance was determined by one-way ANOVA with Tukey's HSD post-hoc test. Data are expressed as mean ± SD.

Cadiolipin species analysis did not yield robust mechanistic insight into SS-31 benefits in VML-injured muscle, so analysis of the mitochondrial proteome was investigated for uninjured, VML saline, and VML SS-31 at 28-days post-injury (tissue collected from Experimental 2). A mitochondrial enrichment factor was calculated for each sample by dividing the total abundance of all proteins classified as mitochondrial, based on the MitoCarta 3.0 database (Rath et al., 2021), relative to the total protein abundance as previously described (McLaughlin et al., 2020). There was a statistical trend ($p=0.077$) for a difference between uninjured and VML saline (**Figure 6A**). To account for this statistical trend and provide greater rigor to the broader proteomic analysis, all mitochondrial protein abundances were normalized by the mitochondrial enrichment factor for each sample (McLaughlin et al., 2020).

Proteomics data analysis showed that VML induces significant changes in grouped oxidative phosphorylation proteins (**Figure 6B,** $p = 0.033$), but not dehydrogenases (**Figure 6B,** $p = 0.0184$). SS-31 does not alter these proteins (**Figure 6B,** $p = 0.674$). All protein abundances linked to an individual complex were summed and then expressed as a percentage of the maximum abundance across the samples to determine the relative expression of the complex (**Figure 6C**). VML-Saline had a 11% lower relative complex-IV proteome (**Figure 6C**, $p=0.012$) and, conversely, a 13% greater relative complex-V proteome (**Figure 6C**, $p=0.030$) compared to uninjured (**Figure 6C**). There was no significant difference in relative complex abundances for VML+SS-31.

A primary goal of this study was to interrogate redox balance after VML injury and with SS+31 intervention. All protein abundances linked to antioxidant enzymes were summed and then expressed as a percentage of the maximum abundance across the samples. VML+Saline had a 20% greater mitochondrial ROS proteome compared to Uninjured (**Figure 6D**, $p = 0.027$).

After normalizing individual protein abundances by the mitochondrial enrichment factor and using a Bonferroni adjusted p-value correction, there were no statistical differences for individual proteins within the electron transport chain and redox circuit (**Figure 6E**, adj. p ≥0.101).

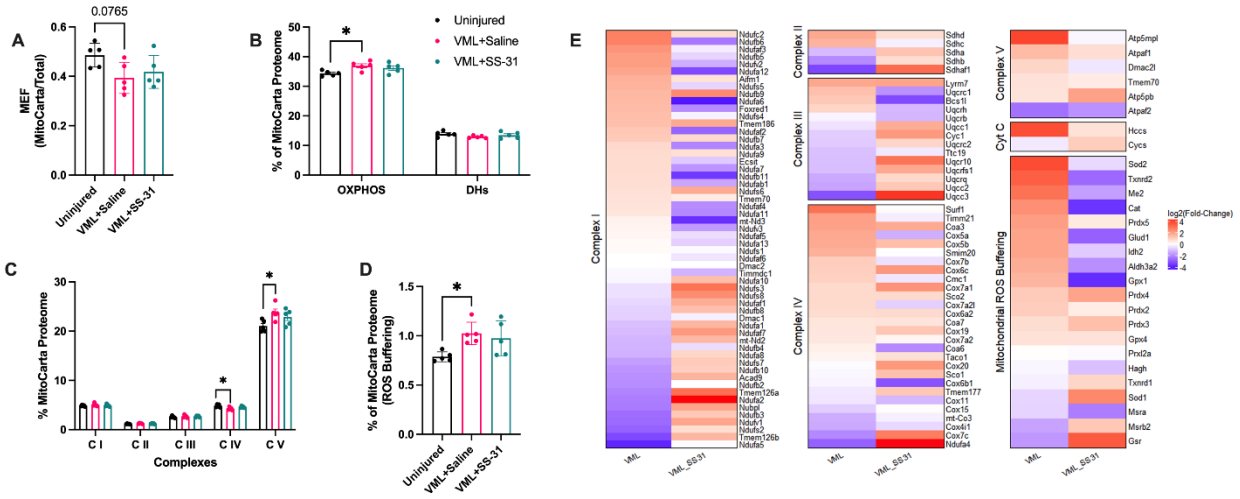

Figure 4.6. Effect of VML injury and SS-31 intervention on the mitochondrial-enriched proteome. **A:** Mitochondrial enrichment factor (MEF) score for each sample. **B:** MEF-normalized abundances for proteins identified as part of oxidative phosphorylation (OXPHOS) and dehydrogenases (DHs) using MitoCarta 3.0. **C:** MEF-normalized abundances of proteins contributing to mitochondrial complex I through V using MitoCarta 3.0. **D:** MEF-normalized abundances of proteins contributing to the reactive oxygen species (ROS) redox circuit using MitoCarta 3.0. **E:** A log2 fold-change (FC) heatmap of individual proteins within the electron transport chain complex I through V and the ROS redox circuit. The log2FC is relative to Uninjured and arranged from largest positive to largest negative in the VML-Saline group. Statistical significance was determined by one-way ANOVA with Bonferroni adjusted p-value. Data are expressed as mean ± SD. *p < 0.05.

3.4 *Effect of SS-31 on rehabilitation adaptive capability post-injury*

To determine if the beneficial effects of SS-31 on mitochondrial ROS emission and mitochondrial function would improve rehabilitation adaptive capability, we compared muscle strength and mitochondrial outcomes after 6-weeks of voluntary wheel running in cohorts of VML-injured mice that either received 14-days of saline or SS-31 immediately following injury. There was no difference in running distance between VML+Saline+Rehabilitation and VML+SS-31+Rehabilitation (**Figure 7A,** $p = 0.908$). At the study endpoint, body weight was 8% less in the VML+SS-31+Rehabilitation mice compared to VML+Saline (**Figure 7B**, $p = 0.022$). There were no statistically significant differences across groups for VML-injured gastrocnemius raw mass nor mass normalized by body mass, blood glucose disposal, body mass-normalized peak-isometric torque, nor muscle mass-normalized peak-isometric torque (**Figure 7B-H,** $p = 0.999$).

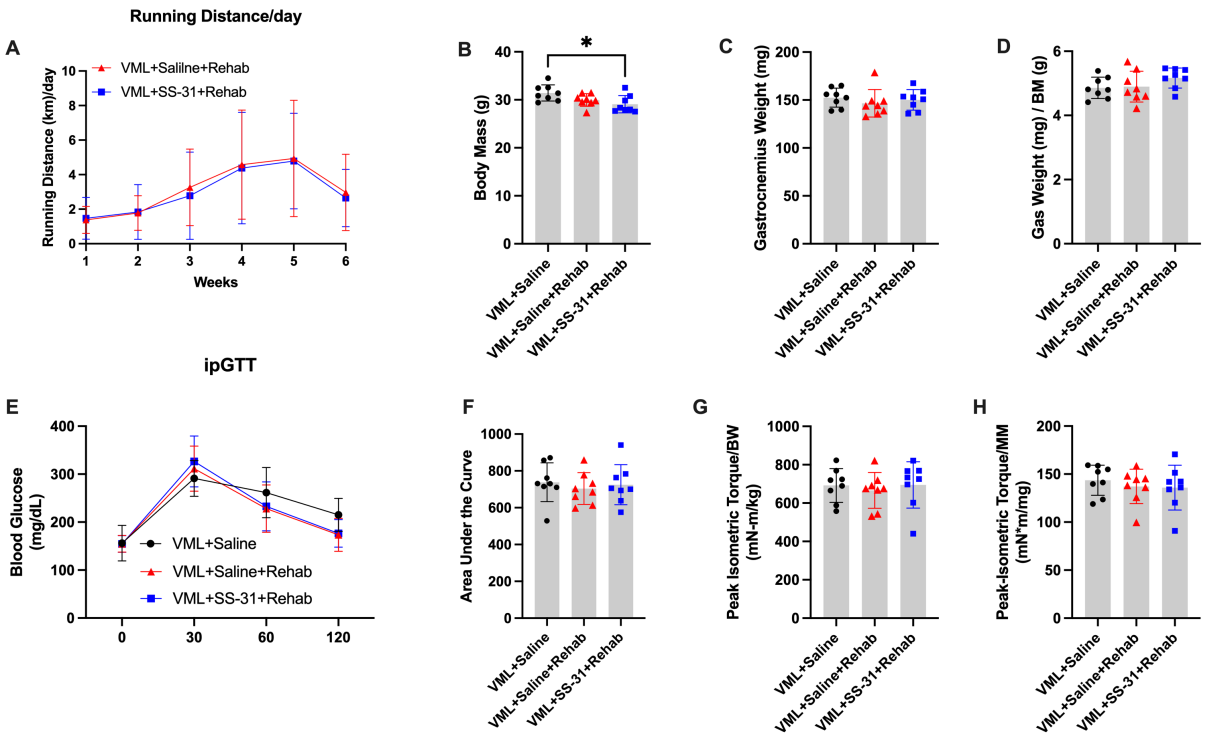

Figure 4.7. Effect SS-31 on morphologic and contractile adaptations to rehabilitation after VML injury. **A:** Average daily wheel running distance by week. **B-D:** Body mass, VML-injured gastrocnemius muscle mass, and body mass-normalized muscle mass at 8-weeks post-injury. **E-F:** Two-hour blood glucose response to a single, fasted glucose challenge and calculated area under the curve at 8-weeks post-injury. **G:** *In vivo* body mass-normalized peak-isometric torque of the hindlimb plantar flexors at 8-weeks post-injury. **H:** *In vivo* muscle mass-normalized peak-isometric torque of the hindlimb plantar flexors at 8-weeks post-injury. Statistical significance was determined by one-way ANOVA with Tukey's HSD post-hoc test. Data are expressed as mean ± SD. *$p < 0.05$.

The influence of SS-31 on metabolic adaptations to rehabilitation was explored next. Consistent with a previous finding (Schifino et al., 2023), rehabilitation alone did not significantly alter carbohydrate-mediated (**Figure 8A, B**, p = 0.543) or fat-mediated (**Figure 8F, G**, p = 0.143) JO_2 (VML+Saline vs. VML+Saline+Rehabilitation); however, the carbohydrate-mediated respiratory conductance was 26% greater in VML+SS-31+Rehabilitation muscle fiber bundles compared to VML+Saline (**Figure 7C,** p = 0.025) despite there being no statistical difference in maximal JO_2 between the two groups (**Figure 7B,** p = 0.132). For fat substrates, maximal JO_2 and respiratory conductance was 84% and 67% higher in the VML+SS-31+Rehabilitation and VML+Saline+Rehabilitation compared to VML+Saline (**Figure 7G, H**, max JO_2; p = 0.002 and conductance; p=0.021).

For Δψm, the results suggest that both rehabilitation groups exhibited a less polarized Δψm compared to the VML+Saline when utilizing both carbohydrate and fat substrates (**Figure 8D**). Notably, mitochondrial bioenergetic efficiency plots showed a left and upward shift in the rehabilitation groups, independent of saline or SS-31 **(Figure 8E)**, reflecting enhanced respiratory capacity coupled with a depolarized Δψm at any given energy demand. These results suggest that the rehabilitation groups are more efficient at utilizing Δp for ATP synthesis compared to VML+saline controls (no rehabilitation) and that electrons are appropriately used in Complex-IV to reduce O_2 to 2 H_2O. ROS emissions were 63% and 48% less in muscle fiber bundles from VML+SS-31+Rehabilitation mice for carbohydrate and fat substrates, respectively, compared to the VML-Saline (**Figure 8K, L**, $p \leq 0.001$). Additionally, carbohydrate-derived ROS production was reduced in both rehabilitation groups, independent of SS-31 intervention (**Figure 8K**, $p \leq 0.010$). There was no statistical difference in ROS production for fat substrate across groups; however, AoxBC was 22% and 32% greater in the fiber bundles from VML+SS-

31+Rehabilitation with carbohydrates and fat substrates, respectively, compared to VML-Saline (**Figure 8K, L**, $p \leq 0.001$).

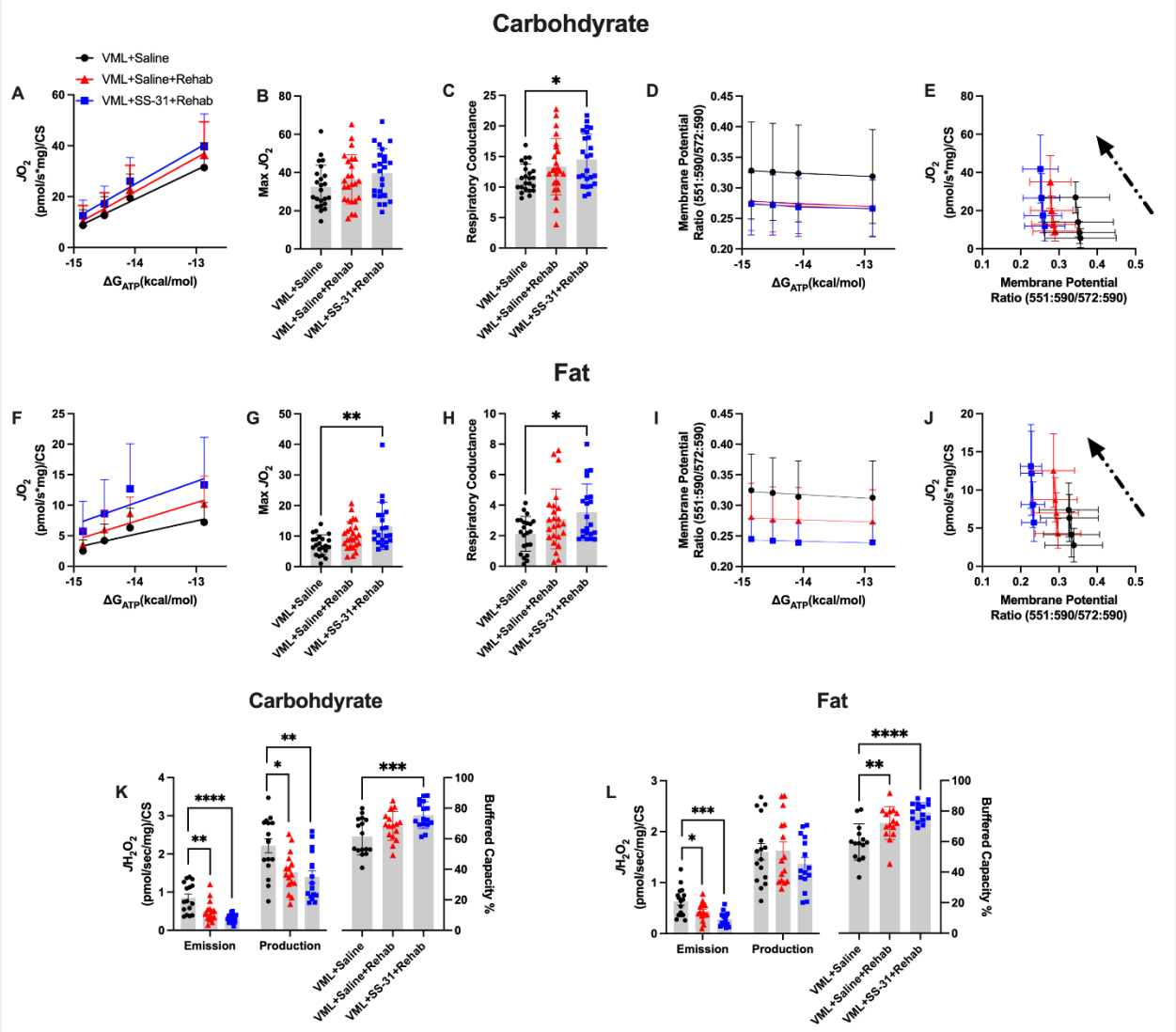

Figure 4.8. Effect of SS-31 metabolic adaptations to rehabilitation after VML injury. **A,F:** The relationship between ATP re-synthesis demand (ΔG_{ATP}) and mitochondrial oxygen consumption (JO_2) normalized to citrate synthase (CS) activity for carbohydrate and fat substrates, respectively, at 8-weeks post-injury. **B,G:** Maximal JO_2 for carbohydrate and fat substrates, respectively, at 8-weeks post-injury. **C,H:** Respiratory conductance for carbohydrate and fat substrates, respectively, at 8-weeks post-injury. **D,I:** The relationship between ΔG_{ATP} and mitochondrial membrane potential for carbohydrate and fat substrates, respectively, at 8-weeks post-injury. **E,J:** The relationship between JO_2 and mitochondrial membrane potential (i.e., bioenergetic efficiency) for carbohydrate and fat substrates, respectively, at 8-weeks post-injury. The arrows indicate the up, leftward shift with rehabilitation and rehabilitation with SS-31 intervention. **K,L:** Reactive oxygen species emission, production, and antioxidant buffer capacity for carbohydrate and fat substrates, respectively, at 8-weeks post-injury. Statistical significance was determined by one-way ANOVA with Tukey's HSD post-hoc test. Data are expressed as mean ± SD. *p < 0.05, **p < 0.01, ***p < 0.001, and ****p < 0.0001. dpi, days post-injury. AoxBC, antioxidant buffering capacity. ROS, reactive oxygen species.

4. Discussion

The objectives of this study were to interrogate the role of mitochondrial ROS in the mitochondrial pathophysiology associated with VML injury (Heo et al., 2023; McFaline-Figueroa et al., 2022, 2023; Southern et al., 2019) and to determine if augmenting the antioxidant buffering capacity of VML-injured muscle improve its adaptive capability to rehabilitation. Our findings reveal that the disrupted mitochondrial bioenergetics after VML injury are associated with greater mitochondrial ROS production that is not adequately buffered by endogenous antioxidant enzymes. Manipulating the AoxBC with SS-31 led to greater respiratory capacity and bioenergetic efficiency, strengthening the causal relationship between ROS and mitochondrial dysfunction in the context of VML. Our findings also reveal that manipulating the AoxBC with antioxidant SS-31 partially improved rehabilitation capability. These findings establish a clear relationship between VML injury and redox imbalance, highlighting the role of oxidative stress in driving the chronic sequelae of VML.

The direct quantification of mitochondrial ROS emissions herein strongly supports the argument that bioenergetic inefficiency generates excessive ROS in VML-injured muscle. *In vivo*, mitochondrial respiration is tightly coupled to ATP demand, where increased energy requirements promote ADP-driven oxidative phosphorylation, leading to $\Delta\psi m$ dissipation as protons flow through ATP synthase. However, VML injury-induced hyperpolarized $\Delta\psi m$ with lower respiratory capacity would reflect a dysregulation to effectively utilize the Δp for ATP production. Moreover, the data showed electron flow congestion (e.g., reduced respiratory conductance) within the electron transport chain. This potentially causes electron backflow and superoxide production at complexes-I, -II, and -III. Together with bioenergetic inefficiency after

VML injury, ROS emission and AoxBC were compromised in mitochondria from VML-injured skeletal muscle.

The antioxidant SS-31 was selected to address ROS emissions in VML-injured muscle because SS-31 is known to localize within mitochondria, enhancing oxidative phosphorylation efficiency and improving the coupling between Δψm and ATP synthesis as its primary mechanism of action (Szeto, 2014). Consistent with previous studies (Anderson et al., 2009; Campbell et al., 2019; Pharaoh et al., 2023), the current study indicates improved bioenergetic efficiency, revealing enhanced respiratory capacity (i.e., electron conductance), improved electron flow within the electron transport chain along with less polarized Δψm at any given energy demand following SS-31 treatment in VML-injured mitochondria. These results suggest that mitochondria from SS-31-treated skeletal muscle possess an improved capacity to accept electrons at complex-IV, facilitating more efficient oxygen consumption while reducing electron congestion and subsequent superoxide leakage from complexes I-III. We note that to fully elucidate the coupling between bioenergetic efficiency (e.g., $J\mathrm{O}_2$ vs. Δψm) and ATP re-synthesis, the ATP synthesis rate (JATP) and the P:O (ATP production to oxygen consumption) ratio are needed in parallel with current bioenergetic assessments. This approach would provide a more precise quantification of mitochondrial ATP coupling efficiency per oxygen and, thus, a more accurate comprehensive diagnosis of overall mitochondrial bioenergetics.

The exact mechanism of SS-31 beneficial effects in VML-injured muscle remains unclear. SS-31 accumulates in mitochondria up to a 1,000 times and binds to the cardiolipin-rich inner-mitochondrial membrane (Birk et al., 2013; K. Zhao et al., 2004), enabling it to play a crucial role in preserving mitochondrial function (Birk et al., 2014) while exhibiting low toxicity and favorable pharmacokinetics (Allingham et al., 2022; Karaa et al., 2020, 2023; Reid

Thompson et al., 2021). Unexpectedly, neither VML injury nor SS-31 had an effect on cardiolipin remodeling. We hypothesize a number of potential mechanisms coupling SS-31 to mitochondrial function based on the previous works and the current results. First, SS-31 may reduce ROS through indirect mechanisms that protect against electron leakage at complex-I through -III by enhancing electron flow through the electron transport chain. The prevention of electron gridlock and backflow minimizes ROS production at key sites. This could be associated with the functional improvement of complexes in the electron transport chain. Chavez et al. demonstrated that SS-31 cross-linked with various subunits of the complex-III, -IV, and -V (Chavez et al., 2020). Second, the beneficial effects of SS-31 may be partially mediated by improving mitochondrial redox balance through an enhanced NADPH-dependent antioxidant defense system. A protein-protein interactome analysis indicated that SS-31 directly binds to IDH2 (Chavez et al., 2020) to potentially regulate redox homeostasis by generating NADPH. This study suggests that it is plausible that when SS-31 interacts with IDH2, its positive charges may contribute to widening the cleft between the enzyme's domains, potentially influencing IDH2 activity (Chavez et al., 2020).

Unexpectedly, despite functional data strongly demonstrating the impacts of VML and SS-31 intervention on mitochondrial bioenergetics and redox balance, there was minimal evidence of VML or SS-31 intervention affecting the mitochondrial proteome. This suggests the involvement of various regulatory factors, such as post-translational modifications, subcellular localizations, conformational changes, and protein-protein interactions (Bakhtina et al., 2023). Other studies showed the role of SS-31 in maintaining redox homeostasis. For example, Hou et al. found that SS-31 administration significantly inhibited the expression of the thioredoxin-interacting protein, which inhibits thioredoxin and reduces antioxidant function in diabetic

conditions (Hou et al., 2016). Moreover, SS-31 reduced thiol-based redox alterations in aged muscle mitochondria (Campbell et al., 2019). Taken together, these findings suggest that SS-31 not only reduces mitochondrial ROS production at its source but also enhances the cell's ability to detoxify ROS, thereby preventing oxidative damage in VML-injured mitochondria, although more comprehensive multi-omics approaches are needed to capture the full complexity of VML injury and further target molecular mechanisms to optimize therapeutic strategies.

Pre-treatment of SS-31 prior to rehabilitation post-VML injury had only modest effects on the adaptive capability of the remaining muscle. Importantly, there was no benefit of SS-31 on muscle strength adaptations, both for muscle strength relative to body mass and muscle strength relative to muscle mass, a marker of muscle quality. The most straightforward interpretation of this is that ROS emissions and oxidative stress are not the primary determinants of poor contractile adaptations to rehabilitation after VML injury. VML injury is marked by a reduction in muscle fiber recruitment due to damaged neuromuscular junctions, a loss in the total number of muscle fibers due to a lack of muscle regeneration, and changes in muscle fiber force transmission throughout the muscle due to fibrotic tissue deposition. Although ROS emissions may play a role in these changes, attenuating the ROS emissions with SS-31 is not effective at overcoming the totality of the pathophysiology and improving the adaptive capability to rehabilitation.

Evidence supporting the effectiveness for SS-31 pre-treatment to bolster metabolic adaptive capability to rehabilitation was modest. Compared to VML-injured mice with no rehabilitation, SS-31-treated mice had notable improvements in respiratory conductance, bioenergetic efficiency, ROS emissions, and AoxBC with rehabilitation; however, there were no statistically significant differences in outcomes between SS-31-treated and saline-treated

rehabilitation groups. Moreover, Saline-treated mice also had notable improvements in bioenergetic efficiency and ROS emissions.

Taken together, this study provides compelling evidence that VML injury significantly impairs mitochondrial bioenergetic efficiency and disrupts redox balance, contributing to metabolic dysfunction. SS-31 treatment effectively restores mitochondrial function by improving electron transport efficiency, reducing oxidative stress, and maintaining redox homeostasis. Additionally, the combination of SS-31 with rehabilitation demonstrates a synergistic effect, partially amplifying these benefits and highlighting the potential of an integrative therapeutic approach to ameliorate the metabolic pathophysiology associated with VML-injured muscle. Despite these promising outcomes, a gap remains between current therapeutic interventions and the muscle function following VML injury. Therefore, further studies are required to find the most effective regenerative and rehabilitative strategies to restore muscle function following VML and to prove the molecular mechanisms of the strategy.

References

Allingham, M. J., Mettu, P. S., & Cousins, S. W. (2022). Phase 1 Clinical Trial of Elamipretide in Intermediate Age-Related Macular Degeneration and High-Risk Drusen: ReCLAIM High-Risk Drusen Study. *Ophthalmology Science*, *2*(1), 100095. https://doi.org/10.1016/j.xops.2021.100095

Anderson, E. J., Lustig, M. E., Boyle, K. E., Woodlief, T. L., Kane, D. A., Lin, C.-T., Price, J. W., Kang, L., Rabinovitch, P. S., Szeto, H. H., Houmard, J. A., Cortright, R. N., Wasserman, D. H., & Neufer, P. D. (2009). Mitochondrial H2O2 emission and cellular redox state link excess fat intake to insulin resistance in both rodents and humans. *The Journal of Clinical Investigation*, *119*(3), 573–581. https://doi.org/10.1172/JCI37048

Bakhtina, A. A., Pharaoh, G. A., Campbell, M. D., Keller, A., Stuppard, R. S., Marcinek, D. J., & Bruce, J. E. (2023). Skeletal muscle mitochondrial interactome remodeling is linked to functional decline in aged female mice. *Nature Aging*, *3*(3), 313–326. https://doi.org/10.1038/s43587-023-00366-5

Birk, A. V., Chao, W. M., Bracken, C., Warren, J. D., & Szeto, H. H. (2014). Targeting mitochondrial cardiolipin and the cytochrome c/cardiolipin complex to promote electron transport and optimize mitochondrial ATP synthesis. *British Journal of Pharmacology*, *171*(8), 2017–2028. https://doi.org/10.1111/bph.12468

Birk, A. V., Liu, S., Soong, Y., Mills, W., Singh, P., Warren, J. D., Seshan, S. V., Pardee, J. D., & Szeto, H. H. (2013). The mitochondrial-targeted compound SS-31 re-energizes ischemic mitochondria by interacting with cardiolipin. *Journal of the American Society of Nephrology: JASN*, *24*(8), 1250–1261. https://doi.org/10.1681/ASN.2012121216

Brand, M. D. (2016). Mitochondrial generation of superoxide and hydrogen peroxide as the source of mitochondrial redox signaling. *Free Radical Biology & Medicine*, *100*, 14–31. https://doi.org/10.1016/j.freeradbiomed.2016.04.001

Brand, M. D., & Nicholls, D. G. (2011). Assessing mitochondrial dysfunction in cells. *The Biochemical Journal*, *435*(2), 297–312. https://doi.org/10.1042/BJ20110162

Campbell, M. D., Duan, J., Samuelson, A. T., Gaffrey, M. J., Merrihew, G. E., Egertson, J. D., Wang, L., Bammler, T. K., Moore, R. J., White, C. C., Kavanagh, T. J., Voss, J. G., Szeto, H. H., Rabinovitch, P. S., MacCoss, M. J., Qian, W.-J., & Marcinek, D. J. (2019). Improving mitochondrial function with SS-31 reverses age-related redox stress and improves exercise tolerance in aged mice. *Free Radical Biology & Medicine*, *134*, 268–281. https://doi.org/10.1016/j.freeradbiomed.2018.12.031

Chavez, J. D., Tang, X., Campbell, M. D., Reyes, G., Kramer, P. A., Stuppard, R., Keller, A., Zhang, H., Rabinovitch, P. S., Marcinek, D. J., & Bruce, J. E. (2020). Mitochondrial protein interaction landscape of SS-31. *Proceedings of the National Academy of Sciences of the United States of America*, *117*(26), 15363–15373. https://doi.org/10.1073/pnas.2002250117

Fisher-Wellman, K. H., Davidson, M. T., Narowski, T. M., Lin, C.-T., Koves, T. R., & Muoio, D. M. (2018). Mitochondrial Diagnostics: A Multiplexed Assay Platform for Comprehensive Assessment of Mitochondrial Energy Fluxes. *Cell Reports*, *24*(13), 3593-3606.e10. https://doi.org/10.1016/j.celrep.2018.08.091

Gelman, S. J., Naser, F., Mahieu, N. G., McKenzie, L. D., Dunn, G. P., Chheda, M. G., & Patti, G. J. (2018). Consumption of NADPH for 2-HG Synthesis Increases Pentose Phosphate

Pathway Flux and Sensitizes Cells to Oxidative Stress. *Cell Reports*, *22*(2), 512–522. https://doi.org/10.1016/j.celrep.2017.12.050

Heo, J., Schifino, A. G., McFaline-Figueroa, J., Miller, D. L., Hoffman, J. R., Noble, E. E., Greising, S. M., & Call, J. A. (2023). Differential effects of Western diet and traumatic muscle injury on skeletal muscle metabolic regulation in male and female mice. *Journal of Cachexia, Sarcopenia and Muscle*, *14*(6), 2835–2850. https://doi.org/10.1002/jcsm.13361

Hou, Y., Li, S., Wu, M., Wei, J., Ren, Y., Du, C., Wu, H., Han, C., Duan, H., & Shi, Y. (2016). Mitochondria-targeted peptide SS-31 attenuates renal injury via an antioxidant effect in diabetic nephropathy. *American Journal of Physiology. Renal Physiology*, *310*(6), F547-559. https://doi.org/10.1152/ajprenal.00574.2014

Johnson, J. M., Ferrara, P. J., Verkerke, A. R. P., Coleman, C. B., Wentzler, E. J., Neufer, P. D., Kew, K. A., de Castro Brás, L. E., & Funai, K. (2018). Targeted overexpression of catalase to mitochondria does not prevent cardioskeletal myopathy in Barth syndrome. *Journal of Molecular and Cellular Cardiology*, *121*, 94–102. https://doi.org/10.1016/j.yjmcc.2018.07.001

Johnson, J., Mercado-Ayón, E., Clark, E., Lynch, D., & Lin, H. (2021). Drp1-dependent peptide reverse mitochondrial fragmentation, a homeostatic response in Friedreich ataxia. *Pharmacology Research & Perspectives*, *9*(3), e00755. https://doi.org/10.1002/prp2.755

Karaa, A., Bertini, E., Carelli, V., Cohen, B. H., Enns, G. M., Falk, M. J., Goldstein, A., Gorman, G. S., Haas, R., Hirano, M., Klopstock, T., Koenig, M. K., Kornblum, C., Lamperti, C., Lehman, A., Longo, N., Molnar, M. J., Parikh, S., Phan, H., … MMPOWER-3 Trial Investigators. (2023). Efficacy and Safety of Elamipretide in Individuals With Primary

Mitochondrial Myopathy: The MMPOWER-3 Randomized Clinical Trial. *Neurology*, *101*(3), e238–e252. https://doi.org/10.1212/WNL.0000000000207402

Karaa, A., Haas, R., Goldstein, A., Vockley, J., & Cohen, B. H. (2020). A randomized crossover trial of elamipretide in adults with primary mitochondrial myopathy. *Journal of Cachexia, Sarcopenia and Muscle*, *11*(4), 909–918. https://doi.org/10.1002/jcsm.12559

Karaa, A., Haas, R., Goldstein, A., Vockley, J., Weaver, W. D., & Cohen, B. H. (2018). Randomized dose-escalation trial of elamipretide in adults with primary mitochondrial myopathy. *Neurology*, *90*(14), e1212–e1221. https://doi.org/10.1212/WNL.0000000000005255

Koves, T. R., Zhang, G.-F., Davidson, M. T., Chaves, A. B., Crown, S. B., Johnson, J. M., Slentz, D. H., Grimsrud, P. A., & Muoio, D. M. (2023). Pyruvate-supported flux through medium-chain ketothiolase promotes mitochondrial lipid tolerance in cardiac and skeletal muscles. *Cell Metabolism*, *35*(6), 1038-1056.e8. https://doi.org/10.1016/j.cmet.2023.03.016

Larsen, S., Nielsen, J., Hansen, C. N., Nielsen, L. B., Wibrand, F., Stride, N., Schroder, H. D., Boushel, R., Helge, J. W., Dela, F., & Hey-Mogensen, M. (2012). Biomarkers of mitochondrial content in skeletal muscle of healthy young human subjects. *The Journal of Physiology*, *590*(14), 3349–3360. https://doi.org/10.1113/jphysiol.2012.230185

Lynch, D. R., & Farmer, G. (2021). Mitochondrial and metabolic dysfunction in Friedreich ataxia: Update on pathophysiological relevance and clinical interventions. *Neuronal Signaling*, *5*(2), NS20200093. https://doi.org/10.1042/NS20200093

McFaline-Figueroa, J., Hunda, E. T., Heo, J., Winders, E. A., Greising, S. M., & Call, J. A. (2023). The bioenergetic “CK Clamp” technique detects substrate-specific changes in

mitochondrial respiration and membrane potential during early VML injury pathology. *Frontiers in Physiology*, *14*, 1178213. https://doi.org/10.3389/fphys.2023.1178213

McFaline-Figueroa, J., Schifino, A. G., Nichenko, A. S., Lord, M. N., Hunda, E. T., Winders, E. A., Noble, E. E., Greising, S. M., & Call, J. A. (2022). Pharmaceutical Agents for Contractile-Metabolic Dysfunction After Volumetric Muscle Loss. *Tissue Engineering. Part A*, *28*(17–18), 795–806. https://doi.org/10.1089/ten.TEA.2022.0036

McLaughlin, K. L., Hagen, J. T., Coalson, H. S., Nelson, M. A. M., Kew, K. A., Wooten, A. R., & Fisher-Wellman, K. H. (2020). Novel approach to quantify mitochondrial content and intrinsic bioenergetic efficiency across organs. *Scientific Reports*, *10*(1), 17599. https://doi.org/10.1038/s41598-020-74718-1

Mettu, P. S., Allingham, M. J., & Cousins, S. W. (2022). Phase 1 Clinical Trial of Elamipretide in Dry Age-Related Macular Degeneration and Noncentral Geographic Atrophy: ReCLAIM NCGA Study. *Ophthalmology Science*, *2*(1), 100086. https://doi.org/10.1016/j.xops.2021.100086

Mitchell, W., Ng, E. A., Tamucci, J. D., Boyd, K. J., Sathappa, M., Coscia, A., Pan, M., Han, X., Eddy, N. A., May, E. R., Szeto, H. H., & Alder, N. N. (2020). The mitochondria-targeted peptide SS-31 binds lipid bilayers and modulates surface electrostatics as a key component of its mechanism of action. *The Journal of Biological Chemistry*, *295*(21), 7452–7469. https://doi.org/10.1074/jbc.RA119.012094

Munro, D., Banh, S., Sotiri, E., Tamanna, N., & Treberg, J. R. (2016). The thioredoxin and glutathione-dependent H2O2 consumption pathways in muscle mitochondria: Involvement in H2O2 metabolism and consequence to H2O2 efflux assays. *Free Radical Biology & Medicine*, *96*, 334–346. https://doi.org/10.1016/j.freeradbiomed.2016.04.014

Murphy, M. P. (2009). How mitochondria produce reactive oxygen species. *The Biochemical Journal*, *417*(1), 1–13. https://doi.org/10.1042/BJ20081386

Pennington, E. R., Funai, K., Brown, D. A., & Shaikh, S. R. (2019). The role of cardiolipin concentration and acyl chain composition on mitochondrial inner membrane molecular organization and function. *Biochimica Et Biophysica Acta. Molecular and Cell Biology of Lipids*, *1864*(7), 1039–1052. https://doi.org/10.1016/j.bbalip.2019.03.012

Pharaoh, G., Kamat, V., Kannan, S., Stuppard, R. S., Whitson, J., Martín-Pérez, M., Qian, W.-J., MacCoss, M. J., Villén, J., Rabinovitch, P., Campbell, M. D., Sweet, I. R., & Marcinek, D. J. (2023). The mitochondrially targeted peptide elamipretide (SS-31) improves ADP sensitivity in aged mitochondria by increasing uptake through the adenine nucleotide translocator (ANT). *GeroScience*, *45*(6), 3529–3548. https://doi.org/10.1007/s11357-023-00861-y

Prola, A., Blondelle, J., Vandestienne, A., Piquereau, J., Denis, R. G. P., Guyot, S., Chauvin, H., Mourier, A., Maurer, M., Henry, C., Khadhraoui, N., Gallerne, C., Molinié, T., Courtin, G., Guillaud, L., Gressette, M., Solgadi, A., Dumont, F., Castel, J., … Pilot-Storck, F. (2021). Cardiolipin content controls mitochondrial coupling and energetic efficiency in muscle. *Science Advances*, *7*(1), eabd6322. https://doi.org/10.1126/sciadv.abd6322

Quinlan, C. L., Perevoschikova, I. V., Goncalves, R. L. S., Hey-Mogensen, M., & Brand, M. D. (2013). The determination and analysis of site-specific rates of mitochondrial reactive oxygen species production. *Methods in Enzymology*, *526*, 189–217. https://doi.org/10.1016/B978-0-12-405883-5.00012-0

Quinlan, C. L., Perevoshchikova, I. V., Hey-Mogensen, M., Orr, A. L., & Brand, M. D. (2013). Sites of reactive oxygen species generation by mitochondria oxidizing different substrates. *Redox Biology*, *1*(1), 304–312. https://doi.org/10.1016/j.redox.2013.04.005

Rath, S., Sharma, R., Gupta, R., Ast, T., Chan, C., Durham, T. J., Goodman, R. P., Grabarek, Z., Haas, M. E., Hung, W. H. W., Joshi, P. R., Jourdain, A. A., Kim, S. H., Kotrys, A. V., Lam, S. S., McCoy, J. G., Meisel, J. D., Miranda, M., Panda, A., … Mootha, V. K. (2021). MitoCarta3.0: An updated mitochondrial proteome now with sub-organelle localization and pathway annotations. *Nucleic Acids Research*, *49*(D1), D1541–D1547. https://doi.org/10.1093/nar/gkaa1011

Raymond-Pope, C. J., Basten, A. M., Bruzina, A. S., McFaline-Figueroa, J., Lillquist, T. J., Call, J. A., & Greising, S. M. (2023). Restricted physical activity after volumetric muscle loss alters whole-body and local muscle metabolism. *The Journal of Physiology*, *601*(4), 743–761. https://doi.org/10.1113/JP283959

Reid Thompson, W., Hornby, B., Manuel, R., Bradley, E., Laux, J., Carr, J., & Vernon, H. J. (2021). A phase 2/3 randomized clinical trial followed by an open-label extension to evaluate the effectiveness of elamipretide in Barth syndrome, a genetic disorder of mitochondrial cardiolipin metabolism. *Genetics in Medicine: Official Journal of the American College of Medical Genetics*, *23*(3), 471–478. https://doi.org/10.1038/s41436-020-01006-8

Schifino, A. G., Cooley, M. A., Zhong, R. X., Heo, J., Hoffman, D. B., Warren, G. L., Greising, S. M., & Call, J. A. (2024). Tibial bone strength is negatively affected by volumetric muscle loss injury to the adjacent muscle in male mice. *Journal of Orthopaedic*

Research: Official Publication of the Orthopaedic Research Society, *42*(1), 123–133. https://doi.org/10.1002/jor.25643

Schifino, A. G., Raymond-Pope, C. J., Heo, J., McFaline-Figueroa, J., Call, J. A., & Greising, S. M. (2023). Resistance wheel running improves contractile strength, but not metabolic capacity, in a murine model of volumetric muscle loss injury. *Experimental Physiology*, *108*(10), 1282–1294. https://doi.org/10.1113/EP091284

Smith, C. D., Schmidt, C. A., Lin, C.-T., Fisher-Wellman, K. H., & Neufer, P. D. (2020). Flux through mitochondrial redox circuits linked to nicotinamide nucleotide transhydrogenase generates counterbalance changes in energy expenditure. *The Journal of Biological Chemistry*, *295*(48), 16207–16216. https://doi.org/10.1074/jbc.RA120.013899

Southern, W. M., Nichenko, A. S., Tehrani, K. F., McGranahan, M. J., Krishnan, L., Qualls, A. E., Jenkins, N. T., Mortensen, L. J., Yin, H., Yin, A., Guldberg, R. E., Greising, S. M., & Call, J. A. (2019). PGC-1α overexpression partially rescues impaired oxidative and contractile pathophysiology following volumetric muscle loss injury. *Scientific Reports*, *9*(1), 4079. https://doi.org/10.1038/s41598-019-40606-6

Sparagna, G. C., Johnson, C. A., McCune, S. A., Moore, R. L., & Murphy, R. C. (2005). Quantitation of cardiolipin molecular species in spontaneously hypertensive heart failure rats using electrospray ionization mass spectrometry. *Journal of Lipid Research*, *46*(6), 1196–1204. https://doi.org/10.1194/jlr.M500031-JLR200

Szeto, H. H. (2014). First-in-class cardiolipin-protective compound as a therapeutic agent to restore mitochondrial bioenergetics. *British Journal of Pharmacology*, *171*(8), 2029–2050. https://doi.org/10.1111/bph.12461

Szeto, H. H., & Birk, A. V. (2014). Serendipity and the discovery of novel compounds that restore mitochondrial plasticity. *Clinical Pharmacology and Therapeutics*, *96*(6), 672–683. https://doi.org/10.1038/clpt.2014.174

Szeto, H. H., & Liu, S. (2018). Cardiolipin-targeted peptides rejuvenate mitochondrial function, remodel mitochondria, and promote tissue regeneration during aging. *Archives of Biochemistry and Biophysics*, *660*, 137–148. https://doi.org/10.1016/j.abb.2018.10.013

Williams, A. S., Crown, S. B., Lyons, S. P., Koves, T. R., Wilson, R. J., Johnson, J. M., Slentz, D. H., Kelly, D. P., Grimsrud, P. A., Zhang, G.-F., & Muoio, D. M. (2024). Ketone flux through BDH1 supports metabolic remodeling of skeletal and cardiac muscles in response to intermittent time-restricted feeding. *Cell Metabolism*, *36*(2), 422-437.e8. https://doi.org/10.1016/j.cmet.2024.01.007

Zhao, H., Li, H., Hao, S., Chen, J., Wu, J., Song, C., Zhang, M., Qiao, T., & Li, K. (2017). Peptide SS-31 upregulates frataxin expression and improves the quality of mitochondria: Implications in the treatment of Friedreich ataxia. *Scientific Reports*, *7*(1), 9840. https://doi.org/10.1038/s41598-017-10320-2

Zhao, K., Luo, G., Giannelli, S., & Szeto, H. H. (2005). Mitochondria-targeted peptide prevents mitochondrial depolarization and apoptosis induced by tert-butyl hydroperoxide in neuronal cell lines. *Biochemical Pharmacology*, *70*(12), 1796–1806. https://doi.org/10.1016/j.bcp.2005.08.022

Zhao, K., Zhao, G.-M., Wu, D., Soong, Y., Birk, A. V., Schiller, P. W., & Szeto, H. H. (2004). Cell-permeable peptide antioxidants targeted to inner mitochondrial membrane inhibit mitochondrial swelling, oxidative cell death, and reperfusion injury. *The Journal of Biological Chemistry*, *279*(33), 34682–34690. https://doi.org/10.1074/jbc.M402999200

Supplemental Figures

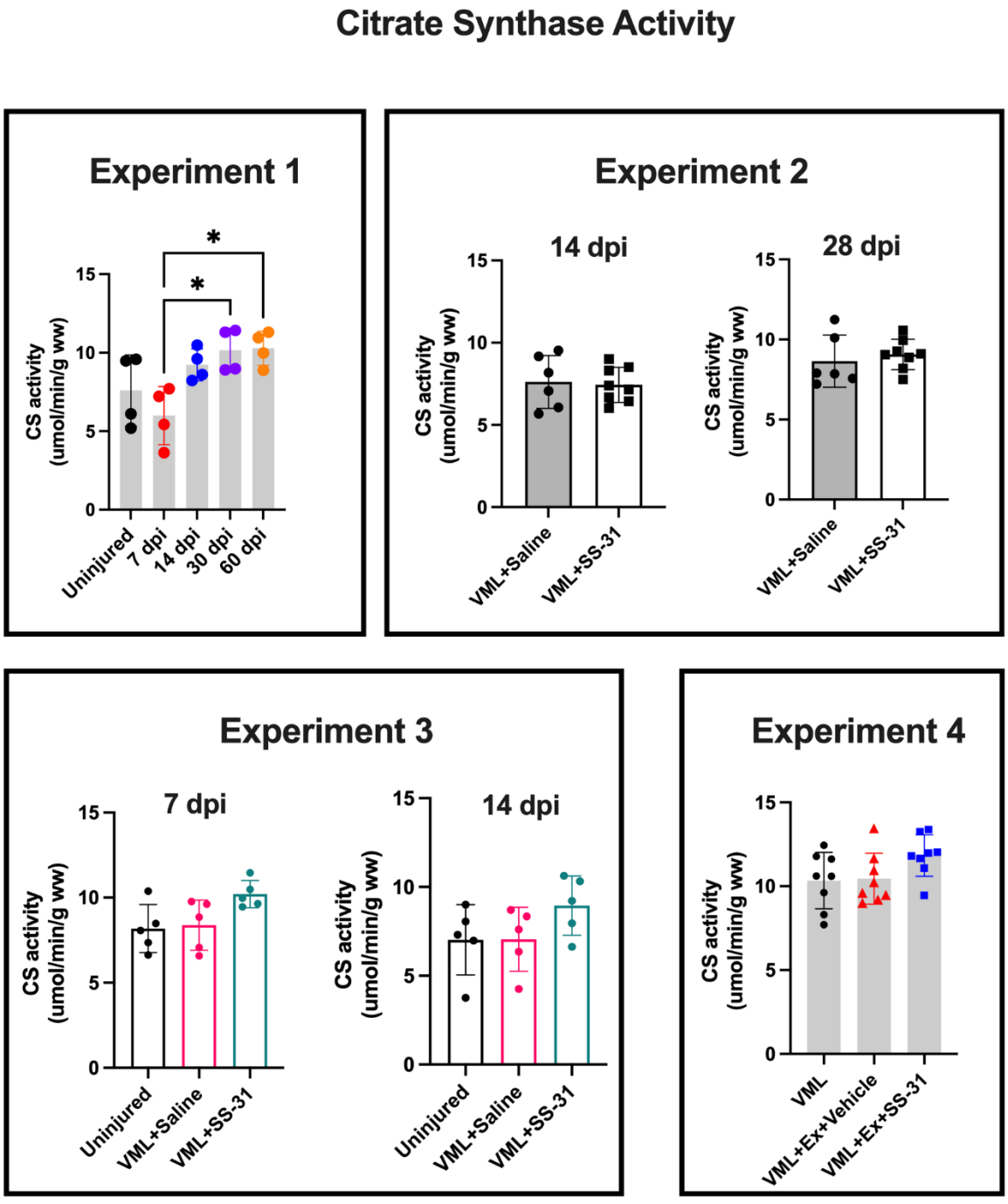

Supplemental Figure 4.1. CS activity in all experiments.

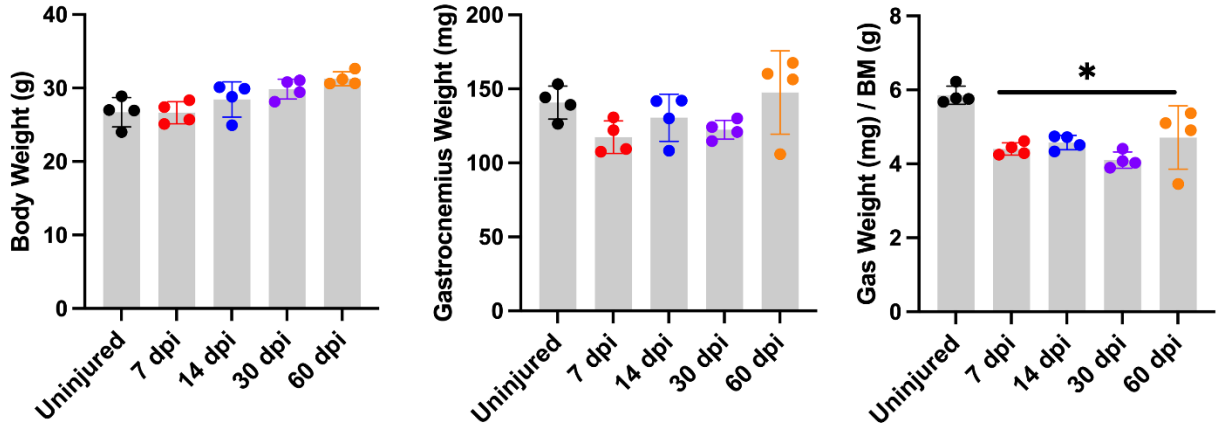

Supplemental Figure 4.2. Experiment 1 (timecourse analysis); body weight, muscle mass, and normalized muscle mass.

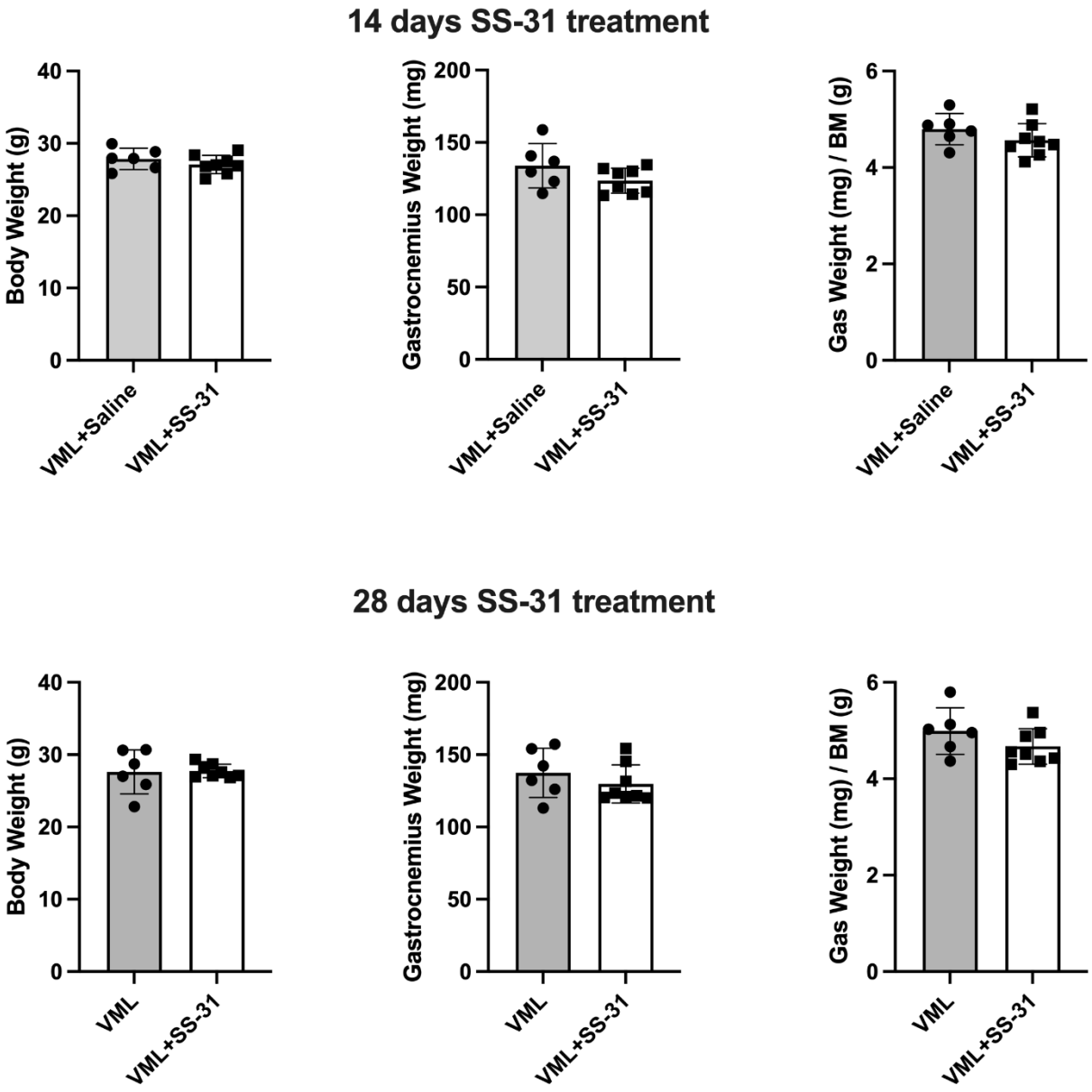

Supplemental Figure 4.3. Experiment 2 (VML vs. SS-31). Effects of SS-31 on body weight, muscle mass, and normalized muscle mass after VML injury.

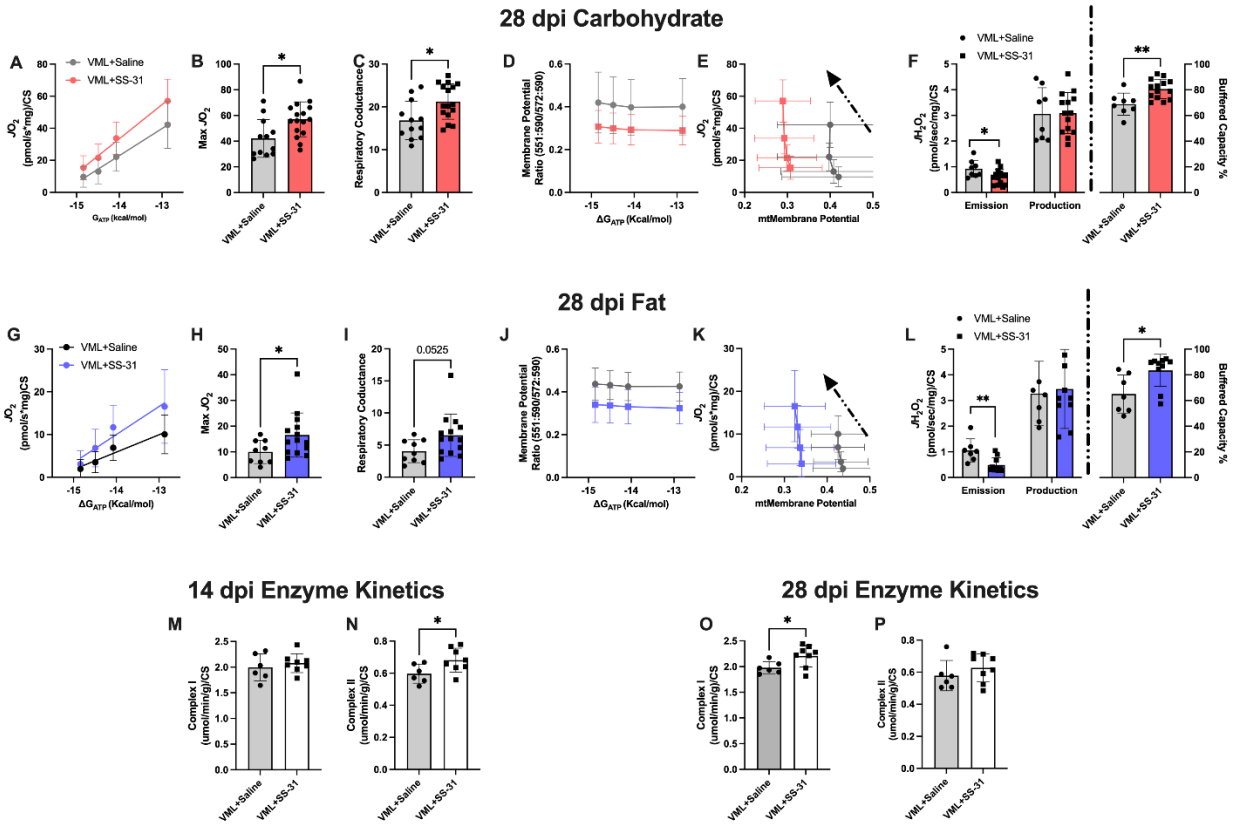

Supplemental Figure 4.4. Experiment 2 (VML vs. SS-31). Effects of SS-31 on mitochondrial function and ROS after VML injury.

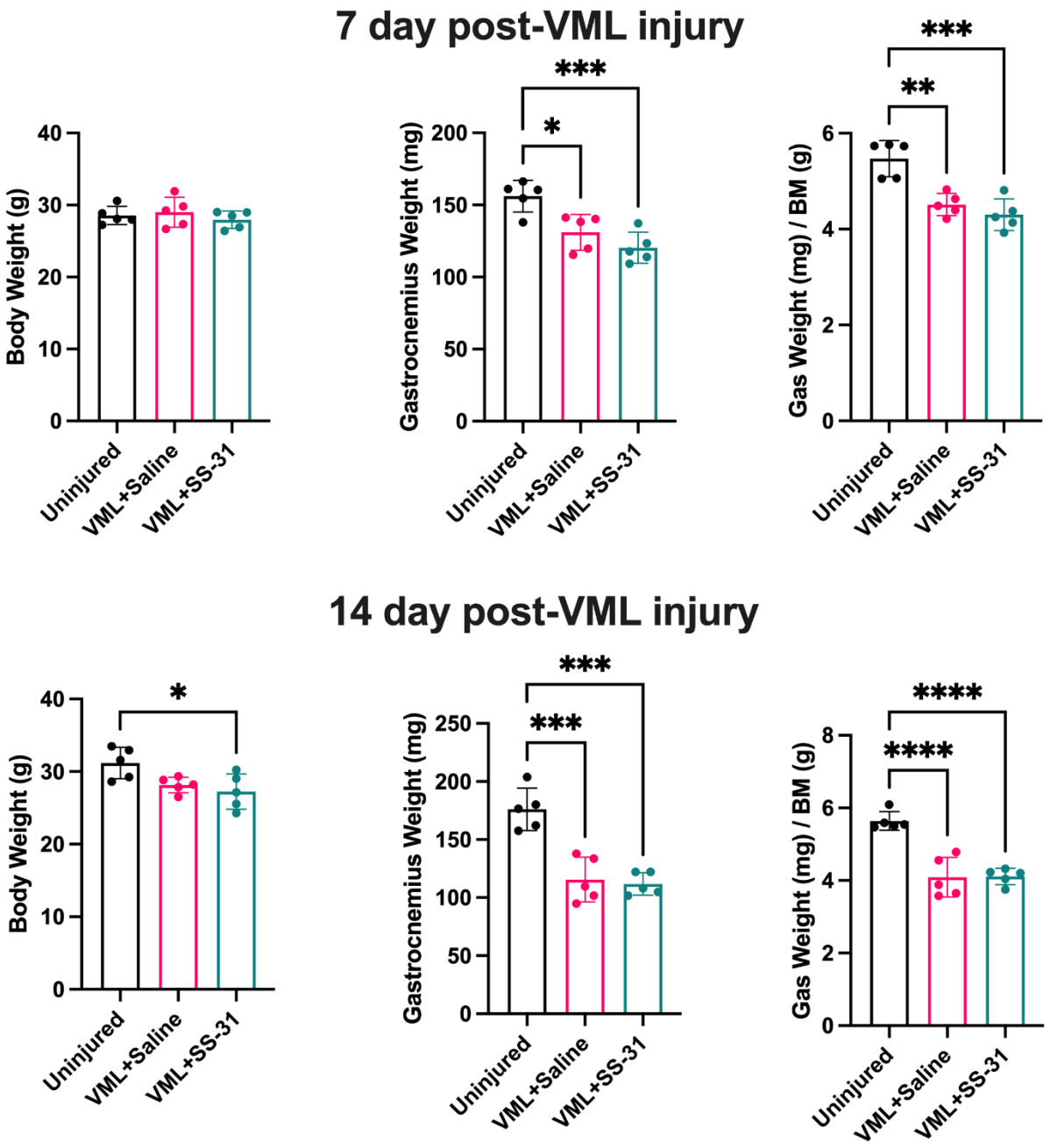

Supplemental Figure 4.5. Experiment 3 (site-specific ROS). Effects of SS-31 on body weight, muscle mass, and normalized muscle mass after VML injury.

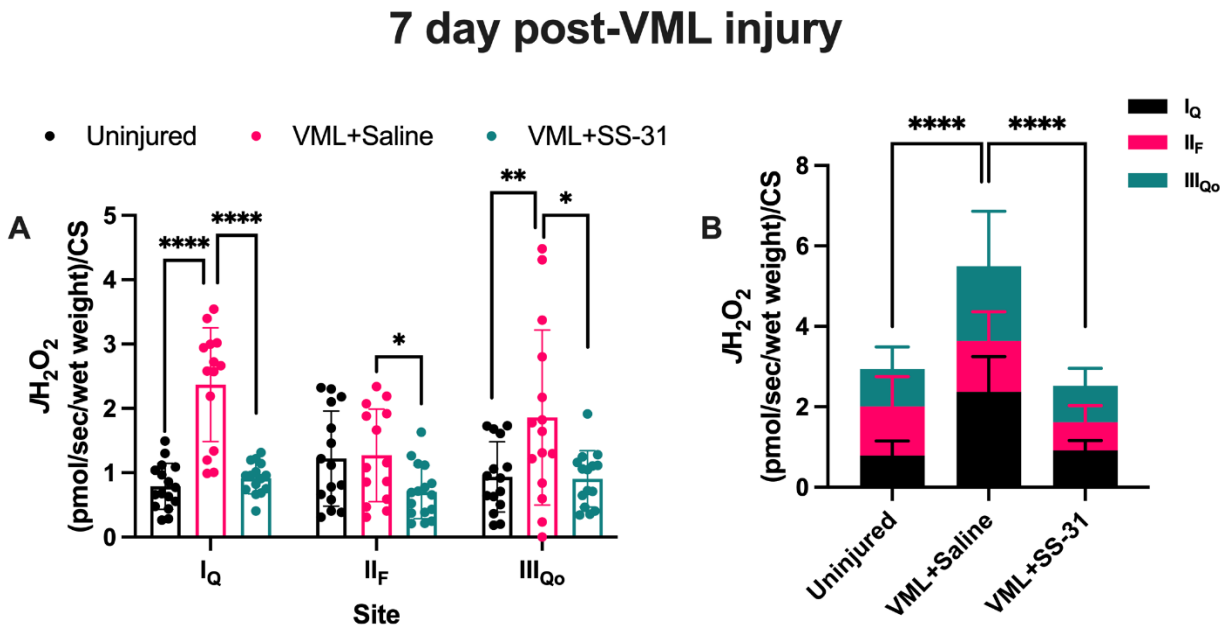

Supplemental Figure 6. Experiment 3 (site-specific ROS). Effects of 7 days treatment of SS-31 on site-specific ROS after VML injury.

CHAPTER 5

17-β ESTRADIOL MITIGATES OVARIECTOMY-INDUCED MITOCHONDRIAL DYSFUNCTION AND REACTIVE OXYGEN SPECIES IN VML-INJURED FEMALE MICE[4]

[4] Junwon Heo, David L. Miller, Jessica R. Hoffman, Reese Groover, Sarah M. Greising, Jarrod A. Call. To be submitted to *Journal of Physiology or American Physiological Journal*

Abstract

The objective of this study is to investigate the role of 17β-estradiol (E2) in modulating mitochondrial bioenergetics and reactive oxygen species (ROS) homeostasis following volumetric muscle loss (VML) injury in female mice. Female C57BL/6J mice were divided into three groups: VML+Sham surgery (VML), VML+Ovariectomized (OVX)+Placebo pellets (VML+OVX+Placebo), and VML+OVX+Estradiol (E2) pellets (VML+OVX+E2). At age 12 weeks of age, OVX surgery was performed, followed by either placebo or E2 pellets implantation. Two weeks after OVX surgery, unilateral VML surgery was conducted on the hindlimb plantar flexors (gastrocnemius, soleus, plantaris muscles). At 3- and 7-days post-injury (dpi), ROS emissions, antioxidant buffering capacity (AoxBC), and transcriptomic profiles were evaluated in the gastrocnemius muscle. At 60 dpi, mitochondrial respiratory capacity, ROS emissions, and AoxBC were measured in permeabilized muscle fibers. The results demonstrated that (a) VML injury led to significant impairments in mitochondrial bioenergetics, increased ROS production, and diminished antioxidant defenses. (b) OVX exacerbates VML-induced decrease in antioxidant defense. However, (c) E2 replacement mitigated these disruptions, improving mitochondrial bioenergetics and AoxBC under E2-deficient condition following VML injury. RNA sequencing and gene set enrichment analysis revealed key shifts in mitochondrial maintenance, oxidative phosphorylation, and metabolic pathways, highlighting the crucial role of E2 in mitochondrial adaptation following traumatic injury in female mice. These findings suggest the therapeutic potential of estradiol in restoring metabolic homeostasis and redox balance following traumatic muscle injury, particularly in naturally or surgically estrogen-deficient conditions. **Key words:** Volumetric Muscle Loss Injury, Sex Differences, Ovarian Hormone , Mitochondria, Reactive Oxygen Species

INTRODUCTION

Volumetric muscle loss (VML) injury results in the non-recoverable loss of muscle mass and function. VML is a significant concern for both military personnel and the general population (Garg et al., 2015; Owens et al., 2008). VML injury can result secondary to any of the 150,000 open fractures or 30,000 gunshot wounds, 36,000 chainsaw accidents, and 13,000 soft-tissue sarcomas that occur annually in the USA. VML leads to irrecoverable muscle loss and various complications, such as fibrosis (Hoffman et al., 2022), metabolic dysfunction (Dalske et al., 2021; Southern et al., 2019), inflammation (Larouche et al., 2023), and permanent functional deficits (Mintz et al., 2020). Research directed toward understanding VML pathophysiology and identifying effective therapies has overwhelmingly focused on male subjects in part due to the higher prevalence of VML in male military servicemembers; however, this has created a knowledge gap in understanding how traumatic muscle injuries may differ between the sexes.

Recently, we published a study that presented evidence of metabolic and biochemical sex differences following a VML injury. Importantly, female mice were not as susceptible to metabolic dysfunction with a combined VML injury and Western Diet compared to male mice (Heo et al., 2023). More recently, we've been interrogating redox balance in the muscle that remains after a VML injury (*Data is not shown here*). Redox balance considers the amount of reactive oxygen species (ROS) produced and the ROS reduction to water via the antioxidant buffering capacity of the tissue. My preliminary data indicates that there is indeed an increase in ROS production (in both males and females) following a VML injury. Intriguingly, the antioxidant buffering capacity of the tissue is depressed at 7- and 14 days after VML injury in males but has already returned to uninjured levels by 14 days post-injury in females. This

suggests a slight protection from redox imbalance in female mice against VML injury compared to males; however, the molecular mechanisms of this protection remain unclear.

Emerging evidence indicates that ovarian hormones play an important role in regulating skeletal muscle contractile function (Greising et al., 2011), metabolism (Torres, Kew, et al., 2018), and redox balance (Bellanti et al., 2013). For example, removing all ovarian hormones through a technique called ovariectomy (OVX) leads to lower mitochondrial dysfunction (Torres, Kew, et al., 2018) and antioxidant gene expression (Baltgalvis et al., 2010; Bellanti et al., 2013) in female mice. On the other hand, 17ß-estradiol treatment, an ovarian hormone, improves all of these factors when repleted after an OVX (Baltgalvis et al., 2010; Bellanti et al., 2013; Torres, Kew, et al., 2018). However, the extent to which ovarian hormones, and 17ß-estradiol in particular, exert these actions in the context of traumatic muscle injury is poorly unknown.

Therefore, the current study aims to investigate the role of estradiol in modulating mitochondrial bioenergetics and ROS homeostasis in female mice subjected to VML injury. We hypothesize that OVX impaired mitochondrial bioenergetics, increased reactive oxygen species, and reduced antioxidant buffering capacity, which is mitigated by estradiol repletion. To test this hypothesis, we evaluated mitochondrial bioenergetics, ROS emission/production, and antioxidant buffering capacity at multiple time points (3, 7, and 60 days post-injury) in VML-injured female mice with and without estradiol replacement. Physiological, metabolic, mitochondrial, and transcriptomic parameters were analyzed to elucidate the protective effects of estradiol on muscle bioenergetics and oxidative stress regulation in the context of VML injury. This study provides valuable insights into potential therapeutic approaches aimed at improving muscle recovery in estrogen-deficient conditions, such as menopause or ovarian dysfunction.

Methods

Animal protocol

All procedures and animal care guidelines were approved and conducted in accordance with the guidelines and regulations of the Institutional Animal Care and Use Committee at the University of Georgia. Procedures were carried out in compliance with the Animal Welfare Act, and the Implementing Animal Welfare Regulations in compliance with the principles of the Guide for the Care and Use of Laboratory Animals. Male and female C57BL/6J mice that were the offspring of breeding pairs obtained from The Jackson Laboratory (stock: 000664) were used for this study.

Study design

Ovariectomy or sham surgery was conducted at 12 weeks of age. 17β-estradiol designed to release 0.18 mg of E2 for 60 days or placebo pellets (Innovative Research of America, Inc.) was inserted at the time of surgery (Baltgalvis et al., 2010; Kararigas et al., 2025). Two weeks later, at age 14 weeks, mice will undergo a unilateral VML surgery from the center of plantar flexor muscles (gastrocnemius/plantaris/soleus). Terminally, 3, 7, and 60 day-post VML injury, uterine mass was recorded as a secondary marker of circulating estrogen levels (Wood et al., 2007). All mice will have access to phytoestrogen-free food (Harlan-Teklad; #2019) to completely exclude exogenous estrogen intake.

Surgical creation of VML injury

VML injury was performed on the posterior compartment of anesthetized (isoflurane inhalation 1.5-3.0%) mice under aseptic surgical conditions as described previously [17, 22]. Mice received buprenorphine (Patterson Veterinary Supply, Inc.; 1.2mg/kg; s. q.) prior to surgery and again at 12- and 24-hours post-surgery for pain management. A single incision was made in

the mid-gastrocnemius to expose posterior compartment muscles. A 4-mm biopsy punch was employed to induce VML (female; 20.17±3.94 mg) from the center of the plantar flexor muscles (gastrocnemius/plantaris/soleus) complex. The skin incision was closed using 6.0 silk suture (ETHICON, 668G S32), and mice were monitored through recovery.

Intraperitoneal glucose tolerance test (ipGTT)

One week before harvest, an intraperitoneal glucose tolerance test (ipGTT) was conducted following glucose injection (2.0g/kg body weight, i.p.) during the light-cycle in the animal facility. After 6 hours of fasting, blood glucose was evaluated before injection and again at 15, 30, 60, and 120 min after injection.

Mitochondrial respiration

High-resolution oxygen respiratory measurements were conducted on permeabilized gastrocnemius fiber bundles using an Oroboros Oxygraph-2K (Oroboros Instruments, Innsbruck, Austria) with a modified creatine kinase (CK) energetic clamp technique (Fisher-Wellman et al., 2018; McFaline-Figueroa et al., 2023). This method precisely controls the extramitochondrial ATP:ADP ratio and ΔG_{ATP} by utilizing excess CK along with defined concentrations of creatine, phosphocreatine (PCr), and adenylates to simulate physiological energy demand shifts. To assess mitochondrial respiratory capacity under near-exercise conditions, fiber bundles were energized with either carbohydrate (5 mM pyruvate, 2 mM malate) or fat (40 μM palmitoyl-carnitine, 2 mM malate) substrates in the presence of CK (20 U/mL), PCr (1 mM), and ATP (5 mM). Cytochrome c (10 μM) was added to verify mitochondrial integrity, followed by sequential PCr titrations (6, 12, 15 mM) to progressively lower ΔG_{ATP} to resting conditions. This approach enables measurement of the linear relationship between ATP:ADP (ΔGATP) and oxygen flux

(JO_2), allowing estimation of respiratory conductance, where a steeper slope indicates greater sensitivity and improved kinetics. The CK clamp models energetic demands and thermodynamic constraints comparable to in vivo conditions. To normalize results, oxygen flux rates were adjusted for tissue wet weight and citrate synthase (CS) activity to account for differences in mitochondrial content (Larsen et al., 2012).

Mitochondrial membrane potential

The Δψm was measured fluorometrically in buffer Z containing 5 mM creatine, using a spectrofluorometer (FluoroMax Plus-C; Horiba Instruments Inc., Irvine, CA, USA) (Fisher-Wellman et al., 2018; McFaline-Figueroa et al., 2023). The membrane potential was assessed with tetramethylrhodamine methyl ester (TMRM) at 30°C, in accordance with the CK clamp assay protocol and with constant stirring. TMRM excitation/emission [(572/590 nm)/(551/590 nm)] fluorescence is quenched, meaning the 572/551 ratio increases with greater mitochondrial membrane polarization. To our knowledge, the 572/551 ratio is represented here as there has been no report validating the conversion of the 572/551 ratio to millivolts in permeabilized muscle fiber.

ROS emission, ROS production, Antioxidants buffering capacity and site-specific ROS

The ROS emission and production were measured in buffer Z supplemented with Amplex Ultrared (5 µM), Cu-Zn superoxide dismutase (25 units/ml), and horseradish peroxidase (1 U/mL) detection system of H2O2 (Ex:Em 565:600), as previously described [8] with a minor modification. After recording the basal rate, ROS emission was assessed by adding 5 mM pyruvate and 2 mM malate (carbohydrate substrates), or 40 µM palmitoyl-carnitine and 5 mM malate (fat substrates). ROS production was assessed by the addition of 1 µM auranofin, an

inhibitor of thioredoxin, and 100 μM carmustine (BCNU), an inhibitor of glutathione reductase. The AoxBC (percentage of ROS buffered by antioxidant enzymes thioredoxin and glutathione reductase) reflects the percentage of ROS produced but not emitted (i.e., (ROS production – ROS emission) / ROS production) x 100) (Smith et al., 2020).

Assessment of mitochondrial enzyme activities

CS activity was assessed using a spectrophotometer (Molecular Devices, San Jose, CA, USA) as previously described (Heo et al., 2023; McFaline-Figueroa et al., 2022). CoA-SH, a byproduct generated by the CS-catalyzed reaction between oxaloacetate and acetyl-CoA, reacts with 5′, 5′-Dithiobis 2-nitrobenzoic acid (DTNB) to produce TNB, which is detected by absorbance at 412 nm.

RNA Sequencing

Total RNA was extracted from mouse gastrocnemius muscle using the RNeasy Fibrous Tissue Mini Kit (Qiagen) and quantified with the NanoDrop One spectrophotometer. RNA was collected from E2-deficient mice 3- and 7-days post-VML injury with or without E2. Libraries were prepared using Illumina TruSeq. Samples were run with at least 20 million paired-end reads using Novoseq 6000 (Illumina) (Novogene, Sacramento, CA). Fastq files were aligned using HISAT2 to GRCm38.p3. Samples were then quantified using salmon through Illumina Dragen v3.7.5 on Amazon Web Services. Gene count files were converted to a counts matrix using tximport (Soneson et al., 2015). The counts matrix was used as input into DESeq2 to evaluate differential gene expression (Love et al., 2014).

Gene Set Enrichment Analysis (GSEA) was performed to identify pathways enriched in differentially expressed genes (DEGs). The analysis was conducted using the Molecular Signatures Database (MSigDB) Hallmark gene sets (h.all.v7.5.1.symbols.gmt) and

Mitochondrial gene sets (custom-curated mitochondrial pathways) to assess the functional enrichment of mitochondrial processes (Liberzon et al., 2015). DEGs were ranked based on their signal-to-noise ratio (or log2 fold-change) and subjected to preranked GSEA using the GSEA software or the fgsea package in R. Significance was determined based on normalized enrichment scores (NES) and false discovery rate (FDR) adjusted p-values ($q < 0.05$).

Statistical analysis

All statistical analyses were determined using JMP Pro statistical software (version 16.0.0 SAS Institute, Cary, NC, USA), and figures were created using GraphPad Prism (version 9.4.1, GraphPad Software, San Diego, CA, USA). All data are represented as mean±standard deviation (SD). Data were analyzed by one-way ANOVA using an alpha level of 0.05.

RESULTS

The effects of VML injury on mitochondrial bioenergetics and mitochondrial ROS in different time points

Consistent with previous reports employing the CK clamp to explore mitochondrial function after VML injury, there are profound changes in both carbohydrate-fueled JO_2 from 7- to 60-days after VML injury (**Figure 1B and C**). Interestingly, fat-induced maximal JO_2 and respiratory conductance were reduced 7- to 30-days post-VML injury; however, after 60 days after VML injury, both maximal JO_2 and respiratory conductance were rebounded to the Uninjured level (**Figure 1G and H**). The relationship between the proton motive force (Δp) and the mitochondrial membrane potential (Δψm) is critical because, *in vivo*, the energy derived from Δp influences how effectively ATP synthase can drive the ATP/ADP ratio away from equilibrium (Fisher-Wellman et al., 2018; Koves et al., 2023). Therefore, the mitochondrial capacity to regulate the connection between JO_2 and Δψm is a key marker of respiratory efficiency and their ability to respond to energy demands, referred to in this paper as "bioenergetic efficiency". Although we did not statistically analyze the bioenergetic efficiency plots (Fisher-Wellman et al., 2018; Koves et al., 2023), the data indicate that groups with volumetric muscle loss (VML) exhibit a mostly downward and to the left shift in the relationship between JO_2 and Δψm compared to uninjured groups (**Figure 1E and J**). The data reflects that VML-injured mitochondria have a lower JO_2 capacity with a similar- or less mitochondrial Δψm at any given energy demand, suggesting that after VML injury, mitochondria are less responsive depending on the different energy demand.

To determine the extent to which the impaired bioenergetic efficiency after VML injury was associated with ROS, the rate of H_2O_2 (JH_2O_2) was assessed using carbohydrate- or fat-

substrates in the presence of endogenous antioxidant buffering systems (ROS emission) and when endogenous antioxidants were inhibited (ROS production). Compared to uninjured, carbohydrate-mediated ROS emission (**Figure 1K**, $p \leq 0.019$) and production (**Figure 1K**, $p = 0.026$) were significantly higher in VML-injured fiber bundles until 14 days post-injury; however, H_2O_2 emission was markedly less in 30- and 60-days post VML injury (**Figure 1K**, $p \leq 0.001$). Similarly, fat-derived H_2O_2 emission and production were significantly greater by 14-days post-VML injury (**Figure 1M**, emission; $p \leq 0.008$ and production; $p \leq 0.022$). Carbohydrate-induced AoxBC was 35% less at 7-days post-injury (**Figure 1L right**, $p = 0.005$); however, AoxBC was 30%, 31%, and 38% greater in 14-, 30-, and 60-days post-VML injury compared to the VML-injured group **(Figure 1L right**, $p = 0.048$). Intriguingly, there were no changes in fat-mediated AoxBC (**Figure 1K right**, $p \leq 0.999$). Taken together, these data suggest that 7-days post-VML injury is a critical threshold for mitochondrial AoxBC in female mice.

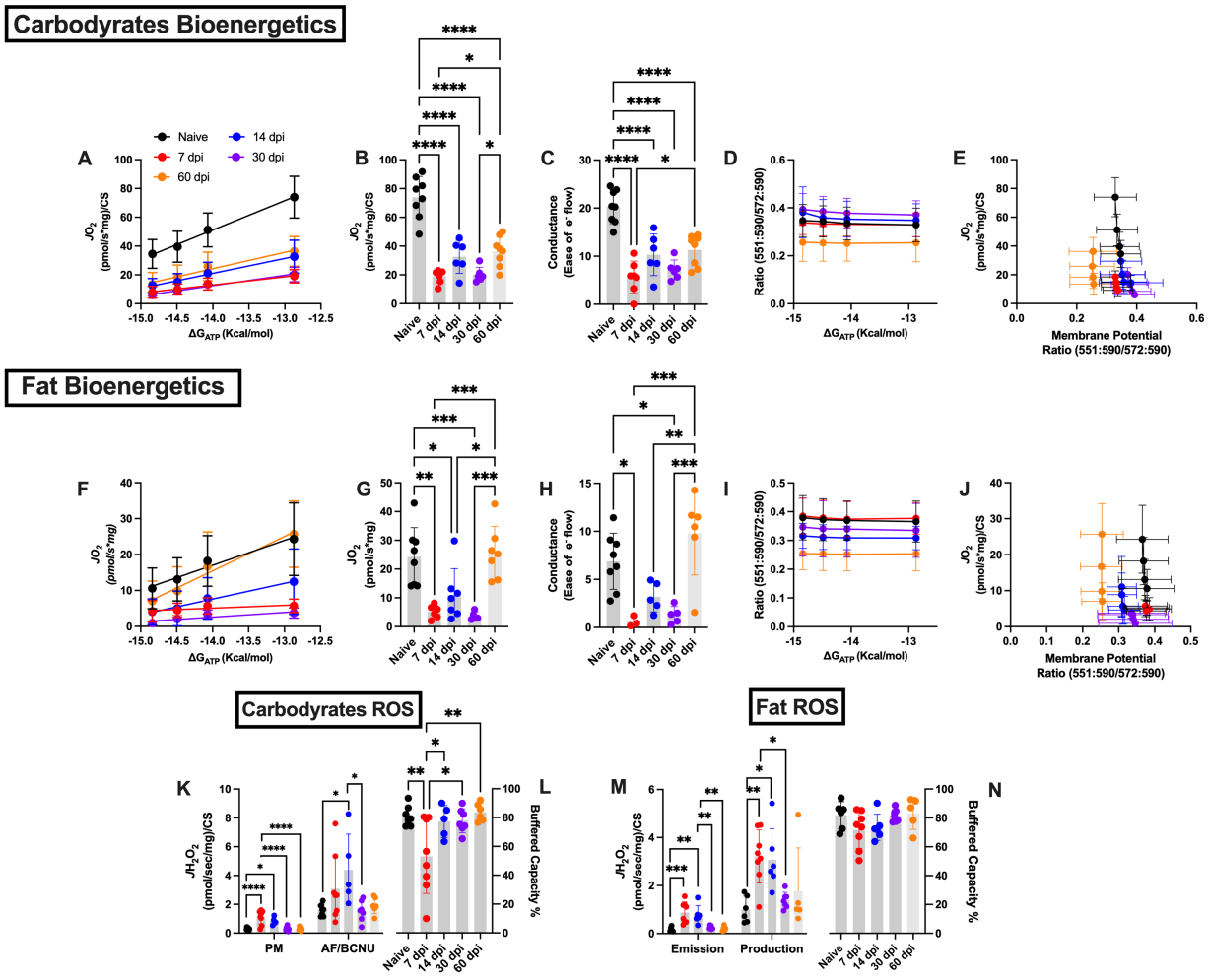

Figure 5.1. Time course of permeabilized muscle fiber bundle mitochondrial bioenergetics and reactive oxygen species after volumetric muscle loss injury. **A,F:** The relationship between ATP re-synthesis demand (ΔG_{ATP}) and mitochondrial oxygen consumption (JO_2) normalized to citrate synthase (CS) activity for carbohydrate and fat substrates, respectively. **B,G:** Maximal JO_2 for carbohydrate and fat substrates, respectively. **C,H:** Respiratory conductance for carbohydrate and fat substrates, respectively. **D,I:** The relationship between ΔG_{ATP} and mitochondrial membrane potential for carbohydrate and fat substrates, respectively. **E,J:** The relationship between JO_2 and mitochondrial membrane potential (i.e., bioenergetic efficiency) for carbohydrate and fat substrates, respectively. The arrows indicate the down, rightward shift with VML injury. **K,M:** reactive oxygen species emission, production, and **L,M:** antioxidant buffer capacity for carbohydrate and fat substrates, respectively. Statistical significance was determined by one-way ANOVA with Tukey's HSD post-hoc test. Data are expressed as mean ± SD. *p < 0.05, **p < 0.01, ***p < 0.001, and ****p < 0.0001. dpi, days post-injury.

The role of 17ß-estradiol on mitochondrial ROS and AoxBC at 3- and 7-days post-VML injury.

Combining the current findings with previously published evidence, we found that females are less prone to VML-induced ROS, especially having greater AoxBC than males. These findings prompted us to explore potential sex difference mechanisms in protecting against increased ROS following VML injury. Thus, we did ovariectomize surgery 2 weeks before the VML surgery and implanted either E2 or placebo pellets in the mice. Following 3- and 7-days post-VML injury, mitochondrial ROS emission, production, and antioxidant buffering capacity (AoxBC) were measured to explore whether ovarian hormone would be the potential mechanistic regulator of sex difference in this animal model.

The uterine mass, as a secondary marker of successful OVX surgery, was 82% and 78% lower in the VML+OVX+Placebo group compared to the VML+Sham group after 3- and 7-days post-VML injury (**Figure 2D and H,** $p \leq 0.001$); however, the uterine mass was significantly greater in the E2-treated group compared to the placebo group (**Figure 2D and H,** $p \leq 0.001$). The body weights at 3- and 7-days post-VM injury were 16% and 13% greater than in the VML+Sham group (**Figures 2A and E,** $p \leq 0.005$). There were decreasing trends in body weight in the VML+OVX+E2 group relative to the VML+OVX+Placebo group, but not significant (**Figures 2A and E,** $p = 0.0502$ and $p = 0.297$). Absolute muscle mass was not significantly altered at both 3 and 7 days post-VM injury (**Figure 2B and F,** $p = 0.981$). Notably, normalized muscle mass by body weight at 7 days post-VM injury was 14% lower in the VML+OVX+Placebo group compared to the VML+Sham group (**Figure 2G,** $p = 0.001$), which rebounded with 17ß-estradiol repletion (**Figure 2G,** $p = 0.003$).

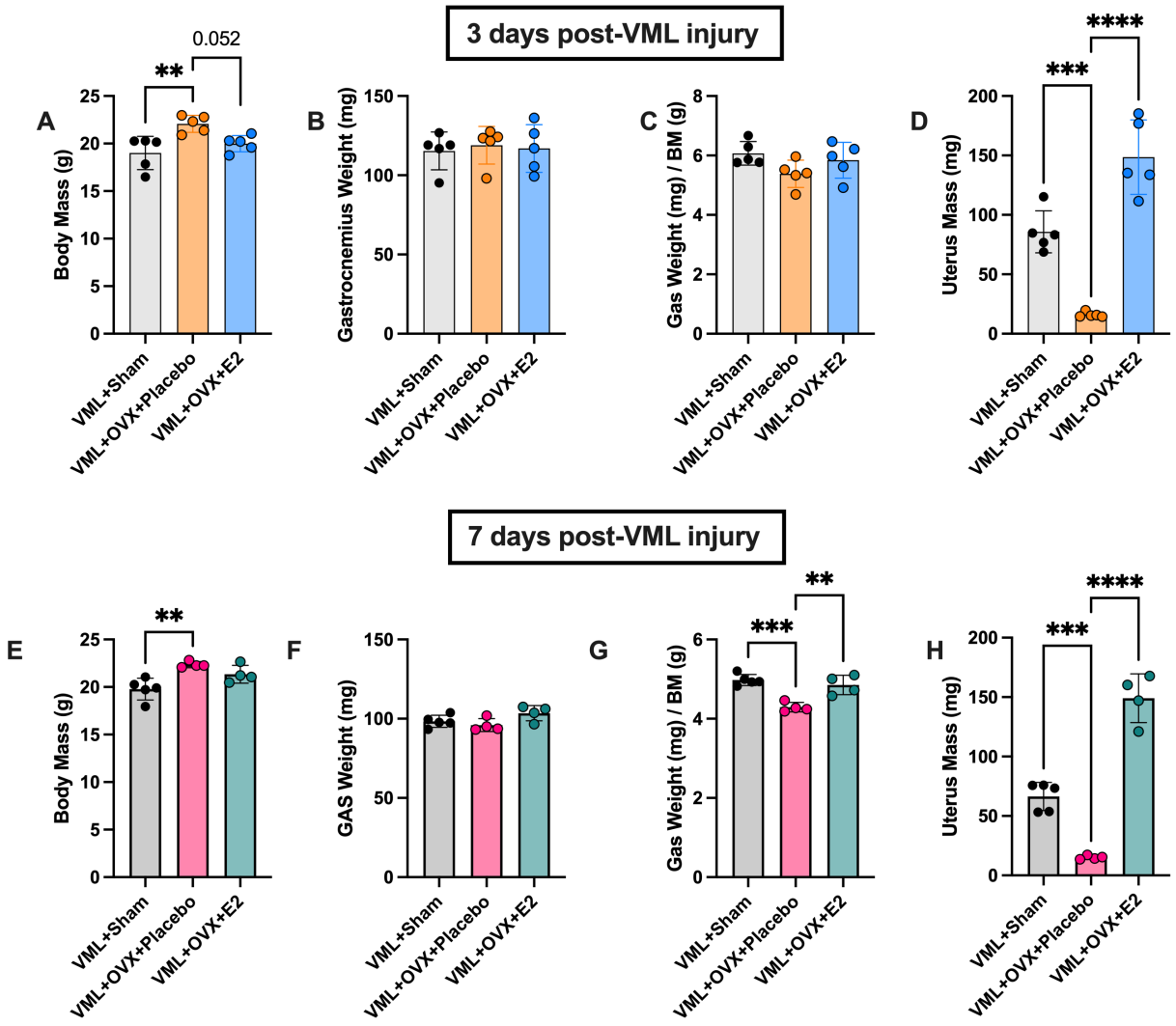

Figure 5.2. Effect of 17ß-estradiol on body mass and gastrocnemius muscle mass. **A-C:** Effect of 17ß-estradiol on body mass, VML-injured gastrocnemius muscle mass, and body mass-normalized gastrocnemius muscle mass at 3-days post-injury. **E-G:** Effect of 17ß-estradiol on body mass, VML-injured gastrocnemius muscle mass, and body mass-normalized gastrocnemius muscle mass at 7-days post-injury. **D,H:** Effect of 17ß-estradiol on uterus mass at 3- and 7-days post-injury. Statistical significance was determined by one-way ANOVA with Tukey's HSD post-hoc test. Data are expressed as mean ± SD. dpi, days post-injury.

The role of 17ß-estradiol on mitochondrial ROS and AoxBC at 3- and 7-days post VML injury.

We sought to investigate the role of 17ß-estradiol on ROS emission, ROS production, and AoxBC using carbohydrate and fat substrates in 3- and 7-days post-VML injury (**Figure 3**). After 3 days post-VML injury, both ROS emissions and production from permeabilized fiber bundles were not altered across all groups from carbohydrates substrates (**Figure 3A and B,** $p \leq 0.991$). Fat-mediated AoxBC was 26% less in the VML+OVX+Placebo group compared to the VML+Sham (**Figure 3D,** $p = 0.015$); however, the AoxBC was 35% greater in the VML+OVX+E2 relative to the VML+OVX+Placebo group (**Figure 3D,** $p = 0.010$). At 7-days post-VML injury, there were no changes in carbohydrate-fueled ROS emission and production across the groups (**Figure 3E,** $p = 0.998$). Fat-derived ROS emission was 64% greater in the VML+OVX+Placebo than the VML+Sham group (**Figure 3G,** $p = 0.026$); however, ROS emission was 51% lower after E2 repletion in the VML+OVX+E2 groups compared to the VML+OVX+Placebo group (**Figure 3G,** $p = 0.004$). Carbohydrate-mediated AoxBC was 25% less in the VML+OVX+Placebo (**Figure 3F,** $p = 0.040$); however, no changes occurred after E2 repletion, despite increasing trends (**Figure 3F,** $p = 0.122$). Fat-derived AoxBC was not significantly reduced in the VML+OVX+Placebo despite decreasing trends (**Figure 3H,** $p = 0.113$). The VML+OVX+E2 group has 30% greater fat-induced AoxBC compared to the VML+OVX+Placebo (**Figure 3H,** $p = 0.012$).

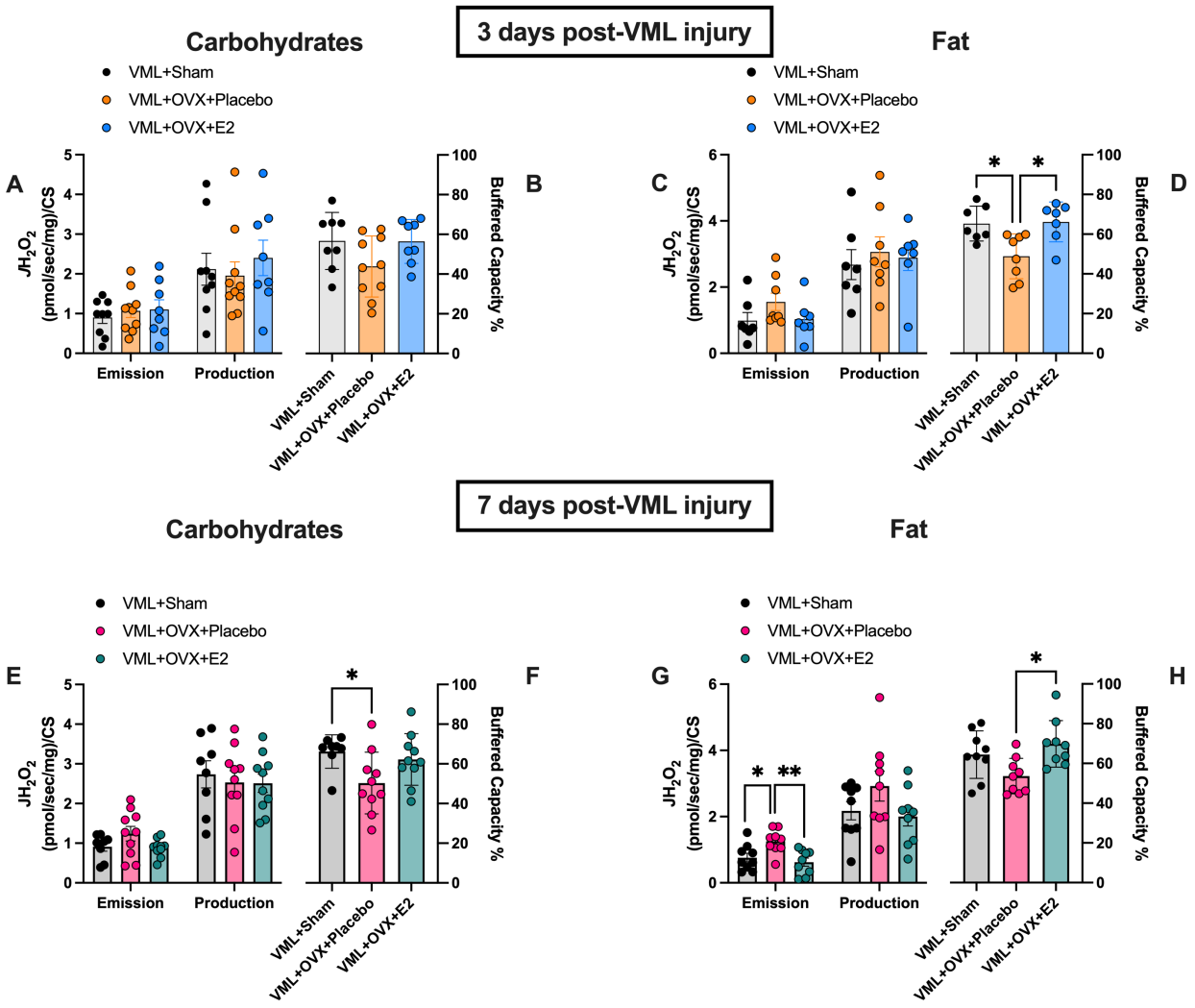

Figure 5.3. Effect of 17ß-estradiol on permeabilized muscle fiber bundle reactive oxygen species after VML injury. **A-D:** Reactive oxygen species emission, production, and antioxidant buffer capacity for carbohydrate and fat substrates, respectively, at 3-days post-injury. **E-H:** Reactive oxygen species emission, production, and antioxidant buffer capacity for carbohydrate and fat substrates, respectively, at 7-days post-injury. Statistical significance was determined by one-way ANOVA with Tukey's HSD post-hoc test. Data are expressed as mean ± SD. *p < 0.05, **p < 0.01, ***p < 0.001, and ****p < 0.0001. dpi, days post-injury. AoxBC, antioxidant buffering capacity. ROS, reactive oxygen species.

The effects of 17ß-estradiol on gene transcriptomes Post-VML Injury

To investigate the molecular signaling of estradiol (E2) in the context of VML injury after OVX, bulk RNA sequencing analysis was done at two different post-VML time points, 3- and 7-dpi. Differential gene expression analysis was done in two different ways: first, by examining the loss of ovarian hormones (OVX vs. Sham, OVX Effect), and second, by examining the role of estradiol (E2 vs. OVX, E2 Effect).

In the context of VML injury, the loss of ovarian hormones resulted in 163 and 11 DEGs at 3- and 7-dpi, respectively (**Table 1**), and only 1 gene was associated with the mitochondrial transcriptome (*Gpt2*) (**Figure 4A**). In contrast, the effect of E2 resulted in 141 and 691 DEGs at 3- and 7-dpi (**Table 1**), and 9 mito-DEGs (**Figure 4A**).

In contrast to individual DEG analysis, gene set enrichment analysis (GSEA) helps elucidate what changes in the entire transcriptome were a result of OVX or E2. GSEA is a type of overrepresentation analysis that determines the degree to which a given set of genes is present at either extreme of a ranked gene list, returning an enrichment score that is normalized to account for differences in both gene set size and in correlations between gene sets and the expression dataset (Subramanian et al., 2005). For statistical comparisons, the false-discovery rate (FDR) Benjamini-Hochberg adjusted p-value was applied to account for multiple testing. All genes were pre-ranked by the Wald statistic and passed through GSEA utilizing hallmark GSEA.

Of the 50 total hmGSEAs, there were 17 significant at 3-dpi and 30 significant at 7-dpi for the OXV vs. Sham analysis (OVX Effect; **Figure 4B**). Notably, among the significant hmGSEAs, Estrogen Response Early was upregulated at 3-dpi, and Oxidative Phosphorylation

was downregulated. At 7-dpi, oxidative phosphorylation and fatty acid metabolism were upregulated, whereas glycolysis was downregulated along with estrogen response late.

There were 21 significant hmGSEAs at 3-dpi and 36 at 7-dpi for the E2 vs. OVX analysis (E2 Effect, **Figure 4B**). At 3-dpi, oxidative phosphorylation and fatty acid metabolism were downregulated in E2 relative to OVX, and at 7-dpi, the trend reversed as oxidative phosphorylation and fatty acid metabolism were upregulated in E2 relative to OVX. This coincided with the downregulation of glycolysis and estrogen response late.

Because the hmGSEA revealed significant changes in the regulation of metabolic-associate gene sets, all genes were passed through GSEA utilizing the Broad Institute's MitoCarta3.0, a resource for mitochondria gene sets (Rath et al., 2021), to specifically evaluate mitochondrial pathway regulation. Of the 119 mito-GSEAs, there were 32 significant at 3-dpi (all downregulated) and 69 at 7-dpi (all upregulated) for the OVX vs. Sham analysis (OVX Effect; **Figure 4B**). Notable categories of downregulated pathways at 3-dpi include: mitochondrial maintenance (e.g., mitophagy genes), fuel preference (e.g., TCA cycle), and electron transport chain (e.g., complex-IV genes) (**Table 2**). Notable categories of upregulated pathways at 7-dpi include mitochondrial maintenance, fuel preference, electron transport chain, and antioxidants (**Table 2**).

Of the 119 mito-GSEAs, there were 10 significant at 3-dpi (9 downregulated) and 54 significant at 7-dpi (all upregulate) for the E2 vs. OVX analysis (E2 Effect, **Figure 5**). There were two primary categories for downregulated pathways at 3-dpi: mitochondrial maintenance and fuel preference (**Table 2**). The notable categories for upregulated pathways at 7-dpi are: mitochondrial maintenance, fuel preference, electron transport chain, and antioxidants (**Table 2**).

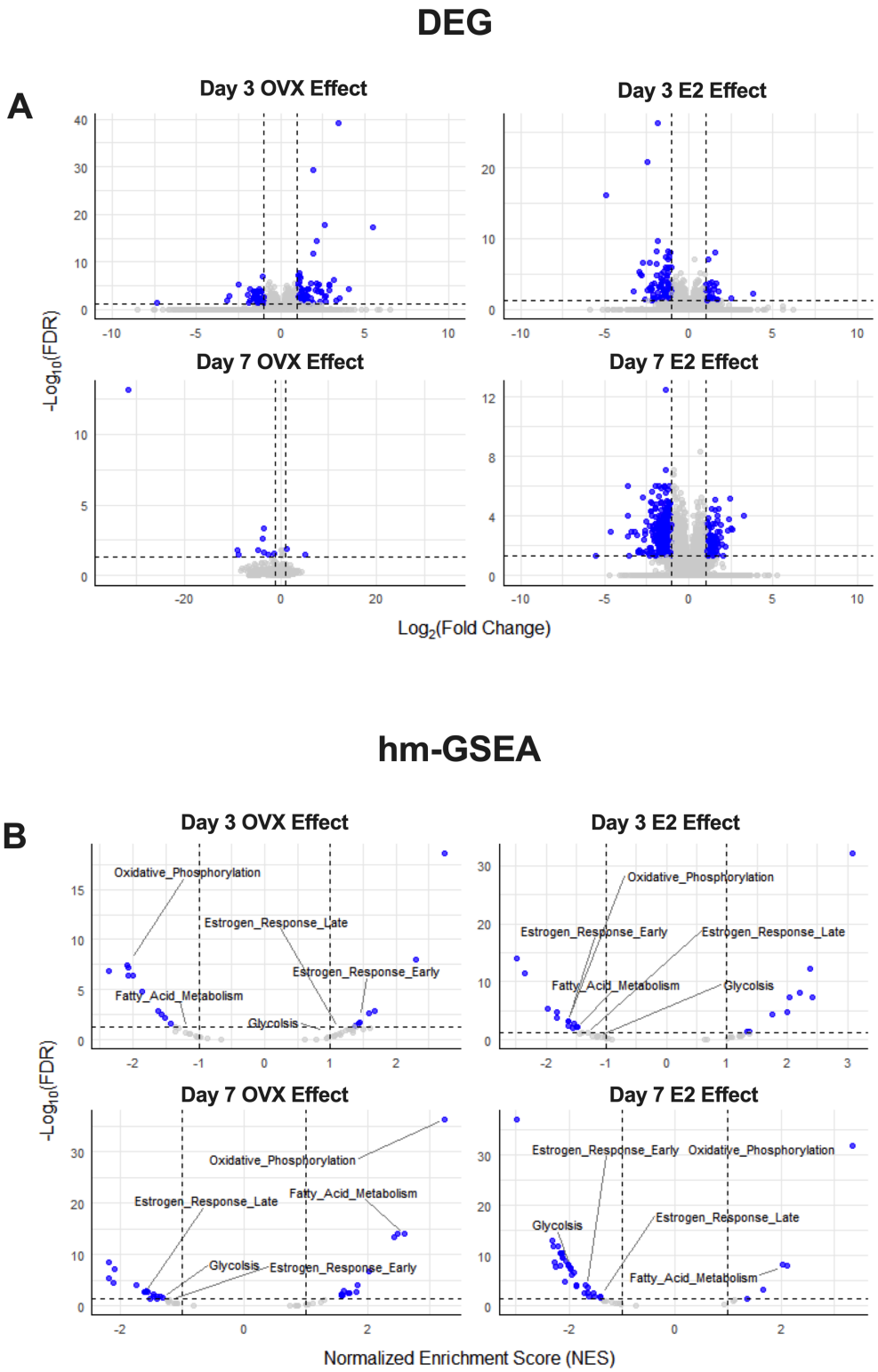

Figure 5.4. Effect of OVX and 17ß-estradiol on differentially expressed genes and hallmark gene set enrichment analysis after VML injury. **A:** Volcano plots showing differential gene expression (DEG). **B:** Volcano plots showing hallmark Gene Set Enrichment Analysis (hmGSEA).

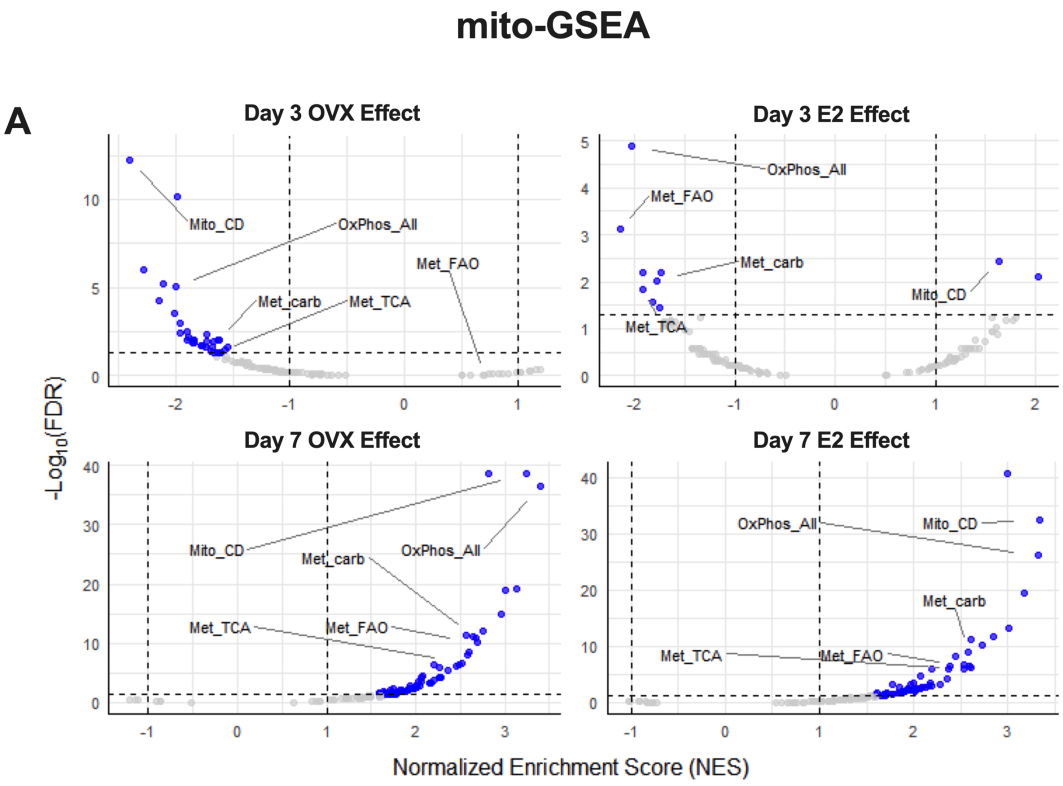

Figure 5.5. Effect of OVX and 17ß-estradiol on mitochondrial gene set enrichment analysis after VML injury.

The effects of 17ß-estradiol on body weight, muscle mass, fat mass, and blood glucose levels Post-VML Injury

To determine if the long-term effects of 17ß-estradiol would attenuate mitochondrial ROS emission and mitochondrial dysfunction following OVX and VML injury, we compared muscle mitochondrial outcomes 8 weeks after VML injury that either received 17ß-estradiol or placebo. At the study endpoint, body weight was 21% greater in the VML+OVX+Placebo mice compared to VML+Sham (**Figure 6A**, $p = 0.001$), which is 13% less in the VML+OVX+E2 group compared to the VML+OVX+Placebo (**Figure 6A**, $p = 0.002$). Absolute muscle mass was 15% and 10% greater in the VML+OVX+E2 mice compared to the VML+Sham and VML+OVX+Placebo, respectively (**Figure 6B**, $p \leq 0.026$). Body mass-normalized muscle mass was 15% lower in the VML+OVX+Placebo relative to the VML+Sham (**Figure 6C**, $p = 0.040$); however, it was 26% higher in the VML+OVX+E2 mice (**Figure 6C**, $p = 0.001$). Uterus mass was markedly reduced in both OVX groups compared to the VML+Sham (**Figure 6D**, $p \leq 0.001$), which is rebounded by E2 replacement (**Figure 6D**, $p = 0.041$). Visceral fat mass was 390% and 164% greater in both OVX groups compared to the VML+Sham (**Figure 6E**, $p \leq 0.014$). Between the OVX groups, the VML+OVX+E2 mice have 46% lower visceral fat mass compared to the VML+OVX+Placebo mice (**Figure 6E**, $p = 0.001$). The area under the curve (AUC) from the ip glucose tolerance test (ipGTT) was greater in the VML+OVX+Placebo group compared to the VML+Sham (**Figure 6F,** $p = 0.006$), which was reduced by E2 replacement (**Figure 6F** $p = 0.002$).

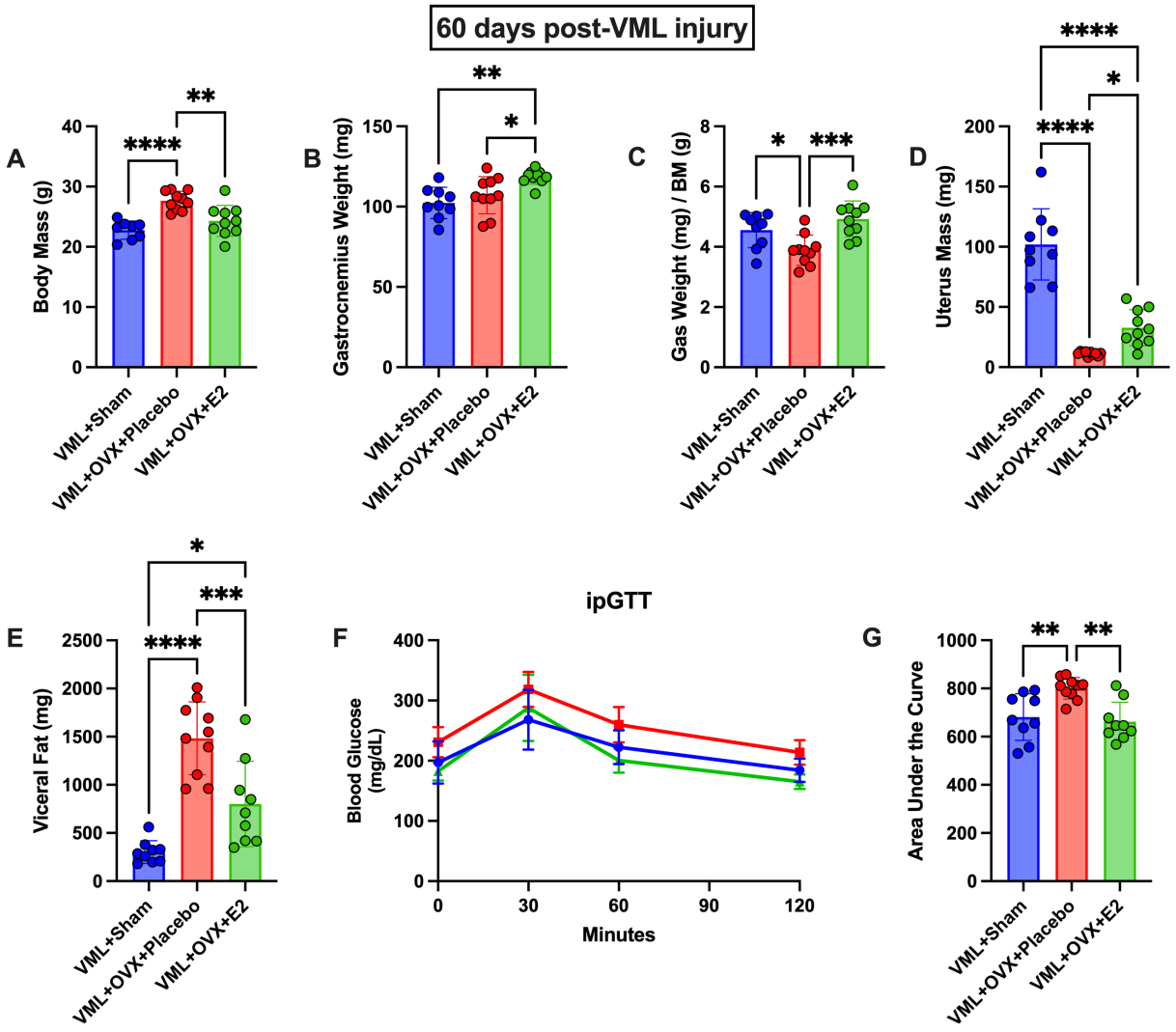

Figure 5.6. Effect 17ß-estradiol on morphologic adaptations 60-days post-VML injury. **A-D:** Body mass, VML-injured gastrocnemius muscle mass, body mass-normalized muscle mass at 8-weeks post-injury, and uterus mass. **E:** Visceral fat mass. **F-G:** Two-hour blood glucose response to a single, fasted glucose challenge and calculated area under the curve at 8-weeks post-injury. Statistical significance was determined by one-way ANOVA with Tukey's HSD post-hoc test. Data are expressed as mean ± SD. *p < 0.05.

The effects of long-term 17ß-estradiol on mitochondrial bioenergetics and ROS Post-VML Injury

Both carbohydrate- and fat-mediated maximal JO_2 were 30% and 44% lower in the VML+OVX+Placebo group **(Figure 7B, G**, $p \leq 0.008$); however, both JO_2 was 49% and 92% greater in VML+OVX+E2 muscle fibers compared to the VML+OVX+Placebo muscle (**Figure 7B, G**, $p \leq 0.001$). Carbohydrate-mediated respiratory conductance was 30% greater in the VML+OVX+E2 compared to the VML+OVX+Placebo (**Figure 7C**, $p = 0.023$), although there was no change between VML+Sham and VML+OVX+Placebo (**Figure 7C,** $p = 0.343$). For fat substrates, respiratory conductance was 41% less in the VML+OVX+Placebo compared to the VML+Sham (**Figure 7H,** $p = 0.023$); however, the conductance was 81% greater in the VML+OVX+E2 than in VML+OVX+Placebo (**Figure 7H,** $p = 0.003$). For Δψm, the results suggest that both rehabilitation groups exhibited a less polarized Δψm compared to the VML+Saline when utilizing both carbohydrate and fat substrates (**Figure 7D,I**). Notably, mitochondrial bioenergetic efficiency plots showed a left and upward shift in the VML+OVX+E2 groups (**Figure 7E,J**), reflecting enhanced respiratory capacity coupled with a depolarized Δψm at any given energy demand. These results suggest that the E2 group is more efficient at utilizing Δp for ATP synthesis compared to VML+OVX+Placebo mice and that electrons are appropriately used in Complex-IV to reduce O_2 to 2 H_2O.

ROS emission from both carbohydrate and fat substrates was 65% and 95% greater, respectively, in the VML+OVX+Placebo compared to the VML+Sham mice (**Figure 7K,M**, $p \leq 0.006$). There was no statistical difference in ROS production for both substrates across group. Both carbohydrate- and fat-mediated AoxBC were 27% and 40% less, respectively, in the VML+OVX+Placebo compared to the VML+Sham mice (**Figure 7L,N**, $p \leq 0.001$); however,

they were 40% and 61% greater in the VML+OVX+E2 muscle fiber bundles relative to the VML+OVX+Placebo muscle (**Figure 7L,N**, $p \leq 0.001$).

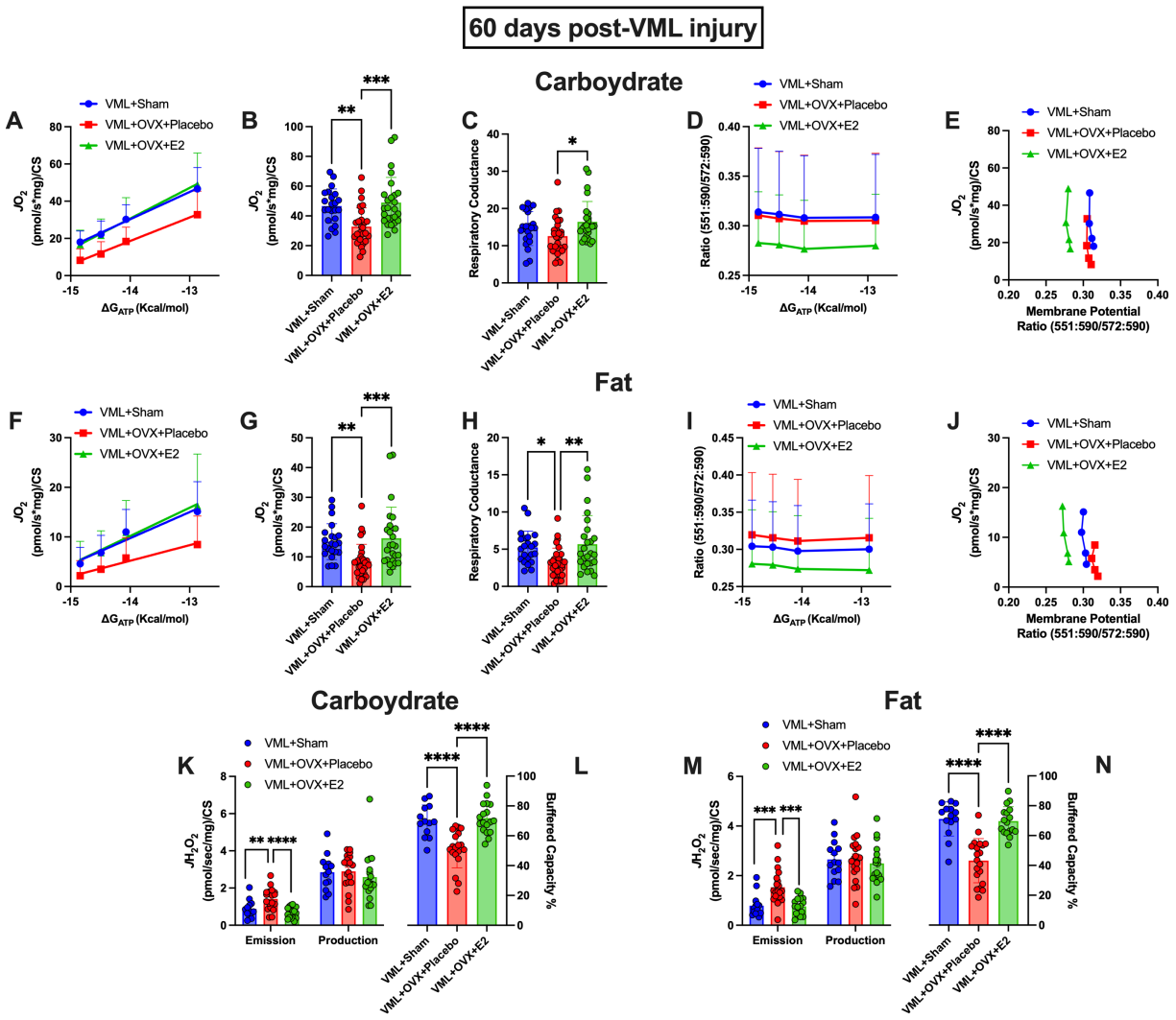

Figure 5.7. Effect of 17ß-estradiol metabolic adaptations after VML injury. **A,F:** The relationship between ATP re-synthesis demand (ΔG_{ATP}) and mitochondrial oxygen consumption (JO_2) normalized to citrate synthase (CS) activity for carbohydrate and fat substrates, respectively, at 8-weeks post-injury. **B,G:** Maximal JO_2 for carbohydrate and fat substrates, respectively, at 8-weeks post-injury. **C,H:** Respiratory conductance for carbohydrate and fat substrates, respectively, at 8-weeks post-injury. **D,I:** The relationship between ΔG_{ATP} and mitochondrial membrane potential for carbohydrate and fat substrates, respectively, at 8-weeks post-injury. **E,J:** The relationship between JO_2 and mitochondrial membrane potential (i.e., bioenergetic efficiency) for carbohydrate and fat substrates, respectively, at 8-weeks post-injury. **K-N:** Reactive oxygen species emission, production, and antioxidant buffer capacity for carbohydrate and fat substrates, respectively, at 8-weeks post-injury. Statistical significance was determined by one-way ANOVA with Tukey's HSD post-hoc test. Data are expressed as mean ± SD. *p < 0.05, **p < 0.01, ***p < 0.001, and ****p < 0.0001. dpi, days post-injury. AoxBC, antioxidant buffering capacity. ROS, reactive oxygen species.

Discussion

The present study investigated the role of 17β-estradiol (E2) in regulating mitochondrial bioenergetics and reactive oxygen species (ROS) homeostasis following volumetric muscle loss (VML) injury in E2-deficient female mice. Our findings demonstrate that ovariectomy (OVX) exacerbates mitochondrial dysfunction and oxidative stress following VML injury, whereas E2 replacement effectively alleviates these defects, restoring mitochondrial bioenergetics and antioxidant buffering capacity (AoxBC). Although the protective role of E2 in skeletal muscle metabolism has been previously demonstrated (Campbell et al., 2003; Cavalcanti-de-Albuquerque et al., 2014; Lowe & Kararigas, 2020; Torres, Kew, et al., 2018), this study is the first study to link the protective effects of E2 specifically to metabolic dysfunction following VML injury. These findings highlight the therapeutic potential of estrogen in modulating skeletal muscle metabolic function and emphasize the importance of estrogen signaling pathways in potential treatments for estrogen-deficient conditions following traumatic injury.

Direct measurements of mitochondrial ROS emission conducted in this study robustly support the hypothesis that bioenergetic inefficiency is a primary driver of excessive ROS generation in VML-injured muscle. Under normal physiological conditions, mitochondrial respiration is closely coupled to ATP demand, where heightened energy requirements stimulate ADP-driven oxidative phosphorylation, thereby dissipating mitochondrial membrane potential ($\Delta\psi m$) through proton translocation via ATP synthase. In contrast, VML injury induced a state of mitochondrial hyperpolarization coupled with diminished respiratory capacity, suggesting impaired regulation and utilization of proton motive force (Δp) for efficient ATP synthesis. Moreover, reduced respiratory conductance, indicative of impaired electron transport within the

electron transport chain, was observed, likely causing electron congestion and subsequent electron leak at complexes I, II, and III. This electron backflow plausibly enhances superoxide generation, disrupting mitochondrial ROS homeostasis. Collectively, these observations highlight that bioenergetic inefficiency induced by VML injury significantly compromises mitochondrial ROS handling and antioxidant buffering capacity (AoxBC).

In investigating temporal changes in mitochondrial bioenergetics in females from acute- through long-term VML injury, we observed marked reductions in maximal respiratory capacity (JO_2) and respiratory conductance during the acute phase (30 days post-injury), followed by partial recovery by day 60 post-injury. These defects were paralleled by elevated mitochondrial ROS emission and impaired antioxidant buffering capacity in VML-injured muscle. Although we found that VML injury primarily influences mitochondrial disruptions during the early phase, the main goal of this study is to explore potential mechanisms based on sex differences following VML injury in females. Our previous study (Heo et al., 2023) and preliminary data (*data is not shown here*) indicate sex-based differences. For example, females are less prone to impaired maximal JO_2 and respiratory conductance in response to the combined Western diet and VML injury (Heo et al., 2023). In addition**, Figure 1** and our preliminary study demonstrated that females have a shorter duration of impaired AoxBC than males, showing that after 7-dpi, AoxBX from females has been normalized to the Uninjured levels; however, AoxBC is impaired until 14-days post-VML injury. This sex-specific phenomenon prompted further investigation into the mechanistic role of ovarian hormones, mainly E2, in mitochondrial adaptations and redox homeostasis following VML injury.

It is known that E2 positively modulates redox balance and upregulates antioxidant defenses (Baltgalvis et al., 2010; Bellanti et al., 2013; Torres, Kew, et al., 2018). For example, Glutathione peroxidase 3 (*Gpx3*) mRNA was greater in mice receiving E2 (Baltgalvis et al., 2010). Moreover, E2 ameliorates OVX-induced disrupted cellular redox status (GSH/GSSG) and decreases mitochondrial H_2O_2 emitting potential (Torres, Kew, et al., 2018). In the current study, we found that E2 primarily improved mitochondrial AoxBC, rather than directly reducing individual ROS emission levels in the early phase of VML injury (3- and 7-dpi). Specifically, OVX markedly produced mitochondrial ROS, notably in fat-derived ROS emissions at 7 days post-injury, whereas E2 replacement significantly attenuated OVX-induced mitochondrial ROS emission from fat substrates. With respect to the role of E2 on AoxBC, OVX mice revealed the impairment of mitochondrial AoxBC during early phase of VML injury, while E2-treated mice showed improvement of AoxBC in VML mice without E2. Together, these findings suggest that E2 plays a crucial role in regulating antioxidant defense following muscle traumatic injury rather than directly scavenging the mitochondrial ROS. It is likely that VML itself generates more mitochondrial ROS; therefore, after OVX, the muscle undergoes a compensatory response to the OVX+VML conditions.

RNA sequencing and Gene Set Enrichment Analysis (GSEA) further elucidated mechanistic insights into mitochondrial dysfunction and oxidative stress responses following OVX with or without E2 in VML-injured mice. Hallmark GSEA revealed distinct metabolic shifts between OVX and E2-treated groups. At 3-dpi, OVX mice without E2 exhibited significant suppression of oxidative phosphorylation and fatty acid metabolism pathways, indicative of early mitochondrial dysfunction. By day 7 post-VML injury, mitochondrial-related pathways, including oxidative phosphorylation and fatty acid metabolism, were upregulated in

OVX mice, potentially as a delayed compensatory response. In contrast, E2-treated mice showed early metabolic activation with robust enrichment of oxidative phosphorylation pathways at day 7, suggesting that estrogen repletion would improve mitochondrial adaptation and bioenergetics.

In addition, mitochondrial-specific GSEA analyses further confirmed these metabolic alterations. At day 3 post-injury, OVX mice displayed significant downregulation of mitochondrial gene sets related to mitochondrial RNA metabolism and electron transport chain (ETC) assembly, indicating impaired mitochondrial biogenesis and function. By day 7, there was an upregulation of oxidative phosphorylation genes in OVX mice, reflecting a compensatory metabolic response. Notably, the E2-treated group demonstrated pronounced mitochondrial gene activation at day 7, characterized by enrichment of central mitochondrial dogma genes and complex I genes. These results align with previous findings showing that E2 enhances complex I enzyme activity (Torres, Ryan, et al., 2018) and complex I-mediated respiration (Torres, Kew, et al., 2018) in E2-deficient mice, thereby improving overall muscle mitochondrial adaptations.

Beyond its short-term mitochondrial effects, E2 also influenced long-term mitochondrial bioenergetics and redox homeostasis following traumatic injury. First, consistent with Prior works (Hu et al., 2024; Torres, Kew, et al., 2018), we observed that E2 improves respiratory capacity following OVX and VML injury. Interestingly, our data revealed that E2 influences respiratory conductance in a substrate-dependent manner, showing that fat-fueled mitochondrial respiratory conductance was impaired after OVX but recovered following E2 replacement. However, in carbohydrate substrates, significant effects were observed with E2-treated mitochondria, not with OVX alone. This finding contradicts previous studies. Torres and Kew et al. (Torres, Kew, et al., 2018) demonstrated that E2 did not affect fatty acid-derived

mitochondrial respiration in permeabilized muscle fibers from OVX animals. This discrepancy may result from temporal differences and variations in experimental models. Moreover, it is plausible that early changes in genes-related fatty acid oxidation could sustain the potential for metabolic adaptations over more extended periods. For example, our hm- and mito-GSEA analysis indicates that E2-repleted mice have greater fatty acid metabolism gene expressions over OVX mice. Other studies have reported increased expression of genes associated with fatty acid oxidation following E2 replacement, contributing to the observed improvement in respiratory capacity in our study (Campbell et al., 2003; Cavalcanti-de-Albuquerque et al., 2014). These gene expression alterations potentially explain the respiratory capacity improvements observed in our study, reflecting adaptive mechanisms emerging over a longer duration that are not captured in shorter-term analyses. Nevertheless, there remains limited direct evidence regarding the long-term influence of E2 on fatty acid metabolism, specifically in skeletal muscle. Thus, future studies are needed to elucidate this relationship.

In addition, consistent with previous studies (Baltgalvis et al., 2010; Silva et al., 2022), the current study indicates that after OVX, E2 reduces excessive H_2O_2 emission and restores AoxBC following OVX combined with VML injury. Kristen et al. (Baltgalvis et al., 2010) previously demonstrated that three weeks of E2 repletion increased the mRNA expression of glutathione peroxidase 3 (Gpx3), potentially mediated through estrogen receptor alpha signaling pathways. Furthermore, prolonged E2 supplementation over eight weeks enhanced superoxide dismutase enzymatic activity (Silva et al., 2022). Collectively, these findings emphasize the role of E2 in maintaining redox homeostasis in skeletal muscle under conditions of estrogen deficiency and traumatic muscle injury. However, a gap between the long-term effects of E2 and muscle redox status remains unresolved, warranting future studies.

In conclusion, this study provides novel insights into the protective effects of estrogen on mitochondrial function and redox homeostasis in skeletal muscle following VML injury in E2-deficient female mice. Our findings demonstrate that OVX exacerbates mitochondrial dysfunction, elevates ROS production, and impairs antioxidant defenses, whereas E2 repletion effectively restores mitochondrial bioenergetic efficiency and improves antioxidant defense. Collectively, these data highlight the potential therapeutic target of E2 in mitigating compromised muscle metabolism and redox homeostasis after traumatic injury, underscoring critical sex-specific differences in muscle pathophysiology and repair mechanisms. Underlying molecular mechanisms related to acute and long-term E2 replacement are essential for developing targeted interventions aimed at enhancing recovery outcomes for naturally or surgically induced postmenopausal women suffering from traumatic muscle injuries.

References

Baltgalvis, K. A., Greising, S. M., Warren, G. L., & Lowe, D. A. (2010). Estrogen regulates estrogen receptors and antioxidant gene expression in mouse skeletal muscle. *PloS One*, *5*(4), e10164. https://doi.org/10.1371/journal.pone.0010164

Bellanti, F., Matteo, M., Rollo, T., De Rosario, F., Greco, P., Vendemiale, G., & Serviddio, G. (2013). Sex hormones modulate circulating antioxidant enzymes: Impact of estrogen therapy. *Redox Biology*, *1*(1), 340–346. https://doi.org/10.1016/j.redox.2013.05.003

Cabelka, C. A., Baumann, C. W., Collins, B. C., Nash, N., Le, G., Lindsay, A., Spangenburg, E. E., & Lowe, D. A. (2019). Effects of ovarian hormones and estrogen receptor α on physical activity and skeletal muscle fatigue in female mice. *Experimental Gerontology*, *115*, 155–164. https://doi.org/10.1016/j.exger.2018.11.003

Campbell, S. E., Mehan, K. A., Tunstall, R. J., Febbraio, M. A., & Cameron-Smith, D. (2003). 17beta-estradiol upregulates the expression of peroxisome proliferator-activated receptor alpha and lipid oxidative genes in skeletal muscle. *Journal of Molecular Endocrinology*, *31*(1), 37–45. https://doi.org/10.1677/jme.0.0310037

Cavalcanti-de-Albuquerque, J. P. A., Salvador, I. C., Martins, E. L., Jardim-Messeder, D., Werneck-de-Castro, J. P. S., Galina, A., & Carvalho, D. P. (2014). Role of estrogen on skeletal muscle mitochondrial function in ovariectomized rats: A time course study in different fiber types. *Journal of Applied Physiology (Bethesda, Md.: 1985)*, *116*(7), 779–789. https://doi.org/10.1152/japplphysiol.00121.2013

Dalske, K. A., Raymond-Pope, C. J., McFaline-Figueroa, J., Basten, A. M., Call, J. A., & Greising, S. M. (2021). Independent of physical activity, volumetric muscle loss injury in

a murine model impairs whole-body metabolism. *PloS One*, *16*(6), e0253629. https://doi.org/10.1371/journal.pone.0253629

Fisher-Wellman, K. H., Davidson, M. T., Narowski, T. M., Lin, C.-T., Koves, T. R., & Muoio, D. M. (2018). Mitochondrial Diagnostics: A Multiplexed Assay Platform for Comprehensive Assessment of Mitochondrial Energy Fluxes. *Cell Reports*, *24*(13), 3593-3606.e10. https://doi.org/10.1016/j.celrep.2018.08.091

Garg, K., Ward, C. L., Hurtgen, B. J., Wilken, J. M., Stinner, D. J., Wenke, J. C., Owens, J. G., & Corona, B. T. (2015). Volumetric muscle loss: Persistent functional deficits beyond frank loss of tissue. *Journal of Orthopaedic Research: Official Publication of the Orthopaedic Research Society*, *33*(1), 40–46. https://doi.org/10.1002/jor.22730

Greising, S. M., Baltgalvis, K. A., Kosir, A. M., Moran, A. L., Warren, G. L., & Lowe, D. A. (2011). Estradiol's beneficial effect on murine muscle function is independent of muscle activity. *Journal of Applied Physiology (Bethesda, Md.: 1985)*, *110*(1), 109–115. https://doi.org/10.1152/japplphysiol.00852.2010

Heo, J., Schifino, A. G., McFaline-Figueroa, J., Miller, D. L., Hoffman, J. R., Noble, E. E., Greising, S. M., & Call, J. A. (2023). Differential effects of Western diet and traumatic muscle injury on skeletal muscle metabolic regulation in male and female mice. *Journal of Cachexia, Sarcopenia and Muscle*, *14*(6), 2835–2850. https://doi.org/10.1002/jcsm.13361

Hoffman, D. B., Raymond-Pope, C. J., Sorensen, J. R., Corona, B. T., & Greising, S. M. (2022). Temporal changes in the muscle extracellular matrix due to volumetric muscle loss injury. *Connective Tissue Research*, *63*(2), 124–137. https://doi.org/10.1080/03008207.2021.1886285

Hu, Y., Fang, B., Tian, X., Wang, H., Tian, X., Yu, F., Li, T., Yang, Z., & Shi, R. (2024). Passive exercise is an effective alternative to HRT for restoring OVX induced mitochondrial dysfunction in skeletal muscle. *Frontiers in Endocrinology*, *15*, 1356312. https://doi.org/10.3389/fendo.2024.1356312

Kararigas, G., Ebeling, M. C., Le, G., Lai, S., Cui, C., Cui, Q., & Lowe, D. A. (2025). Transcriptomic Profiling Reveals 17β-Estradiol Treatment Represses Ubiquitin-Proteasomal Mediators in Skeletal Muscle of Ovariectomized Mice. *Journal of Cachexia, Sarcopenia and Muscle*, *16*(1), e13698. https://doi.org/10.1002/jcsm.13698

Koves, T. R., Zhang, G.-F., Davidson, M. T., Chaves, A. B., Crown, S. B., Johnson, J. M., Slentz, D. H., Grimsrud, P. A., & Muoio, D. M. (2023). Pyruvate-supported flux through medium-chain ketothiolase promotes mitochondrial lipid tolerance in cardiac and skeletal muscles. *Cell Metabolism*, *35*(6), 1038-1056.e8. https://doi.org/10.1016/j.cmet.2023.03.016

Larouche, J. A., Wallace, E. C., Spence, B. D., Buras, E., & Aguilar, C. A. (2023). Spatiotemporal mapping of immune and stem cell dysregulation after volumetric muscle loss. *JCI Insight*, *8*(7), e162835. https://doi.org/10.1172/jci.insight.162835

Larsen, S., Nielsen, J., Hansen, C. N., Nielsen, L. B., Wibrand, F., Stride, N., Schroder, H. D., Boushel, R., Helge, J. W., Dela, F., & Hey-Mogensen, M. (2012). Biomarkers of mitochondrial content in skeletal muscle of healthy young human subjects. *The Journal of Physiology*, *590*(14), 3349–3360. https://doi.org/10.1113/jphysiol.2012.230185

Liberzon, A., Birger, C., Thorvaldsdóttir, H., Ghandi, M., Mesirov, J. P., & Tamayo, P. (2015). The Molecular Signatures Database (MSigDB) hallmark gene set collection. *Cell Systems*, *1*(6), 417–425. https://doi.org/10.1016/j.cels.2015.12.004

Love, M. I., Huber, W., & Anders, S. (2014). Moderated estimation of fold change and dispersion for RNA-seq data with DESeq2. *Genome Biology*, *15*(12), 550. https://doi.org/10.1186/s13059-014-0550-8

Lowe, D. A., & Kararigas, G. (2020). Editorial: New Insights into Estrogen/Estrogen Receptor Effects in the Cardiac and Skeletal Muscle. *Frontiers in Endocrinology*, *11*, 141. https://doi.org/10.3389/fendo.2020.00141

McFaline-Figueroa, J., Hunda, E. T., Heo, J., Winders, E. A., Greising, S. M., & Call, J. A. (2023). The bioenergetic "CK Clamp" technique detects substrate-specific changes in mitochondrial respiration and membrane potential during early VML injury pathology. *Frontiers in Physiology*, *14*, 1178213. https://doi.org/10.3389/fphys.2023.1178213

McFaline-Figueroa, J., Schifino, A. G., Nichenko, A. S., Lord, M. N., Hunda, E. T., Winders, E. A., Noble, E. E., Greising, S. M., & Call, J. A. (2022). Pharmaceutical Agents for Contractile-Metabolic Dysfunction After Volumetric Muscle Loss. *Tissue Engineering. Part A*, *28*(17–18), 795–806. https://doi.org/10.1089/ten.TEA.2022.0036

Mintz, E. L., Passipieri, J. A., Franklin, I. R., Toscano, V. M., Afferton, E. C., Sharma, P. R., & Christ, G. J. (2020). Long-Term Evaluation of Functional Outcomes Following Rat Volumetric Muscle Loss Injury and Repair. *Tissue Engineering. Part A*, *26*(3–4), 140–156. https://doi.org/10.1089/ten.TEA.2019.0126

Owens, B. D., Kragh, J. F., Wenke, J. C., Macaitis, J., Wade, C. E., & Holcomb, J. B. (2008). Combat wounds in operation Iraqi Freedom and operation Enduring Freedom. *The Journal of Trauma*, *64*(2), 295–299. https://doi.org/10.1097/TA.0b013e318163b875

Rath, S., Sharma, R., Gupta, R., Ast, T., Chan, C., Durham, T. J., Goodman, R. P., Grabarek, Z., Haas, M. E., Hung, W. H. W., Joshi, P. R., Jourdain, A. A., Kim, S. H., Kotrys, A. V.,

Lam, S. S., McCoy, J. G., Meisel, J. D., Miranda, M., Panda, A., … Mootha, V. K. (2021). MitoCarta3.0: An updated mitochondrial proteome now with sub-organelle localization and pathway annotations. *Nucleic Acids Research*, *49*(D1), D1541–D1547. https://doi.org/10.1093/nar/gkaa1011

Silva, S. B., Honorato-Sampaio, K., Costa, S. P., Domingues, T. E., da Cruz, T. M. M., Rodrigues, C. M., Costa, K. B., Dos Santos, J. M., da Silva Lage, V. K., Gaiad, T. P., Santos, A. P., Dias-Peixoto, M. F., Coimbra, C. C., Dos Reis, A. M., Szawka, R. E., Figueiredo, P. H. S., Costa, H. S., Oliveira, M. X., Mendonça, V. A., & Lacerda, A. C. R. (2022). The superior beneficial effects of exercise training versus hormone replacement therapy on skeletal muscle of ovariectomized rats. *Scientific Reports*, *12*(1), 8764. https://doi.org/10.1038/s41598-022-12739-8

Smith, C. D., Schmidt, C. A., Lin, C.-T., Fisher-Wellman, K. H., & Neufer, P. D. (2020). Flux through mitochondrial redox circuits linked to nicotinamide nucleotide transhydrogenase generates counterbalance changes in energy expenditure. *The Journal of Biological Chemistry*, *295*(48), 16207–16216. https://doi.org/10.1074/jbc.RA120.013899

Soneson, C., Love, M. I., & Robinson, M. D. (2015). Differential analyses for RNA-seq: Transcript-level estimates improve gene-level inferences. *F1000Research*, *4*, 1521. https://doi.org/10.12688/f1000research.7563.2

Southern, W. M., Nichenko, A. S., Tehrani, K. F., McGranahan, M. J., Krishnan, L., Qualls, A. E., Jenkins, N. T., Mortensen, L. J., Yin, H., Yin, A., Guldberg, R. E., Greising, S. M., & Call, J. A. (2019). PGC-1α overexpression partially rescues impaired oxidative and contractile pathophysiology following volumetric muscle loss injury. *Scientific Reports*, *9*(1), 4079. https://doi.org/10.1038/s41598-019-40606-6

Subramanian, A., Tamayo, P., Mootha, V. K., Mukherjee, S., Ebert, B. L., Gillette, M. A., Paulovich, A., Pomeroy, S. L., Golub, T. R., Lander, E. S., & Mesirov, J. P. (2005). Gene set enrichment analysis: A knowledge-based approach for interpreting genome-wide expression profiles. *Proceedings of the National Academy of Sciences of the United States of America*, *102*(43), 15545–15550. https://doi.org/10.1073/pnas.0506580102

Torres, M. J., Kew, K. A., Ryan, T. E., Pennington, E. R., Lin, C.-T., Buddo, K. A., Fix, A. M., Smith, C. A., Gilliam, L. A., Karvinen, S., Lowe, D. A., Spangenburg, E. E., Zeczycki, T. N., Shaikh, S. R., & Neufer, P. D. (2018). 17β-Estradiol Directly Lowers Mitochondrial Membrane Microviscosity and Improves Bioenergetic Function in Skeletal Muscle. *Cell Metabolism*, *27*(1), 167-179.e7. https://doi.org/10.1016/j.cmet.2017.10.003

Torres, M. J., Ryan, T. E., Lin, C.-T., Zeczycki, T. N., & Neufer, P. D. (2018). Impact of 17β-estradiol on complex I kinetics and H2O2 production in liver and skeletal muscle mitochondria. *The Journal of Biological Chemistry*, *293*(43), 16889–16898. https://doi.org/10.1074/jbc.RA118.005148

Wood, G. A., Fata, J. E., Watson, K. L. M., & Khokha, R. (2007). Circulating hormones and estrous stage predict cellular and stromal remodeling in murine uterus. *Reproduction (Cambridge, England)*, *133*(5), 1035–1044. https://doi.org/10.1530/REP-06-0302

Tables

Table 5.1: the results of DEG, hm- and mito-GSEA

Differential gene expression analysis				
OVX Effect	Total Genes (after QC)	Total DEGs	Pos DEGs	Neg DEGs
D3 OVX/SS	19,184	163	90	73
D7 OVX/SS	19,184	11	2	9
E2 Effect	Total Genes (after QC)	Total DEGs	Pos DEGs	Neg DEGs
D3 E2/OVX	19,184	141	33	108
D7 E2/OVX	19,184	691	142	549
Mitochondrial differential gene expression analysis				
OVX Effect	Total Genes (after QC)	Total MitoDEGs	Pos MitoDEGs	Neg MitoDEGs
D3 OVX/SS	1,140	1	0	1
D7 OVX/SS	1,140	0	0	0
E2 Effect	Total Genes (after QC)	Total MitoDEGs	Pos MitoDEGs	Neg MitoDEGs
D3 E2/OVX	1,140	0	0	0
D7 E2/OVX	1,140	9	3	6
Hallmark gene set enrichment analysis				
OVX Effect	Total Gene Sets	Sig Mito Gene sets	Pos Gene sets	Neg Gene sets
D3 OVX/SS	129	17	7	10
D7 OVX/SS	129	30	13	17
E2 Effect	Total Gene Sets	Sig Mito Gene sets	Pos Gene sets	Neg Gene sets
D3 E2/OVX	129	21	9	12
D7 E2/OVX	129	36	5	31
Mitochondrial gene set enrichment analysis				
OVX Effect	Total Gene Sets	Sig Mito Gene sets	Pos Gene sets	Neg Gene sets
D3 OVX/SS	129	32	0	32
D7 OVX/SS	129	69	69	0
E2 Effect	Total Gene Sets	Sig Mito Gene sets	Pos Gene sets	Neg Gene sets
D3 E2/OVX	129	10	1	9
D7 E2/OVX	129	54	54	0

Table 2: the results of mito-GSEA

	Categories, pathways, & normalized enrichment score							
	Mitochondrial Maintenance	NES	Fuel Preference	NES	Electron Transport Chain	NES	Antioxidants	NES
OVX Effect								
D3 OVX/SS	TOMM TIM Mitophagy Autophagy Fusion Import and sorting mtDNA maintenance	-1.67 -1.75 -1.84 -1.86 -1.96 -2.14 -1.68	Carb AA BCAA	-1.62 -1.72 -1.78	C4 C1 OxPhos all	-1.54 -1.97 -2.00		
D7 OVX/SS	TIM Fission Autophagy MICOS complex Fusion Mitophagy mtDNA maintenance	+2.00 +1.95 +1.91 +1.82 +1.77 +1.69 +1.92	FAO Carb Lipids TCA BCAA AA	+2.69 +2.67 +2.56 +2.52 +2.46 +2.06	OxPhos all C1 C4 C3 C5 C2	+3.40 +3.12 +2.59 +2.26 +1.98 +1.88	Detox ROS Detox all	+1.65 +1.64
E2 Effect								
D3 E2/OVX	mtDNA maintenance	+2.00	FAO Lipids TCA Carbs	-2.15 -1.72 -1.92 -1.76	OxPhos all C1	-2.02 -1.87		
D7 E2/OVX	TIM Autophagy Mitophagy Fusion Fission mtDNA maintenance	+2.09 +2.01 +1.94 +1.96 +1.66 +1.71	Lipid BCAA Carb TCA FAO AA Ketones	+2.61 +2.60 +2.58 +2.54 +2.54 +2.45 +1.77	OxPhos all C1 C4 C3 C2	+3.33 +3.02 +2.37 +2.19 +1.83	Detox all	+2.00

CHAPTER 6

DISCUSSION AND CONCLUSIONS

The primary goal of my dissertation was to gain a deeper understanding of mitochondrial adaptations in response to traumatic injury under various conditions, such as Western diets (WD) and a sex-dependent manner. In the first study, I investigated how a WD exacerbates VML-induced metabolic dysfunction in both sexes. The second study examined mitochondrial-targeted antioxidant mitigates VML-induced mitochondrial dysfunction and oxidative stress but not muscle contractile function. Finally, my third study explored the critical role of estrogen (E2) in regulating mitochondrial bioenergetics and redox homeostasis in E2-deficient VML-injured mice. The findings from these studies provide valuable insights into the pathophysiological consequences of VML injury and highlight potential metabolic and therapeutic targets for mitigating mitochondrial dysfunction in this context. The following sections outline the fundamental research questions and how my studies addressed them.

Sex differences in mitochondrial dysfunction in the combination of WD and VML

Given the rising prevalence of obesity affecting muscle metabolism and the fact that amputees with military traumatic injuries are more likely to develop metabolic syndrome than the general population, it is essential to determine how dietary factors worsen mitochondrial dysfunction in the context of VML injury. In Chapter 3, I investigate the interplay between WD-induced obesity and VML injury on contractile and metabolic function in both sexes. One of the key findings was that females are less prone to disrupted mitochondrial bioenergetics in response to the combined

Western diets and VML injury. Due to the higher risk of metabolic syndrome in wounded veterans and trauma patients, it is crucial to develop dietary and clinical strategies that address injury-diet interactions. Understanding sex-specific metabolic responses is essential for effective prevention and treatment.

SS-31 partially enhances exercise rehabilitative capacity by improving mitochondrial bioenergetics and AoxBC following VML injury, but not contractile function

Previously, our lab has demonstrated that VML injury impairs mitochondrial function (particularly mitochondrial respiration and enzymatic function). Additionally, there was only circumstantial evidence that VML injury reduced respiratory capacity with hyperpolarized mitochondrial membrane potential, possibly increasing mitochondrial ROS. However, there was a lack of direct evidence where oxidative stress is a hallmark of VML-injured muscle and its implication on muscle regenerative/rehabilitative capacity. In Chapter 4, I examined mitochondrial bioenergetics, reactive oxygen species (ROS) production, and antioxidant buffering capacity (AoxBC) in a murine model of VML injury, and assessed the therapeutic potential of SS-31, a mitochondria-targeted antioxidant. VML injury impaired mitochondrial function, elevated ROS, and decreased AoxBC. SS-31 treatment enhanced bioenergetic efficiency, lowered ROS levels, and improved AoxBC; however, its effects on muscle mass and contractile function were limited. Although SS-31 partially augments exercise rehabilitative capacity by enhancing metabolic function (i.e., mitochondrial bioenergetics and reducing ROS), it did not significantly enhance muscle strength, suggesting oxidative stress might not be the primary factor limiting muscle recovery post-VML. Future research should identify precise mechanisms and refine therapeutic approaches targeting muscle after VML injury.

The Role of Estradiol in Muscle Bioenergetics and ROS Regulation in E2-deficient female mice following VML injury

Sex-based differences in mitochondrial function and redox homeostasis have emerged as critical factors in muscle injury. Understanding the role of E2 in mitochondrial function and oxidative stress may provide insights into sex-specific therapeutic strategies for muscle injuries, particularly in estrogen-deficient conditions. In Chapter 5, I explore the role of E2 in protecting against mitochondrial dysfunction and oxidative stress following VML injury in E2-deficient female mice. This study demonstrates that E2 replacement alleviated OVX+VML-induced mitochondrial impairments by enhancing mitochondrial bioenergetics and antioxidant buffering capacity. RNA sequencing and gene enrichment analysis revealed significant changes in mitochondrial maintenance, oxidative phosphorylation, and metabolic pathways, highlighting the beneficial role of E2 in mitochondrial adaptation following traumatic injury. These findings underscore the therapeutic potential of estradiol in restoring metabolic balance and redox homeostasis, especially in females suffering from natural or surgical estrogen deficiency.

Future Directions

There are several directions for the future from the results of these studies. First, we identified that a WD exacerbates carbohydrate-supported mitochondrial dysfunction in male mice following VML injury, as indicated by the dysregulation of pyruvate dehydrogenase (PDH). Given the critical role of PDH in mitochondrial metabolism, future studies are needed to focus on elucidating the precise molecular mechanisms underlying PDH dysregulation in response to VML. This could include investigating regulatory factors such as PDH kinases (PDKs) and phosphatases (PDPs), as well as potential therapeutic interventions to restore PDH activity post-

VML injury. Second, our findings demonstrate that VML injury leads to increased mitochondrial reactive oxygen species (ROS) production and impairs antioxidant buffering capacity (AoxBC). To further delineate the molecular pathways contributing to VML-induced mitochondrial dysfunction, comprehensive multi-omics approaches, including cysteine redox proteomics, protein-protein interactome analyses, post-translational mitochondrial proteomics, and metabolomics are needed. These multi-omics approaches will allow us to better understand VML-induced mitochondrial dysregulation, potentially identifying novel molecular targets for therapeutic intervention. Finally, we observed that OVX impairs mitochondrial function and exacerbates mitochondrial ROS, and conversely, E2 mitigates these defects. It could be associated with G protein-coupled estrogen receptor (GPER) signaling. GPER activation has been shown to modulate mitochondrial permeability transition pore (mPTP) opening via ERK signaling and enhance muscle strength in OVX mice. However, the relative contributions of GPER compared to classical estrogen receptors (ERα and ERβ) in skeletal muscle remain unclear. Future research is required to investigate the role of 17β-estradiol on gene expression related to muscle contractility, mitochondrial bioenergetics, and antioxidant responses following VML injury through the mechanisms involving GPER. Employing pharmacological approaches using G1 (a GPER agonist) and G15 (a GPER antagonist) or loss of function model (e.g., GPER KO mouse model) will provide valuable insights into the receptor-specific mechanisms mediating estrogen's protective effects in the context of VML injury.

Conclusions

In closing, this dissertation contributes to the growing body of literature on mitochondrial dysfunction and redox imbalance in VML injury, with a particular emphasis on the influence of diet, sex differences, and therapeutic interventions. Addressing these complex biological

interactions will be essential in developing effective therapeutic strategies to enhance muscle metabolism, regeneration, and functional recovery in individuals suffering from traumatic injuries.